FINAL REPORT: EPA X98429297-0-PA

FATE OF WASTEWATER NUTRIENTS IN FLORIDA KEYS GROUNDWATER

SUMMARY

Wastewater disposal in the Florida Keys poses a potentially serious threat to the ecosystem that the Florida Keys National Marine Sanctuary and the EPA Water Quality Protection Program are charged with protecting. Our study addresses that threat by tracing the fate of wastewater and its associated nutrient load from the point of subsurface injection, through its flowpath through the groundwater system, towards its point of discharge. Our study site is Key Colony Beach, Florida, a residential community with centralized wastewater treatment and disposal. Here, secondarily treated wastewater is injected between 60-90' below the surface through a series of Class V injection wells. We installed a number of monitoring wells surrounding the injection field which allowed us to sample the groundwater system at shallow (typically 25-30'), intermediate (approximately 45') and deeper (60') depths.

Our results, and those of our collaborators at Florida State, show that the wastewater plume rises buoyantly to the bedrock/unconsolidated mud interface at approximately 20' subsurface depth, and then migrates in an easterly – southeasterly direction with the dominant flow path. Slower flow paths and dispersion of the plume causes it to spread in all directions, however. Despite the spread of this plume, which likely extends to the canal on the eastern side of the study area, nutrients are preferentially removed from the plume through interactions in the subsurface. Phosphate is strongly sorbed to the calcite surface of the bedrock limestone, and likely precipitates as an apatite phase (carbonate fluorapatite), rendering it essentially immobile. This conclusion is strongly supported by laboratory experiments performed on natural limestone substrates. Nitrate, on the other hand, exhibits high (several ppm – N) concentrations far from the point of injection, along the most rapid flowpaths. Elsewhere, nitrate concentrations are reduced by a combination of denitrification and nitrate ammonification (microbiological processes favored in the reducing groundwaters).

Overall, we find that secondary treatment of wastewater and its injection into the Key Largo Limestone is followed by effective removal of phosphate, but variably effective removal of nitrate from the wastewater plume. Treatment practices that reduce nitrate and ammonia loadings are indicated by this study.

The results presented here are largely from the M.S. Thesis of Katherine Elliott (1999).

LEE R. KUMP
DEPT. OF GEOSCIENCES
THE PENNSYLVANIA STATE UNIVERSITY
503 DEIKE BUILDING
UNIVERSITY PARK, PA 16802

TABLE OF CONTENTS

BACKGROUND AND APPROACH

The Florida Keys have become a popular retirement and vacation destination, being home to tens of thousands of permanent residents and host to millions of tourists each year (NOAA, 1995). This increase in popularity has coincided with a degradation of offshore water quality, evidenced by large algae blooms in the Florida Bay and Florida Keys, an increase in sponge mortality in near-shore communities in the Middle Keys, large seagrass die-offs in the Florida Bay, and an increase in coral bleaching and disease in the Florida Keys Reef Tract (Sullivan et al., 1996). The Florida Keys National Marine Sanctuary (FKNMS) was established in November of 1990 to preserve the sensitive marine environments surrounding the Keys. In the management plan for the sanctuary, water quality improvement and preservation was one of five issues identified as central to proper sanctuary management (NOAA, 1995).

Various researchers have suggested that wastewater-derived nutrients could be responsible for the observed degradation of water quality in near-shore environments of the Florida Keys (NOAA, 1995). Lapointe and Clark (1992) found elevated inorganic nitrogen and phosphorous concentrations along with low dissolved oxygen in near-shore waters of Florida Bay and the Atlantic Ocean and in water from artificial canals in the Keys. They implicated domestic wastewater as the source of the nutrients. Most wastewater in the Florida Keys is released into the saline groundwater of the islands through on-site disposal systems, including injection wells, cesspools, or septic systems. The aquifer that receives the wastewater discharge in the Upper and Middle Florida Keys is the very porous Key Largo Limestone (KLL), which is hydrologically connected to Florida Bay and the Atlantic Ocean and also to the many canals that cut through the islands. Wastewater disposed of into the groundwater system of the Upper and Middle Keys has the potential to quickly reach these waterbodies.
Lapointe (1987, 1989) has shown that in Florida Bay, just offshore of Big Pine Key and the Content Keys, algal growth is phosphate-limited year-round. Because of these findings, he concluded that wastewater phosphate input into Florida Bay would likely result in a dramatic increase in algal productivity (Lapointe, 1989). Forqurean et al. (1992) found that phosphate also limited seagrass growth in Florida Bay. The eutrophication threat posed by wastewater-phosphate is questioned, however, by the possibility that phosphate is removed in the subsurface (Corbett et al., 2000; Monaghan, 1996; and Lapointe et al., 1990). Monaghan (1996) and Lapointe et al. (1990) hypothesized that the phosphate uptake they observed at small on-site disposal systems is the result of phosphate adsorption and precipitation of an apatite mineral. Additionally, Monaghan (1996) calculated that groundwater surrounding a wastewater injection wells was supersaturated with carbonate fluorapatite. If interaction with the KLL immobilizes phosphate, then wastewater release into the limestone does not present as great a threat of eutrophication of surface waters as proposed by earlier work.

This project was designed to test the hypothesis that wastewater phosphate is immobilized in the saline carbonate groundwater within the KLL through carbonate fluorapatite precipitation induced by wastewater-limestone interaction. To address this hypothesis, both a field study and a laboratory study were conducted. The field study, presented in the next section, was an investigation of the mobility of phosphate at one of the largest volume wastewater injection site in the Middle and Upper Florida Keys in the city of Key Colony Beach (KCB), in the Middle Keys. The goal of the study was to determine if phosphate uptake is occurring, and if so, the extent of that uptake. In the laboratory study presented in the following section, phosphate solutions were reacted with pieces of KLL to test if interaction with KLL causes precipitation of phosphate as carbonate fluorapatite. The approach of this

investigation allowed for a comparison of phosphate chemistry in the field setting with the fate of phosphate observed under controlled conditions in the laboratory.

KEY COLONY BEACH FIELD STUDY

INTRODUCTION

Water quality issues are important in the Florida Keys, a heavily inhabited island chain. The severe coral-bleaching event of 1987 in the Florida Reef Tract, together with increased occurrence of coral disease and death, heightened awareness of the need to understand how human activities in the Keys affect the nearshore marine environments surrounding the islands. These include not only the Florida Reef Tract, but also the seagrass beds of Florida Bay. One potential threat to water quality is the release of nutrients through wastewater disposal. Besides the ecological issues, the problem also has economic consequences for the residents of the Florida Keys, part of Monroe County, Florida:

> "Monroe County's economic base is heavily dependent on tourism and water-related activities. These activities, in turn, depend on waters of consistently high quality. However, pollutant discharges in the Sanctuary, most of which can be attributed to wastewater treatment methods in Monroe County, have degraded the area's water quality." (NOAA 1995, pp. 191).

Most residents dispose of treated wastewater directly into the saline groundwater of the Keys through either shallow injection wells following secondary treatment, septic tanks, or cesspools. In the Upper and Middle Keys, the wastewater is released into the shallow, highly transmissive limestone aquifer of the region. Here, groundwater flow is complex, being influenced by tidal fluctuations and density contrasts between the low-salinity wastewater and the saline groundwater. If mobile, the wastewater-derived nutrients released into the groundwater can induce eutrophication of nearby surface waters, including the canals that are found on many islands.

In this field study, the mobility of wastewater phosphate around shallow injection wells was investigated. The study site was the wastewater treatment plant of Key Colony Beach, one of the largest wastewater injection sites in the Florida Keys. Maximum phosphate mobility was expected here due to the large injection rate. The hypothesis that wastewater-phosphate is immobilized in the carbonate aquifer through the precipitation of carbonate fluorapatite in the saline carbonate groundwater was tested.

GEOLOGY OF THE FLORIDA KEYS

The Florida Keys are a 240 km long arc of low-lying carbonate islands that extend southwest from Soldier Key, 15 km southeast of Miami, to Key West (Figure 1; Halley et al., 1997). The Keys consist of three island groups: the Upper, Middle, and Lower Keys. The Upper Keys are those islands north of and including Upper Matecumbe. The Middle Keys run from Lower Matecumbe to Big Pine Key and are distinguished from the Upper Keys by larger tidal channels between islands. The Upper and Middle Keys are oriented parallel to the arc of the island chain. Conversely, the Lower Keys, from Big Pine Key to Key West (Chiappone, 1996), are oriented roughly perpendicular in their long dimension to the island chain, in a northwest-southeast direction. The Keys form the eastern margin of Florida Bay.

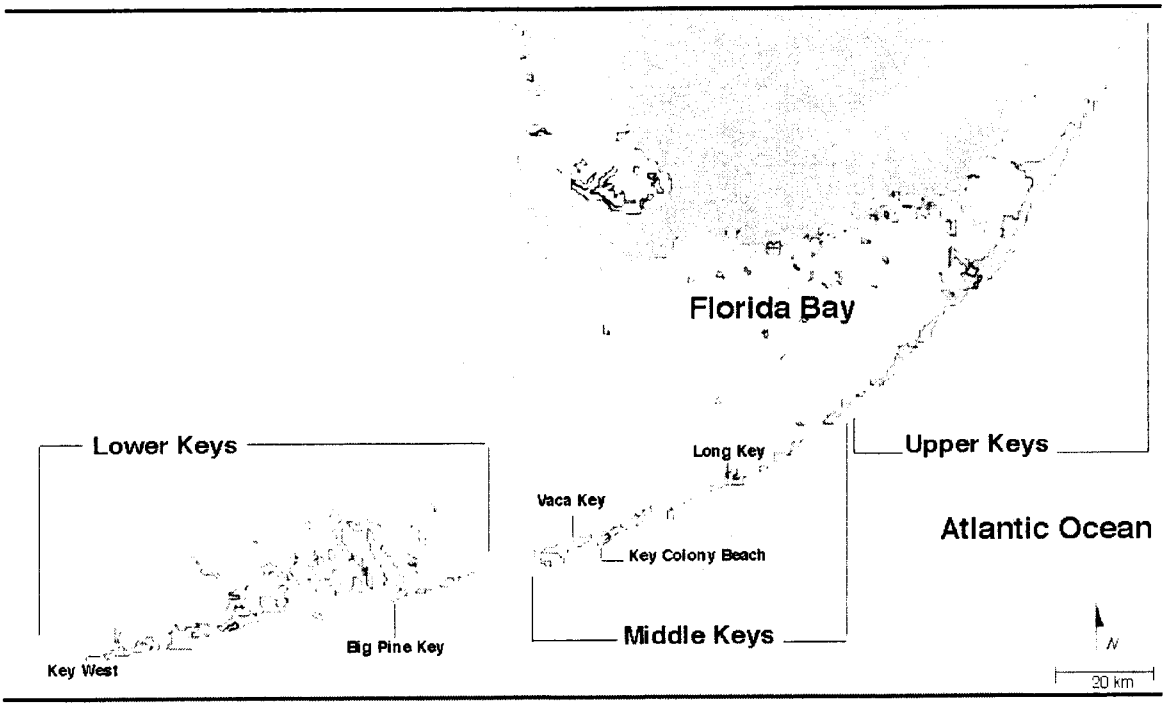

Figure 1. The three island groups of the Florida Keys and the islands discussed in the text are marked on this map of southern Florida (adapted from NOAA, 1995).

The Keys formed during interglacial stages of the Pleistocene, when sea level was up to seven meters higher than at present (Harrison and Coniglio, 1985). The long linear islands of the Upper and Middle Keys emerged as a shelf-margin coral reef during this time (Harrison and Coniglio, 1985). Further south, the Lower Keys formed contemporaneously as ooid shoals (Halley et al., 1997). The Keys are now exposed due to lower Holocene sea levels. The coralline rock of the Upper and Middle Keys is known as the Key Largo Limestone (KLL). This formation consists of skeletal grainstone, packstone and wackestone as well as coral boundstone (Halley et al., 1997) and extends over an area much larger than the Florida Keys (Hoffmeister and Multer, 1968). The ooid grainstone of the Lower Keys is part of the Miami Oolite (MO), also known as the Miami Limestone, which overlies the KLL in the Lower Keys (Halley et al., 1997). The surface contact of the KLL and MO is exposed on Big Pine Key (Hoffmeister and Multer, 1968). The thickness of the MO varies from 3 to 5 m; it generally thickens toward the Atlantic (Halley et al., 1998). The thickness of the KLL ranges from 40 to 90 m (Cunningham et al., 1998). Cunningham et al. (1998) found 50 m of KLL in their drill core from Vaca Key, close to the study site at KCB (Figure 1).

There have been periodic episodes of marine flooding and subaerial exposure of the Florida Plateau (Perkins 1969). Exposure to meteoric waters during the Quaternary has caused minor karstification of the Pleistocene limestone and the development of soilstone crusts (Halley et al., 1997; Perkins, 1969). These features allowed Perkins (1969) to recognize five Pleistocene carbonate chronostratigraphic units, Q1-Q5, each bounded by exposure surfaces. The KLL spans all five of these; the MO is part of the Q4 and Q5 units (Perkins, 1969). Two of these subaerial unconformities are easily recognized and broadly distributed in exposures and cores throughout the Keys. One is the Q3-Q4 contact (known as the Q3 unconformity), which

is marked by the presence of quartz sand, laminations, iron staining, root traces and regions of lower permeability (Perkins, 1977; Halley et al., 1997). The other is the surface exposure of the Keys, the upper boundary of the Q5. The Q3 unconformity in drill cores is generally 7 to 10 meters deeper than the Q5 exposure surface (Coniglio and Harrison, 1983; Harrison and Coniglio, 1985).

The waters surrounding the Florida Keys continue to be areas of active carbonate deposition. Coral is not the only source of recent carbonate sediment; Holocene mud and sand deposits occur in the waters surrounding the islands (Enos, 1969). These are composed of biogenic carbonates such as algal precipitates, bivalve shells and foraminifera (Enos, 1977).

HYDROLOGY OF THE FLORIDA KEYS

Regional groundwater flow in the Keys appears to be across the island chain, from Florida Bay eastward under the Florida Keys to the Atlantic Ocean (Shinn et al., 1997). This flow mirrors the surface water hydrodynamics; Ogden et al. (1994) found that the average flow direction for water in tidal channels between the Upper and Middle Keys was also from the Florida Bay to the Atlantic. A hydrodynamically supported difference in water levels of about ten to twenty cm between Florida Bay and the Atlantic Ocean drives both surface and groundwater flow (Shinn et al., 1997). The resulting groundwater flow is not uniform; tides cause periodic reversals in flow direction (Shinn et al., 1997). The northeast half of Florida Bay is minimally influenced by tides, and at some stages of the Atlantic tidal cycle the water level is higher in the Atlantic Ocean than in Florida Bay. During these times, groundwater flow reverses and proceeds from the Atlantic to the Florida Bay.

Groundwater recharge occurs in the Florida Bay and through meteoric recharge in the Keys. Machusak and Kump (1997) concluded that recharge occurs in hardground areas of Florida Bay, based on the results of observation wells drilled in the area. Within these wells, negative groundwater heads relative to Florida Bay level dominated during typical tidal cycles and salinities were similar to those of the slightly hypersaline water of Florida Bay. As a result of this recharge in the bay, groundwater deeper than 5 m is saline to slightly hypersaline in the Upper and Middle Keys (Monaghan, 1996; Bohlke et al., 1997). Shallow groundwater of the Keys is often less saline, as a result of meteoric recharge or wastewater disposal that occurs on the islands. (Vacher et al., 1992; Monaghan, 1996; Shinn et al., 1994)

The hydraulic conductivity of the KLL is too large to be measured by in-situ techniques such as pump or slug tests. However, Vacher et al. (1992) estimated the hydraulic conductivity of the KLL to be 1,400 m/day using Dupuit-Ghyben-Herzberg analysis. A hydraulic conductivity of the MO of 120 m/day was also estimated using the same technique (Vacher et al., 1992). The large hydraulic conductivity of these formations limits freshwater lens development in the Keys. In the Upper and Middle Keys, freshwater is rarely found, due to the small size of the islands and the large hydraulic conductivity of the KLL. The shallow groundwater of these islands is generally brackish (Monaghan, 1996). Small freshwater lenses do exist within the MO in the larger islands of the Lower Keys, such as Big Pine Key (Hanson, 1980) and Key West (McKenzie, 1990). These lenses have an extensive transition zone between fresh and salt water, and only a small volume of water within them meets the drinking water standard of 250 mg/l chloride (McKenzie, 1990; Hanson, 1980).

The Holocene mud layer is much less permeable than the MO or KLL. Shinn et al. (1994) hypothesized that the mud confines upward groundwater flow from the KLL seaward of the Keys. Their conclusion is supported by the work of Machusak and Kump (1997), who found that the mud layer of Fiesta Key is an effective cap for the groundwater system. This is because of the mud's low hydraulic conductivity, which can be approximated by the values measured for similar unconsolidated Holocene muds from other locals on the Florida Plateau. Enos and Sawatsky (1981) measured the permeability of the upper 50 cm of sediments from

shoals and islands within Florida Bay and Hawk Channel. They found unconsolidated sediments corresponding to a medium to fine grained wackestone lithology have hydraulic conductivities ranging from $5.2*10^{-4}$ to 5.5 m/day. In agreement with these results, Juster and Vacher (1994) found hydraulic conductivities of sediment from mud islands in the Florida Bay to be approximately $8*10^{-2}$ m/day at 50 cm depth and $8*10^{-4}$ m/day at 2 m depth. These results show that the hydraulic conductivity of fine-grained, mud-dominated sediment on the Florida Plateau is 2 to 6 orders of magnitude lower than that of the MO and 3 to 7 orders of magnitude lower than that of the KLL. Thus, the mud acts as a confining layer to water traveling in the much more conductive KLL or MO.

WASTEWATER DISPOSAL IN THE FLORIDA KEYS

The only local sources of freshwater in the Florida Keys are rain, once collected in cisterns, and a few small freshwater lenses in the Lower Keys. These freshwater resources are insufficient for the islands' population. Almost all potable water comes from the Miami area via the Florida Keys aqueduct (Ovide, 1991). Water is pumped from wells in Florida City, south of Miami, that tap the Biscayne Aquifer (Ovide, 1991). This surficial, unconfined aquifer is composed of porous limestone and confined at the bottom by low permeability sand and clay sediments (Kohout, 1987).

Much of this imported freshwater becomes domestic wastewater. Thus, wastewater disposal is an anthropogenic source of freshwater to the groundwater of the Florida Keys. The EPA reported in 1996 that wastewater disposal in the Keys occurs through 10,000 unregulated cesspools, 30,000 septic tanks, over 200 small package plants, and municipal wastewater treatment plants at Key Colony Beach and Key West (USEPA, 1996). Shallow injection wells, which inject at depths ranging from 10 to 30 m, dispose of the treated effluent of the package plants and the treatment plant of Key Colony Beach. These systems together disposed of an average of $6.4*10^{4}$ m^3/day into the groundwater of the Keys in 1991 (Sullivan et al., 1996). This input compares to an average rainfall input of $9.0*10^{5}$ m^3/day (Shooner and Drew, 1982) and an estimated potential evapotranspiration of $9.4*10^{5}$ m^3/day (Henry et al., 1994), given an area of the Florida Keys of 266 km^2 (NOAA, 1995). Due to the water deficit caused by excess potential evapotranspiration little rain recharges the groundwater. Wastewater disposal is the main source of freshwater to the groundwater of the Keys, especially when injected by wells several meters below the shallow water table.

METHODS

SITE DESCRIPTION

The wastewater treatment plant at the city of Key Colony Beach (KCB) was the study site. The city is located a small artificial island east of Vaca Key (Figure 1). This island was created in 1950's by filling a low-lying mangrove forest and surrounding waters (Feiner, 1991) with a dredge and fill operation (Gallagher, 1991). KCB was a 0.36 km^2 mangrove forest before development; it now consists of 1.15 km^2 of filled land (Feiner, 1991; Figure 2).

The centralized wastewater treatment plant of KCB is one of only two in the Keys. Before 1993, the city released treated wastewater into Shelter Bay, to the north of the island (Figure 2). The city now uses a line of six injection wells to dispose of 500 to 1,200 m^3 per day of secondary treated wastewater. A covered cement trough houses the wells, which have inlets of varying heights. Wastewater in the trough must be at a critical height to flow through an inlet. Usually, only the middle two or three wells take in water. The injection wells are cased to a depth of 18 m and to open to the bottom of the borehole at 27 m.

The injection well system at KCB is unusually large. Small package plants with only one injection well are much more common in the Florida Keys. Monaghan (1996) and Corbett et al (in prep.) examined the chemistry of groundwater surrounding the small package plant of Keys Marine Lab (KML) on Long Key, Florida. KML has an injection well that disposes of approximately 3 m^3 of wastewater per day. The wastewater plume was difficult to trace due to this small flux of wastewater. This is not a problem at KCB, due to the much larger volume of wastewater injected. The amount of wastewater injected varies seasonally, due to the increase in population during the winter months.

MONITORING WELL INSTALLATION AND SURVEY

During the month of January 1998, researchers from Florida State University, The Pennsylvania State University (Penn State), and the U.S. Geological Survey (USGS) installed seven piezometer nests, A through G, in the vicinity of the wastewater injection wells (Figure 2). An NX wire-line, hydraulic coring drill with a tungsten carbide bit was used to drill 5.1 cm (2 inch) diameter boreholes for the wells. This equipment retrieves 1.52 m (5 ft) sections of core. Tap water was the drilling fluid. Placement of the piezometer nests was concentrated to the south of the injection line (nests A, B, C, E, and G) for logistical reasons. The wells all fall along one of the two transects shown in Figure 2. Wells E, B, A, C, D fall along the east-west trending transect. Wells F, A, and G fall along the north-south trending transect. These transects cross at A, which is the piezometer nest closest to the main wastewater injection well. This report uses cross-sections along these transects to display results.

Each nest consists of three piezometers with discrete sampling depths (Figure 3). The piezometers are composed of linked sections of 1.52 m long (5 ft), 1.27 cm (0.5 inch) diameter PVC pipe. The deepest 1.52 m (5 ft) section of the pipe is screened along its entire length with small slots in the PVC to make up the sampling interval. To construct a piezometer, the PVC pipe was inserted into the borehole, screened section first. The borehole was then backfilled with quartz sand to pack around the sampling interval; this sand is too coarse to pass into the screen and acts as a sand pack. Portland cement was poured in to grout the hole up to the depth for the next piezometer. Once the cement grout had set, the procedure was repeated for the next piezometer. The cement was judged to be set after probing it with a PVC pipe indicated it had hardened. After all desired piezometers were installed, the upper 30 cm, roughly, of the borehole was cased with 5.08 cm (2 inch) diameter PVC pipe. Then the borehole was backfilled with cement to about 10 cm from the ground surface to fix the position of the piezometers. PVC caps were then fit onto each piezometer. Lastly, the wells were sealed with rubber tension well caps. These caps are flush with the ground and, theoretically, can be stepped on or driven over without harm to pedestrian, vehicle, or well. The three sampling intervals at each location are referred to in this report as the shallow, intermediate, and deep wells (Table 1). The bottom of each sampling interval will be used as the well depth, although each well samples a 1.52 m (5 ft) interval of aquifer. Individual sampling intervals are referred to by the nest and lower depth of sampling interval to the nearest meter; for example, A-18 (Table 1).

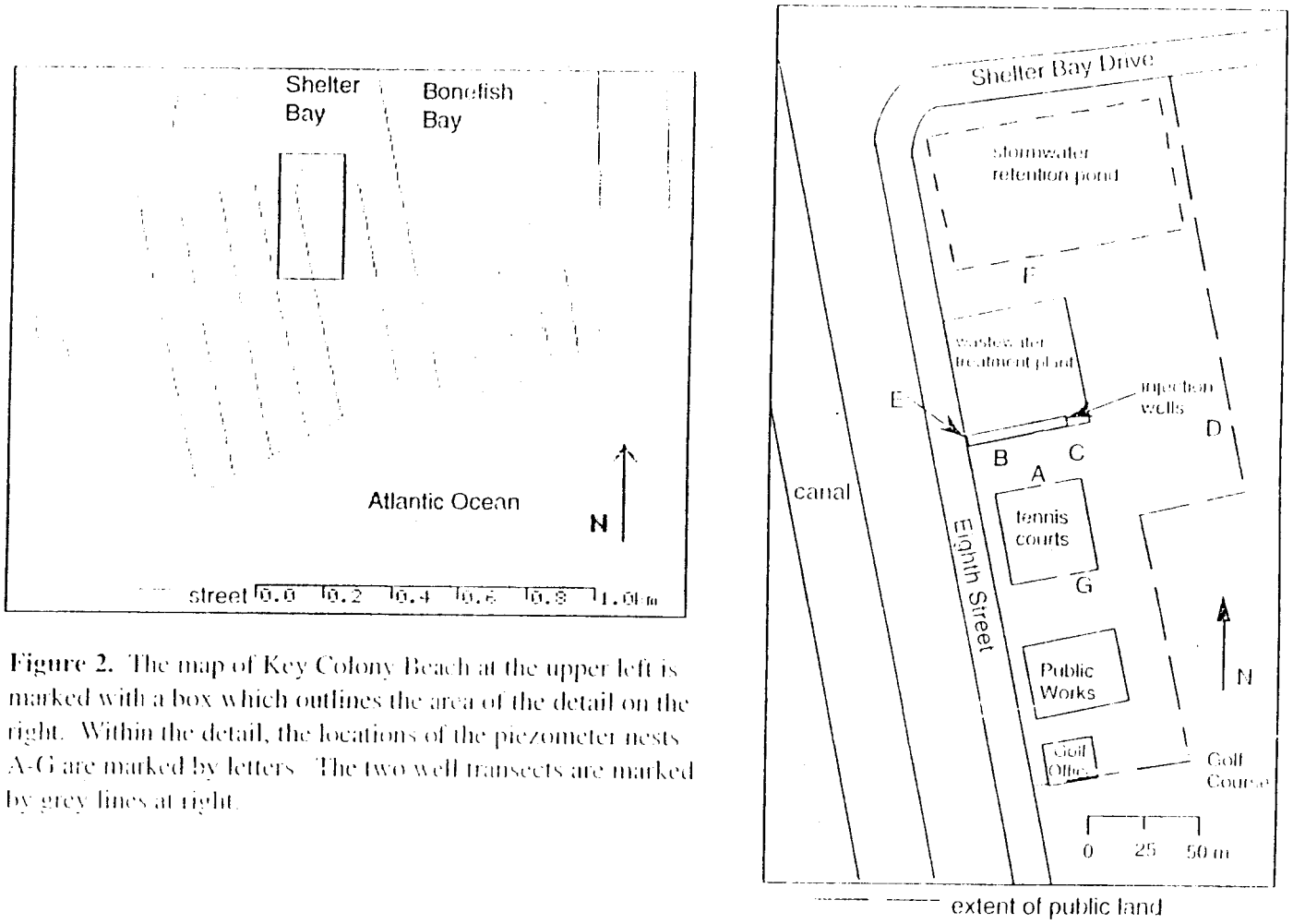

Figure 2. The map of Key Colony Beach at the upper left is marked with a box which outlines the area of the detail on the right. Within the detail, the locations of the piezometer nests A-G are marked by letters. The two well transects are marked by grey lines at right.

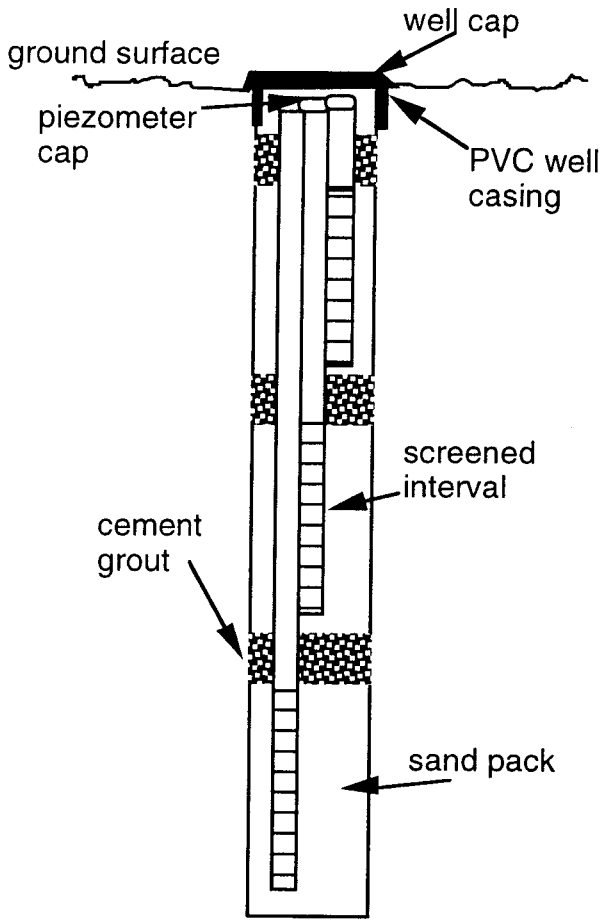

Figure 3. This schematic of the piezometer nest design is not drawn to scale.

Table 1. Depth of each sampling interval its identification.

Piezometer	Sampling Interval Depth, m, and Identification		
Nest	Shallow	Intermediate	Deep
A	3.0-4.6, A-5	7.6-9.1, A-9	16.8-18.3, A-18
B	3.0-4.6, B-5	7.6-9.1, B-9	16.8-18.3, B-18
C	3.0-4.6, C-5	7.6-9.1, C-9	18.3-19.8, C-20
D	3.0-4.6, D-5	7.6-9.1, D-9	12.2-13.7, D-14
E	3.0-4.6, E-5	7.6-9.1, E-9	16.8-18.3, E-18
F	6.1-7.6, F-8	12.2-13.7, F-14	16.8-18.3, F-18
G	3.0-4.6, G-5	7.6-9.1, G-9	16.8-18.3, G-18

The monitoring wells' locations were surveyed in on June 6, 1999 with respect to a benchmark on the wastewater treatment plant premises. D. Ombolski and L. Kump performed the survey using a laser theodolite. Vertical positioning is estimated to be accurate to ± 1 cm.

DRILL CORE CHARACTERIZATION

During drilling, notes were taken on the length of time it took to drill each 1.52 m section of core. This is a qualitative measure of the competence of the formation. Sudden drops of the drill, presumably due to voids, were also noted. The length of core obtained was used to estimate a percent recovery of the core:

$$\% \text{ Recovery} = [\text{length of core} / \text{length of drill pipe}] * 100\% \quad (1)$$

In the laboratory the core lithologies were described in detail. Rock types were classified using the carbonate rock classification of Dunham (1962). Also, the cores were weighed. This weight was used to calculate an upper limit on the porosity by dividing the weight of each 1.52 m section of core by the weight of a block of pure calcite in the shape of the core section, 8387 g.

Samples from selected cores were analyzed by powder x-ray diffraction (XRD) and bulk chemical analysis. Samples were taken from four cores: two from close to the injection wells, A and C, and two from the margins of the study area, F and G (Figure 2). They were sampled at locations at least 30 cm from the end of a core section to avoid anomalies due to core retrieval. Before sampling, the cores were rinsed with tap water to remove sea salt. Slices of cores were taken by cutting through the cores using a water-cooled rotary saw with a tungsten carbide blade. Some sections of core were not intact rock but composed of pebble-size fragments. These intervals were sampled by taking representative fragments. Samples were rinsed after removal. Each sample was cut in two with the rotary saw; one half was used for XRD analysis and the other for bulk chemical analysis. The samples for bulk analysis were weighed to ensure they were at least five grams, which is comfortably over the minimum three grams required for this analysis. Due to the low recovery of the cores drilled, depths of each sample are only approximate. Duplicates of ten percent of the bulk analysis samples were obtained by cutting large bulk analysis samples into two with the same saw.

Enzyme Laboratories (Golden, Colorado) performed the bulk analyses. The samples were ground and fusion digested by Enzyme Laboratories. The digested bulk samples were analyzed with an inductively coupled plasma-atomic emission spectrophotometer (ICP-AES). The laboratory staff analyzed the samples with their standard bulk rock assay. This analysis included the following major oxides with a stated detection limit of 0.1 wt %: Al_2O_3, CaO,

Fe_2O_3, K_2O, MgO, MnO, Na_2O, P_2O_5, SiO_2, and TiO_2. The following trace elements were also analyzed for with a stated detection limit of 2 ppm: Ba, Sr, Sc, Y, and Zr. Other analyzes included Be with a detection limit of 1 ppm, F with a detection limit of 10 ppm, and V with a detection limit of 5 ppm. The weight percent lost on ignition was also reported. Enzyme Laboratories also analyzed the duplicate samples (Appendix H).

The samples were analyzed by powder XRD to determine the their mineralogy and to see if any phosphate phases could be detected. XRD samples were analyzed on a Rigaku Gigerflex with a Dmaz-B controller and vertical goniometer at the Materials Characterization Laboratory, Penn State. This diffractometer uses copper $K\alpha_1$ radiation. Samples were ground and crushed using a ceramic mortar and pestle. The resulting powders were mounted as an acetone slurry on a quartz slide to produce the thin coating of powder required for analysis. Qualitative scans were performed, with a continuous scan at 5 degrees per minute. Most samples were scanned from 10 to 65° 2-theta, which is the appropriate range for the two minerals detected aragonite and calcite. A 2-theta range of 10 to 100° was used for three samples to check for other phases.

WATER SAMPLING AND FIELD ANALYSES

Two sampling campaigns were conducted at KCB during 1998, which will be referred to as the March and June sampling campaigns. The March sampling campaign ran through March 9 to 11, when a comprehensive well sampling was completed. The June sampling campaign occurred on June 6 to 11. First, a comprehensive well sampling was completed on June 6. On June 8 through 11, wells A and B were sampled at twelve-hour intervals to investigate the variability in groundwater nutrient concentrations over a three-day period. Also, KCB workers sampled wastewater every day during the workweek that preceded the June sampling campaign, June 1 through 5.

A standard procedure was followed during each well sampling which followed our EPA approved Quality Assurance Project Plan. First, the well was purged of at least three well volumes of water. In March, this was done with a Masterflex peristaltic pump. In June, a faster Jobsco industrial diaphragm pump Model 30802-0012 was used. After purging, pre-cleaned 250 ml Nalgene screwcap bottles were rinsed three times with sample and then filled using the peristaltic pump. Temperature and pH were measured in one of these bottles using a Hanna HI model 9023 portable pH and temperature meter. The same sample was analyzed for conductivity using an Orion model 115 conductivity meter and discarded.

Prelabeled 250 ml sample bottles were used for alkalinity samples and samples taken for transport to Penn State. Ten percent of alkalinity samples were taken in duplicate. All samples destined for analysis at Penn State were taken in duplicate while ten percent were taken in triplicate for interlaboratory comparison with Florida International University. A sodium thiosulfate solution was added to remove residual chlorine that could react with ammonia according to American Public Heath Association method 4500-NH_3 A (1985). Alkalinity samples were filtered through glass fiber filters and analyzed within twenty-four hours of sampling using a standard hydrochloric acid solution following EPA Method 310.1 (USEPA, 1983).
Field sulfide analyses were conducted during the March 1998 sampling campaign. Sulfide samples were collected in 75 ml glass bottles with stoppers. Immediately, sulfide was fixed as ZnS according to American Public Heath Association's method 4500-S^{2-} A (1985). Even with this pretreatment, analysis was required within several hours (American Public Health Association, 1985). Ten percent of sulfide samples were taken in duplicate.
Sulfide samples were analyzed within twelve hours of sampling. Fixed sulfide samples were pretreated to remove interferences by decanting off the supernatant and refilling bottles with

distilled water according to American Public Heath Association's method 4500-S^{2-} C (1985). Subsequently, sulfide concentration was determined using EPA Method 376.2, a colorimetric methylene blue method with a visual comparison (USEPA, 1983). In this method the sulfide reacts with dimethyl-p-phenylediamine in the presence of ferric chloride to produce a methylene blue dye in a test tube. The color was compared with another test tube in which the sample is treated in the same manner except the dimethyl-p-phenylemediamine was not added. A calibrated methylene blue solution was added dropwise to this second test tube until the blue colors of the solutions in the two tubes matched.
Replicate and duplicate alkalinity and sulfide analyses were performed to assure data quality. Each sulfide and alkalinity sample was analyzed in replicate; the average of the replicates is reported. Duplicate sulfide and alkalinity samples for ten percent of the samples were analyzed; duplicate results are tabulated in Appendix H.

Samples for nutrient, fluoride, oxygen isotope and elemental analysis were frozen for transport to Penn State. In March 1998, these samples were filtered through glass fiber filters before freezing. Unfortunately, June 1998 samples could not be filtered before shipment because of equipment failure. June 1998 samples were thawed and filtered at Penn State before analysis.

During the March 1998 sampling campaign, many of the wells had anomalously high pH readings. It is suspected that the Portland cement grout between sampling depths had not set properly, which caused alkaline conditions. In April of 1998, sulfuric acid was poured into the affected piezometers to clear the unset cement, and then pumped out after several hours. Those treated wells which sample the limestone layer had risen to a normal pH of 7 to 8 by June 1998. Unfortunately, the acid effects of the treatment remained in the treated wells in the mud layer. These wells were also problematic in that they have a very low yield and slow recovery; it was difficult to obtain enough water for sampling. Because of these complications, wells that sampled the mud layer (sampling depths less than 6.09 m) were not sampled during the June 1998 campaign.

During the June 1998 sampling, water level readings were made in four of the wells throughout a twelve-hour period to examine tidal effects. Measurements were made every hour for the intermediate and deep wells of A, B, F, and G. The water level depth was determined by a "homemade" device that consisted of a conductivity probe that beeps when submerged, attached to a 1.5 m-long thin dowel fitted with a metric measuring tape. During the second half of the tidal cycle, the sampling interval was shortened as the tidal reversal approached, to improve the resolution on the time when this reversal occurred.

NUTRIENT ANALYSIS

Samples were analyzed for ammonia, nitrate plus nitrite, and phosphate by automated spectrophotometry on a Technicon Autoanalyzer II according to EPA methods. Ammonia analysis was performed according to Method 350.1, in which alkaline phenol and hypochlorite react with ammonia to form an idophenol blue (USEPA, 1983). Sodium nitroprusside intensifies the blue color. Phosphate analyses were performed using EPA Method 365.1 (USEPA, 1983). This analysis includes all forms of dissolved orthophosphates (PO_4^{3-}, HPO_4^-, $H_2PO_4^-$, and H_3PO_4) and aqueous complexes of those ions plus a small amount of any condensed polyphosphates present (American Public Health Association, 1995; USEPA, 1983). At a pH greater than 7.2, $H_2PO_4^{2-}$ is the dominant species. The result of this analysis will be referred to as "phosphate". In the analysis, phosphate reacts with ammonium molybdate and antimony potassium tartrate to form an antimony-phospho-molybdate complex. This complex is reduced to an intensely blue-colored complex by ascorbic acid. The methods used have a

range from up to one ppm-N for nitrate and ammonia, and up to one ppm P for phosphate. Any samples with higher concentrations were diluted with deionized distilled water. The detection limits for each method were determined during the analysis of each sampling campaign by analyzing a series of increasingly dilute samples until no response by the instrument was observed.

Combined nitrate plus nitrite was analyzed by EPA Method 353.2 with an additional pretreatment for sulfidic samples (USEPA, 1983). In this method, nitrate is reduced to nitrite in a column containing granulated copper-coated cadmium. The reduced nitrate plus original nitrite is reacted with sulfanilamide and N-(1-naphthyl)-ethylenediamine dihydrochloride to form an azo dye. Sulfide interferes with the analysis, so sulfidic samples were first treated by bubbling water-saturated air through acidified samples for an hour to degas hydrogen sulfide. Before analysis, the pH of the samples was adjusted to near-neutral using dilute sodium hydroxide solution. Sulfidic samples were not treated before ammonia or phosphate analysis. Nitrate plus nitrite is referred to simply as nitrate in this study, because it is the more abundant species.

The autoanalyzer was calibrated during each analytical period. It produces a trace of absorbance through time on chart paper; each sample corresponds to a peak in the trace. Six standards were analyzed in the beginning of each run to calibrate the peak height against concentration. The solution matrix affects the background absorbance of the reagents. Because of this, diluted samples or those with low salinity were calibrated with standards made with distilled water, while samples with high salinities were calibrated with seawater standards. Those seawater standards were prepared with unfiltered, low-nutrient water collected from the Gulf Steam seaward of the Florida Reef Tract. Standards were also analyzed periodically throughout an autoanalyzer run to check for drift. If standards were outside a prescribed range, the analytical results were voided. The range of drift allowable was plus or minus three times the standard deviation of twenty replicate analyses of a standard.

Additional quality control procedures were followed according to the EPA approved Quality Assurance Project Plan. All samples were analyzed in replicate on the autoanalyzer. Thus, if a brief chemical or electrical interference occurred, one replicate could still be analyzed. Ten percent of sample duplicates were analyzed. Triplicates samples (numbering ten percent of total samples) collected in June 1998 were analyzed at Florida International University for interlaboratory comparison. Duplicate and triplicate results are tabulated in Appendix

FLUORIDE Analysis

Penn State undergraduate student Tonya McGowen analyzed the June 1998 samples for fluoride (McGowen, 1999, unpubl.) as part of an independent research project. A fluoride sensitive electrode was used in a method similar to that of EPA method 340.2 (USEPA, 1983). However, modifications were made; the complexing buffer solution of Bodkin (1977) was used. Also, the sample and complexing buffer were left to react overnight to ensure all fluoride was liberated from magnesium-fluoride complexes. Measurements were made on a Corning model 135 pH ion meter using an Orion 94-09 fluoride ion selective electrode and a Orion 90-02 double junction reference electrode.

ELEMENTAL ANALYSIS

The Material Characterization Laboratory of Penn State performed elemental analyses of the June 1998 water samples. Samples were analyzed for Al, Ba, Ca, Fe, K, Mg, Mn, Na, P, Si, Sr, and Ti. Analysis was performed on a Leeman Labs PS3000UV inductively coupled plasma-

atomic emission spectrophotometer (ICP-AES). Duplicates of ten percent of the samples were analyzed (Appendix H).

OXYGEN ISOTOPIC ANALYSIS

The oxygen isotopic composition of June samples was determined by the carbon dioxide equilibration method described by Epstein and Mayeda (1953) and Craig (1957). In this procedure 10 ml of water was equilibrated with a measured number of moles of carbon dioxide of a known oxygen isotopic composition at 25°C. Isotopic compositions were reported in delta notation:

$$\delta^{18}O = [(R_{sample} / R_{standard}) - 1] * 1000\ ‰ \quad (2)$$

where: $R = {}^{18}O/{}^{16}O$

Once equilibrium was reached, the oxygen isotopic composition difference between the carbon dioxide and water is governed by the fractionation factor (α):

$$\alpha = R_{CO2} / R_{H2O} = (1000 + \delta^{18}O_{CO2}) / (1000 + \delta^{18}O_{H2O}) \quad (3)$$

where: $R_{CO2} = {}^{18}O/{}^{16}O$ of oxygen in CO_2
$R_{H2O} = {}^{18}O/{}^{16}O$ of oxygen in H_2O

The isotopic composition of the water can then be calculated based on the principle of mass balance:

$$\delta^{18}O_{H2O} = (1-\alpha) * 1000/\alpha + \delta^{18}O_{CO2\ final} * (1/\alpha + 2n_{CO2}/n_{H2O}) - 2n_2 * \delta^{18}O_{CO2\ initial} / n_{H2O} \quad (4)$$

where:
n_{H2O} = moles of water
n_{CO2} = moles of carbon dioxide
$\delta^{18}O_{CO2\ initial}$ = oxygen isotopic composition of CO_2 before equilibration
$\delta^{18}O_{CO2\ final}$ = oxygen isotopic composition of CO_2 after equilibration
$\delta^{18}O_{H2O}$ = oxygen isotopic composition of the H_2O before equilibration
α = CO_2 - H_2O fractionation factor (1.0412 at 25° C; O'Neil et al., 1975)

Salt content affects the fractionation factor between carbon dioxide and saline solutions, but at seawater salinity this effect is small (Craig and Gordon, 1965). For example, Craig and Gordon (1965) carried out duplicate analysis of the same water, adding sodium chloride incrementally to distilled water to achieve the salinity of seawater. The salinity difference changed the result by only 0.03‰. In support of this result, O'Neil and Truesdell (1991) found that sodium chloride had no effect on the fractionation factor up to a concentration of 6.0 molar, but other salts affect the fractionation factor at lower concentrations. Horieta et al. (1993) recommended that any dissolved species with a concentration of greater than 0.1 molal should be considered as contributors to the salt effect. In an analysis of Long Key groundwaters by Monaghan (1996), sodium chloride was the only salt whose concentration exceeded 0.1 molal. Since the expected concentrations of sodium chloride do not add significantly to the salt effect, the oxygen isotope ratios are not corrected for salinity.

Samples were prepared for oxygen-isotope analysis on a glass high-vacuum line (refer to Figure 4). Before equilibration, all dissolved gasses had to be removed from the water sample.

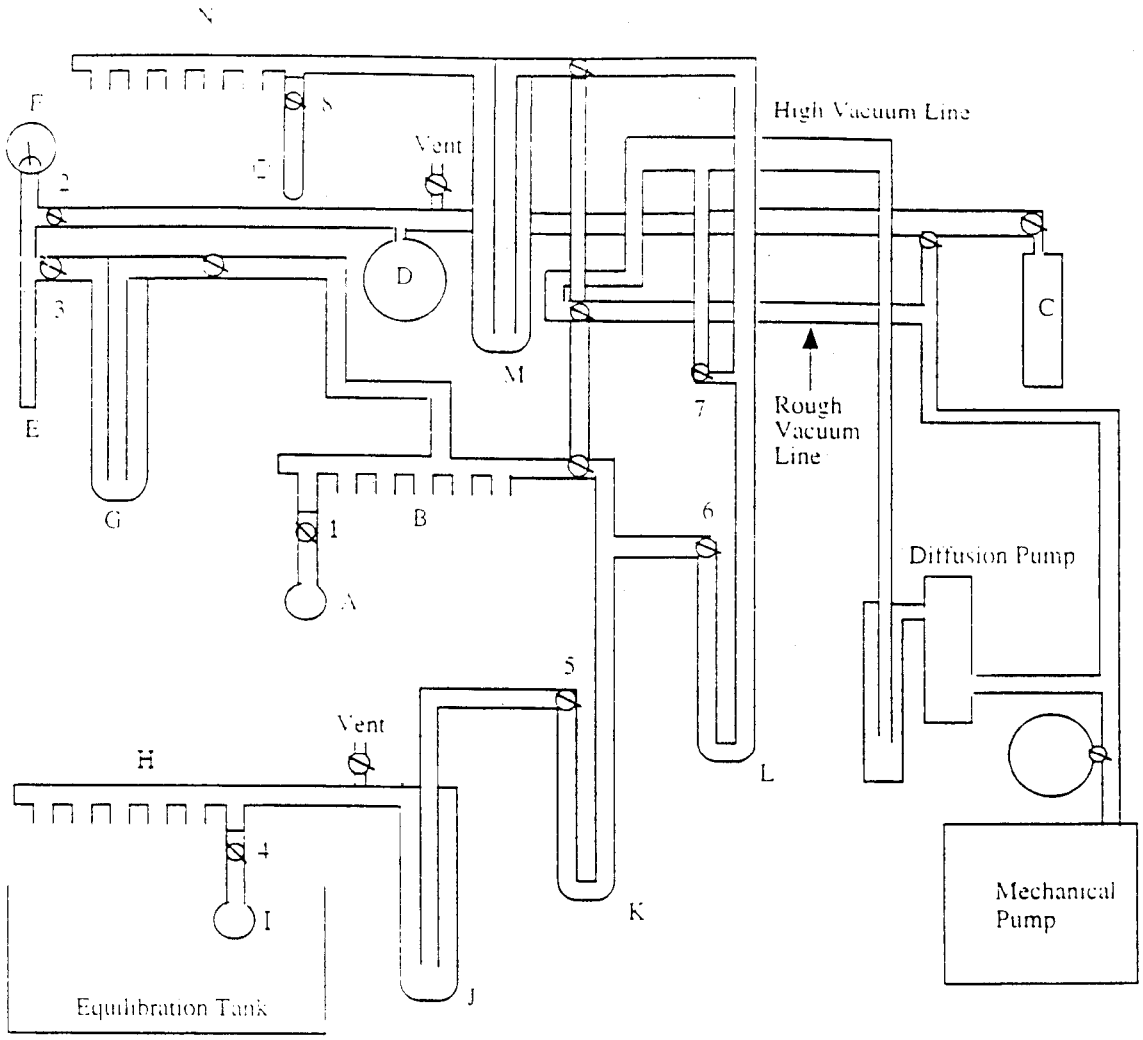

1-8: stopcock valves
A: equilibration vessel
B: sample preparation line
C: CO2 tank
D: expansion volume
E: fixed-volume cold finger, calibrated
F: pressure gage
G: water trap

H: CO2 extraction line
I: equilibration vessel
J: water trap
K: trap
L: trap
M: water trap
N: gas collection line
O: gas sample vessel

Figure 4. This schematic illustration of the vacuum manifold used in the carbon dioxide-water equilibration shows the letters and number referred to in the text.

First, 10 ml of sample was placed in an equilibration vessel, a 50 ml round-bottom flask sealed with a stop cock connector. Six equilibration vessels (A) were attached to the vacuum system (Figure 4) at the sample preparation line (B). Immersing the vessels in liquid nitrogen for 10 minutes froze the water samples. Liquid nitrogen cooled the vessels to the boiling point of nitrogen, -195.8 °C (Lide, 1996). Noncondensible gases were removed by opening valve 1 to expose the samples to vacuum. After attaining a pressure below 10^{-3} mmHg, the vessels were closed off from the vacuum and immersed in hot water to melt the ice. The water was then re-frozen and the sample vessel evacuated again to remove any noncondensible gases released during melting.

The carbon dioxide used in the equilibration was stored in a tank (C) and was transferred into the equilibration vessels through the vacuum line. First, a sample of this carbon dioxide was expanded into volume D. Then, an aliquot was expanded into fixed-volume cold finger E by opening valve 2. The aliquot was isolated in the cold finger between valves 2 and 3. The carbon dioxide was frozen with liquid nitrogen and any remaining noncondensible gasses were pumped away. Then the cold finger E was warmed and the pressure of the carbon dioxide read with gage F. The moles of carbon dioxide were determined from this pressure and the calibrated volume of the cold finger. Valve 3 was then opened to pass the carbon dioxide through trap G. Any water was frozen out in a trap (G), which was kept at the sublimation temperature of carbon dioxide, -78.4 °C (Lide, 1996), by a slush of dry ice and methanol. Then the carbon dioxide was frozen into a reaction vessel cooled with liquid nitrogen (A). Next, stopcock 1 was closed and the equilibration vessel with the sample water and purified carbon dioxide was taken off the sample preparation line (B).

The equilibration vessels were mounted on a shaker in at water bath heated to 25 ± 0.05 °C and allowed to equilibrate. Equilibration of the sample water and carbon dioxide in this system required a minimum of six hours (Schuyler, 1987). After at least six hours, the sample vessels were removed from the bath and attached to the vacuum manifold at the carbon dioxide extraction line (H).

Equilibrated carbon dioxide must be isolated from the sample water for analysis. This procedure was carried out on the same high-vacuum line (Figure 4). The vessels were placed back on the line at H. Each sample was then isolated separately. First, an aliquot of carbon dioxide was removed from an equilibration vessel by quickly opening and closing stopcock 4. This aliquot was held in water trap J by keeping stopcock 5 closed. In trap J the gas was cooled with a dry ice and methanol slush, which freezes water but not carbon dioxide. Next, the carbon dioxide was frozen in liquid nitrogen cooled trap (K) by keeping stopcock 6 closed. After the carbon dioxide was completely frozen, stopcock 5 was closed and stopcock 6 and 7 were opened to pump away noncondensible gasses away. These stopcocks were then closed and trap J was cooled with a dry-ice slush which sublimed the carbon dioxide while retaining frozen water. Next, stopcock 6 was opened to freeze carbon dioxide gas into the liquid nitrogen cooled trap L. After all the carbon dioxide was frozen, stopcock 6 was closed and stopcock 7 was opened to vacuum to again remove noncondensible gasses. Stopcock 7 was then closed and L was cooled with a dry ice slush to sublime the carbon dioxide while retaining water. Any traces were frozen out as the carbon dioxide passed through dry-ice slush trap M on route to being was frozen with liquid nitrogen into a sample tube (O) on the gas collection line (N). Closing stopcock 8 isolated the dried and frozen carbon dioxide into a gas sample tube (O). The sample tube was then removed from the vacuum manifold and taken to the mass spectrometer for analysis.

$\delta^{18}O$ analysis was performed on the same day the equilibrated carbon dioxide was isolated and purified. The measurements were performed on a 60°, 6 inch, Nier-McKinney mass spectrometer described by Deines (1970). During a single isotope analysis of a gas, this machine compared each sample to a working reference twenty times. A computer attached to the mass spectrometer converted the data to standard δ-notation (equation 2). Once the $\delta^{18}O_{CO2}$

final was known, the $\delta^{18}O_{H2O}$ of the sample could be calculated according to equation (4). The precision of isotope analysis of carbon dioxide using this mass spectrometer has been reported as ± 0.05 ‰ (Deines, 1970).

A number of procedures were followed to track $\delta^{18}O$ data quality. A single large-volume of Florida Keys groundwater from KML was used as the reference water. A set of six analyses on this sample was used to determine the standard deviation of the method. An aliquot of the reference water was analyzed during every analytical period. A control chart was drawn, which plots the analysis of the reference water through time. Ten percent of the duplicate samples were also analyzed; duplicate results are tabulated in Appendix H.

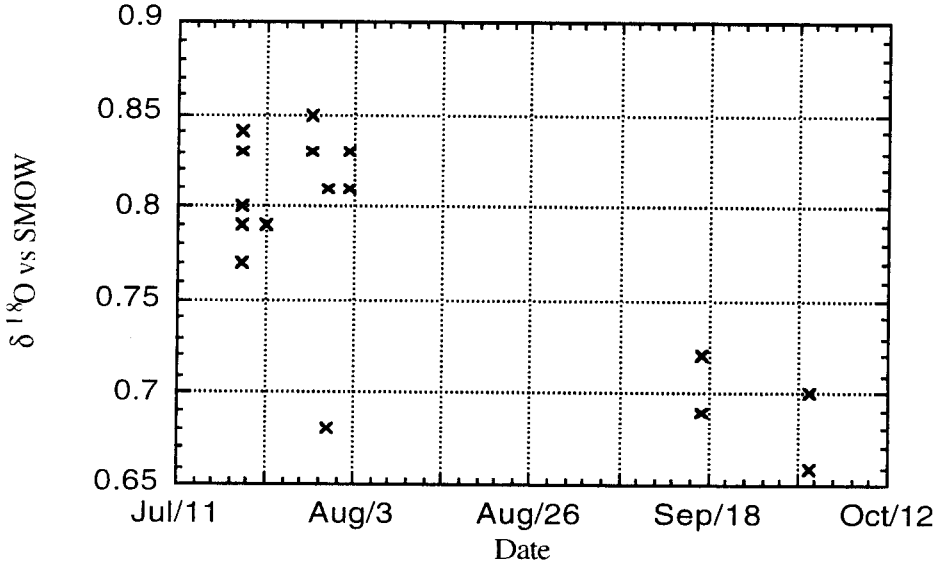

Figure 5. Measured $\delta^{18}O$ values, in ‰, of the reference water thorough time.

The control chart for the reference water analyzed each day showed a 0.15‰ decrease in the $\delta^{18}O$ for this water after a six week hiatus from lab work (Figure 5, data Appendix H). The cause of this shift was not identified. This shift in the reference water measurements caused an uncertainty in the $\delta^{18}O$ values of 0.15‰.

RESULTS

WELL POSITIONS

The results from the well survey are given in Appendix A. These data were used to determine the distance between wells and well elevation. The geographic positions of the wells in the figures presented in this report was determined using the survey results.

DRILL CORE CHARACTERIZATION

Drill logs showed that the study area consists of six meters of unconsolidated carbonate mud overlying KLL grainstone and packstone facies (Figure 6-7). The upper approximately two meters is fill used to create the island. The thickness of this fill varies, and is nearly indiscernible from the natural deposits at depth, but it can be distinguished by its lack of fine

laminations and the presence of a layer of shell debris at its base. The upper surface of the KLL was found below the mud at a depth of 5.79 to 6.40 m. The only other feature common to all the cores is the Q3-Q4 unconformity of Perkins (1977). Its higher density and thin bands of red-brown caliche are characteristic of an exposure surface. The Q3-Q4 in these cores occurs about nine meters deeper than the upper surface of the KLL; this is a similar depth to what has been observed in other site in the Keys. This unit varies in thickness from only a couple to tens of centimeters in the cores.

The KLL at KCB is primarily composed of white chalky grainstone with abundant shell fragments. At this location the KLL is not a fossil reef, unlike the main islands of the Keys. There are coral fragments in core C, but these are small and likely pieces of coral rubble. Of the six cores that are drilled to a depth of at least sixty feet, five show that mud content of the core increases from a grainstone to a packstone around the Q3-Q4 unconformity. (Figures 6-7).

The calculated porosity of the cores is extremely high, from 0.52 to 0.98, while typical core recovery is low (Figure 8, Appendix B). Low core recovery can result from large voids in the rock itself or the loss of loose material (e.g., sand) with the drilling fluid. Both of these factors contribute to the low core recovery at KCB. Karstification has been observed in the KLL of the Keys and voids are the most likely cause of the quick drops of the drill pipe that occurred while drilling. Additionally, sand-size carbonate grains were observed coming out of the borehole with the drilling fluid in some intervals, indicating that material was lost. This was noted in the 12.19-13.72 m (40-45 ft) deep section of cores B, D, E, and G (Figures 6-7). The rock at this depth is either especially friable or poorly consolidated.
Because core material was lost during drilling, little confidence can be put in the porosity estimates based on weight. The three sections with at least 90% core recovery estimate that the porosity of the KLL underlying KCB ranges from 0.52 to 0.60 (Figure 8). This is consistent with conclusion of Shinn et al. (1994) that the porosity of the KLL is at least 0.45. These values are similar to the typical porosity range of 0.4 to 0.7 for coralline KLL in drill cores from the KML site (Monagan, 1996). In the KLL cores, some sections were interpreted as zones of macroporosity, where either no core was recovered or the porosity was found to greater than 0.7 (Monaghan, 1996). At KCB, rock porosity is in the range of 0.5 to 0.6. However, conduits one to two cm in diameter were observed in some of the cores, which can act as paths for rapid fluid flow.

Qualitative x-ray diffraction results show that the cores are composed primarily of calcite with some aragonite (Appendix B); the powder patterns were sharp with no broad peaks characteristic of amorphous or poorly crystalline phases (Figure 9). Aragonite was found in all samples, except one that had no aragonite, core C at 10.4 m depth. Using the I/I_{cor} values from JCPDS (1992), the ratio of the most intense aragonite peak to most intense calcite peak for a fifty-fifty mixture of calcite and aragonite was calculated as 0.5. This ratio is much lower in the samples, equal or less than 0.17, which shows that calcite is the dominant mineral. This interpretation is only qualitative, since the scans were not performed for quantitative analysis.

The average CaO content of the core samples is 57 $\pm$ 1 wt %, while MgO concentrations range from 0.39 to 0.79 wt %. All other elements analyzed for are minor, less than one weight percent (results tabulated in Appendix B). Thus, the bulk analyses of core material support a mineralogy of dominantly low-magnesium calcite, with Mg concentrations in $(Ca,Mg)CO_3$ ranging from 0.61 to 1.2 mol %.

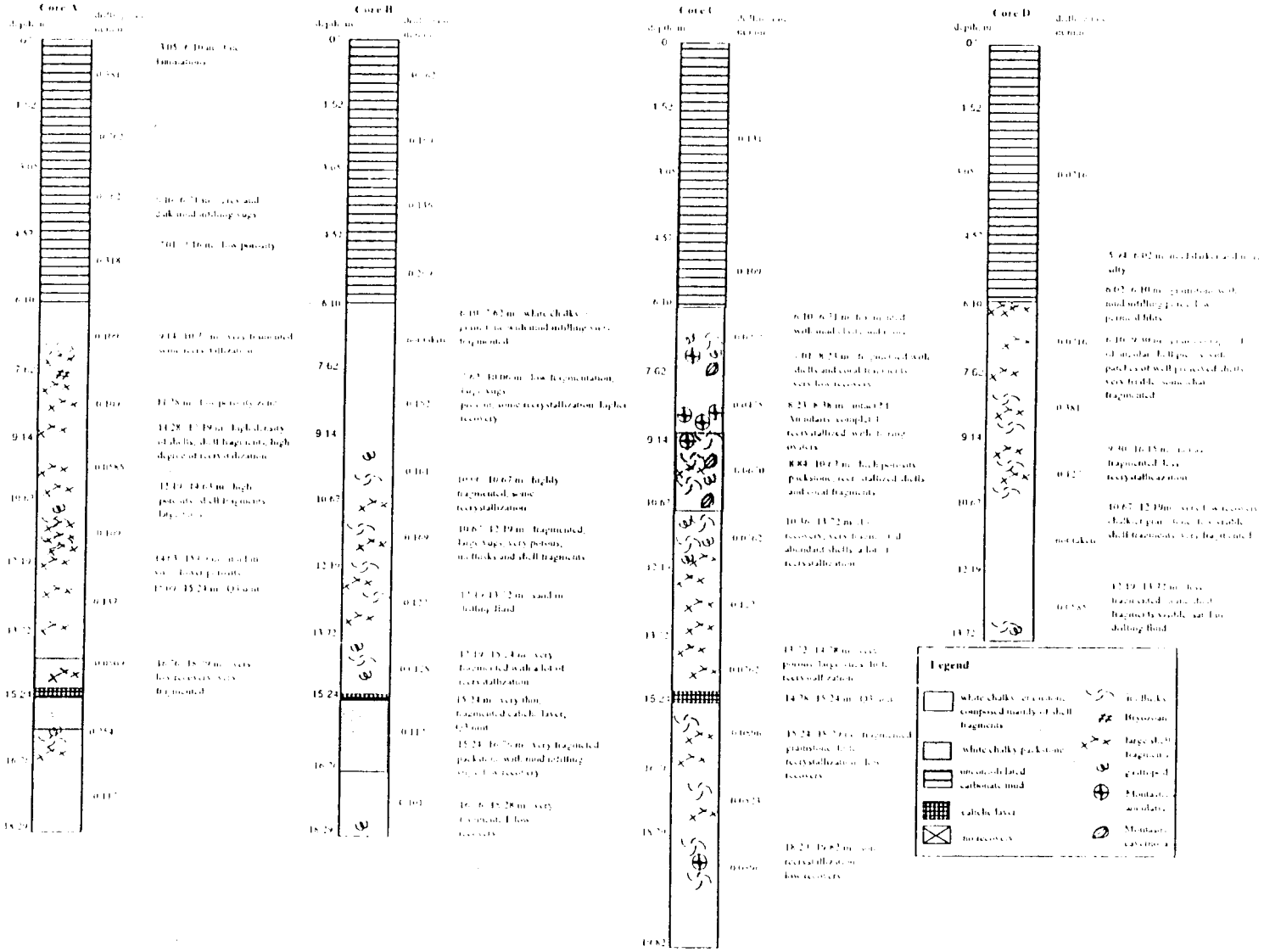

Figure 6. Cores A-D are schematically represented in this figure. Additional notes on core lithology and drilling are presented to the right of each column

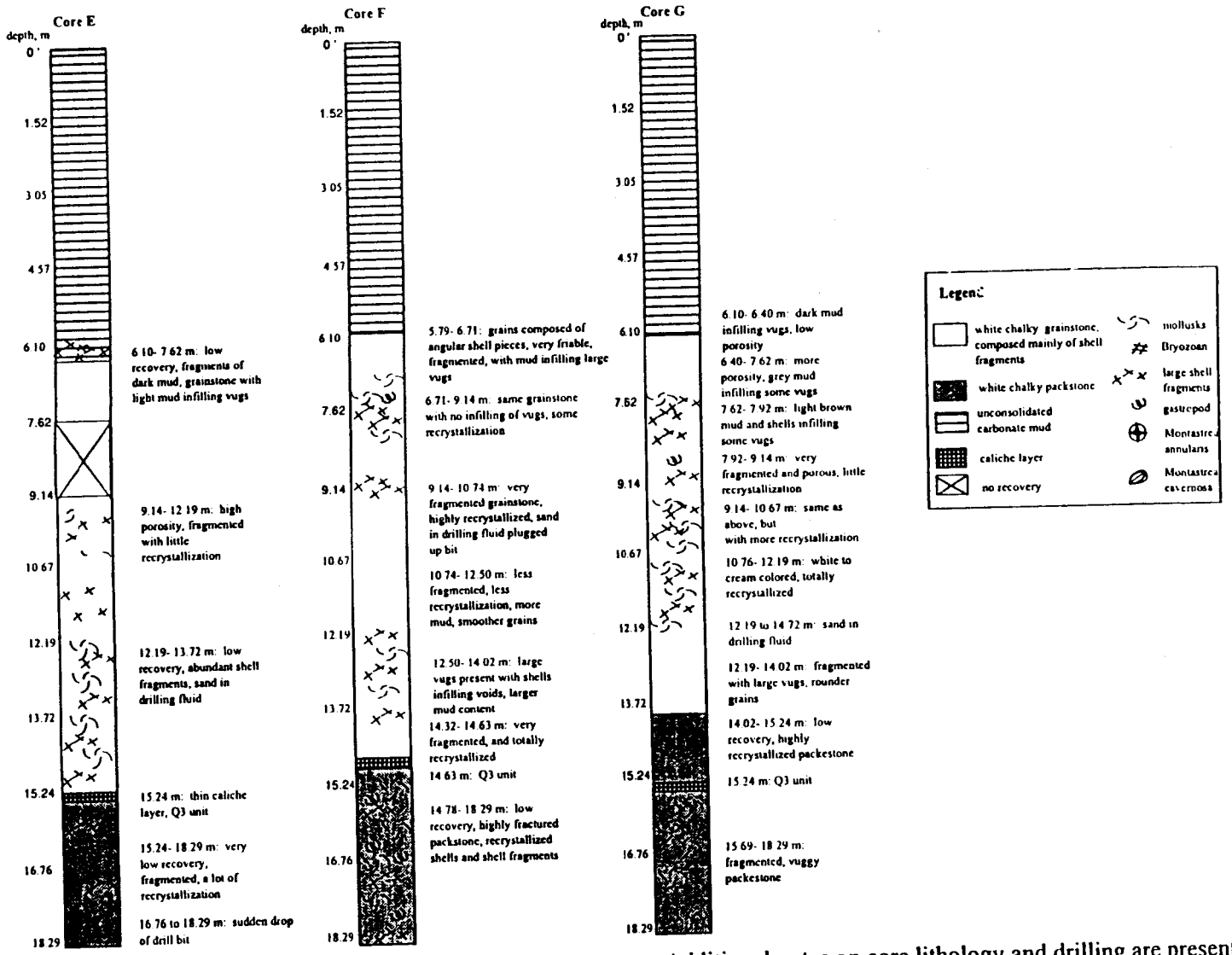

Figure 7. Cores E-G are schematically represented in this figure. Additional notes on core lithology and drilling are presented to the right of each column.

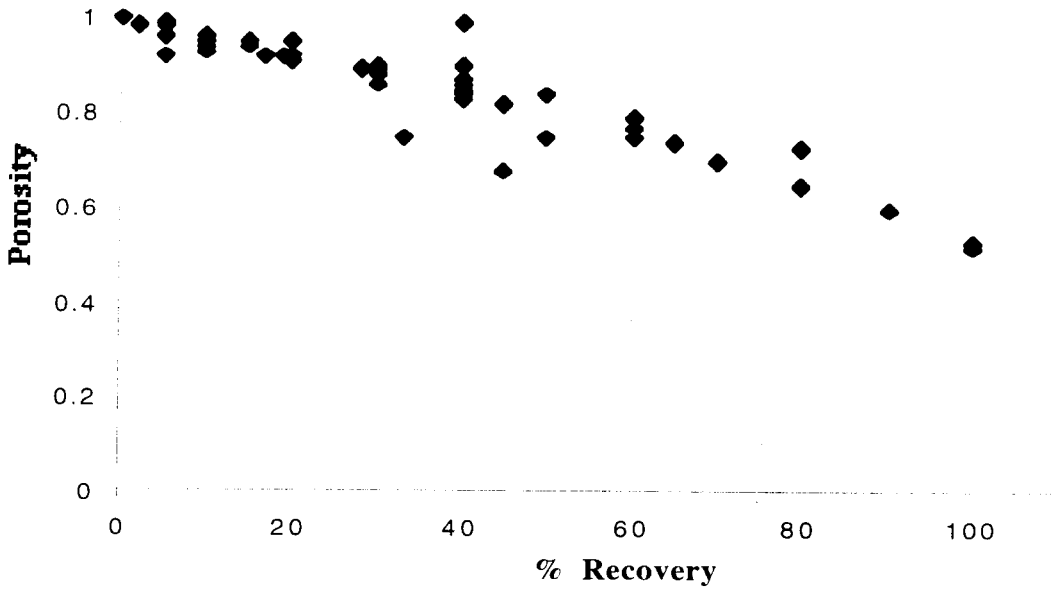

Figure 8. Core porosity versus recovery for each 1.52 (5 ft) section of core.

All of the core samples analyzed, regardless of how close they were to the wastewater injection wells, have similar phosphorous concentrations ranging from 0.02 to 0.09 wt %. Phosphorous and fluorine concentrations of the rock samples do not correlate; a linear regression yields a correlation coefficient of 0.385. The variations in fluoride are instead coupled with strontium, with a correlation coefficient of 0.871. These elements are both calcite impurities that are diagenetically mobile. Rude and Aller (1991) found increasing diagenesis led to lower concentrations of these elements in aragonite and calcite. Phosphorous content of the KLL also did not correlate with distance from the injection wells. The samples from cores near the wastewater injection are not measurably enriched in phosphorous in comparison to those from further away. The observed variations in the phosphorous content of the cores cannot be attributed to wastewater-rock interaction.

WELL WATER LEVEL

Water level monitoring through a tidal cycle showed that the tide propagates in the groundwater through the limestone (Appendix C). Figure 10 shows the tidal cycle measured in a nearby canal in KCB, along with the water levels in studied wells. The well water levels are all normalized to the elevation of the surveying benchmark, set at 0 m, but the canal tide has not been normalized to that benchmark because it was not surveyed. The canal and wells water levels are plotted in this graph using the same distance between tick marks in the y-axis and the same x-axis, which allows a comparison between tidal peak and amplitude in the canal and the wells. The tide did propagate through the KLL at KCB, but the peak of the cycle was broadened relative to that at the canal and lags the canal tide by about one hour. Additionally, the amplitude of the tidal cycle in the wells is about 60% of that measured in the canal.

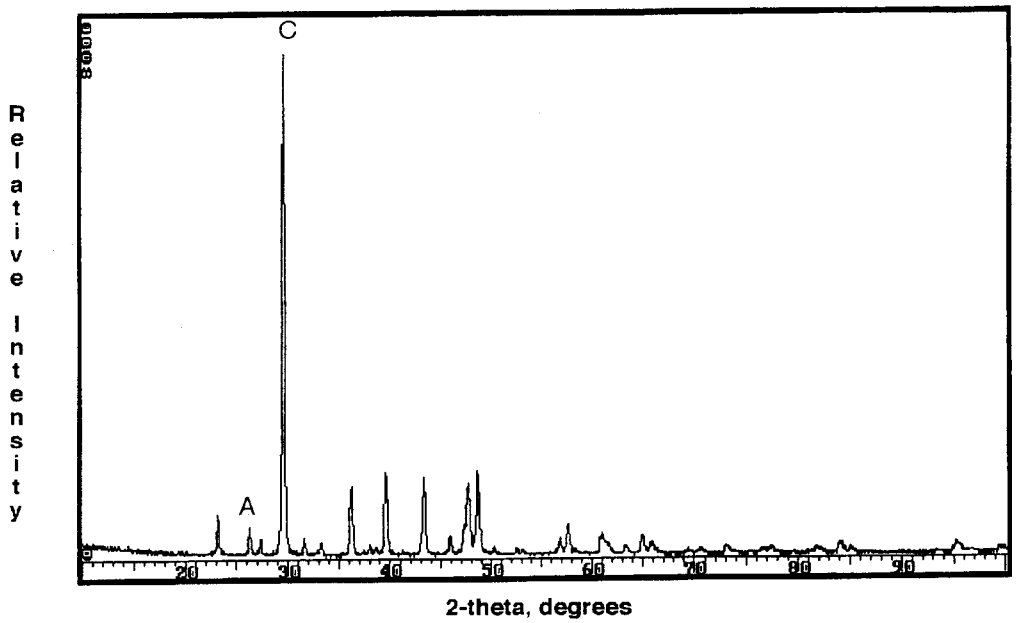

Figure 9. This x-ray powder pattern is from core F, sampled at a depth of 24 m. The A and C mark the most intense peaks of aragonite and calcite, respectively. All peaks larger than the peak marked A are other calcite peaks. This is a typical pattern for the samples analyzed.

Figure 10 is potentially misleading in that it appears that there is a hydraulic head gradient between the intermediate wells (closed symbols, depths of 8-9 m) and the deeper wells (open symbols, depths 14-18 m) of approximately 20 cm. However, these well heights are influenced by the salinity differences between wells. To correct the well heights for salinity, the freshwater head correction of Custodio (1987) was applied. This correction is only appropriate for wells which sample water at the same depth, so in this exercise all well depths were fixed as the depth of the shallowest well, F-8. This depth was used as the elevation head for all wells. The freshwater head correction is calculated by (Custodio, 1987):

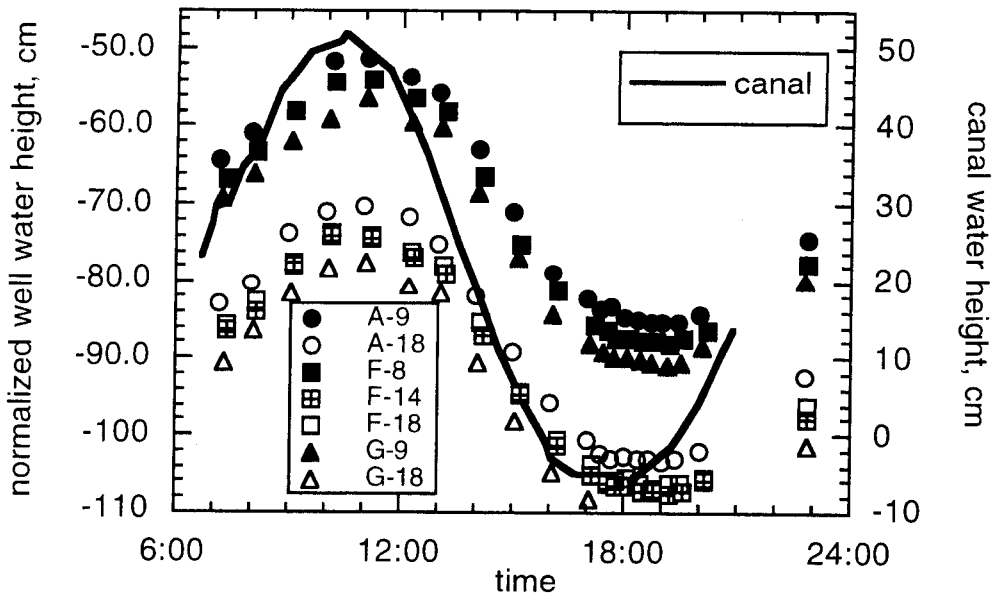

Figure 10. Normalized well water heights through a tidal cycle are plotted here with the tidal cycle in a nearby canal. While the scale is relatively the same, the absolute canal elevations are arbitrarily placed on the diagram.

$$h_f = z + (h_0 - z)\rho_0/\rho_f \qquad (5)$$

where: h_f = corrected freshwater hydraulic head, m
z = elevation head (the bottom of well F-8), m
h_0 = measured hydraulic head, m
ρ_0 = density of water in well, kg/m^3
ρ_f = density of fresh water = 997.0480 kg/m^3

The density of the groundwater in the wells was approximated by using the salinity of the water sampled from the well during June 1998 sampling campaign, which was four days before the tidal study for wells F and G, and the same day for well A. The salinity was converted to density using the International Equation of State of Seawater (Unesco, 1981) at 25°C:

$$\rho_0 = \rho_f + 0.7592383*S - 0.004202*S^{1.5} + (4.8314*10^{-4})S \qquad (6)$$

S is the salinity in psu. The resulting freshwater heads are plotted in Figure 11. With this correction, the large difference between the intermediate wells (solid symbols) and deep wells (open symbols) was substantially reduced, to about 6 cm for wells in the same location.

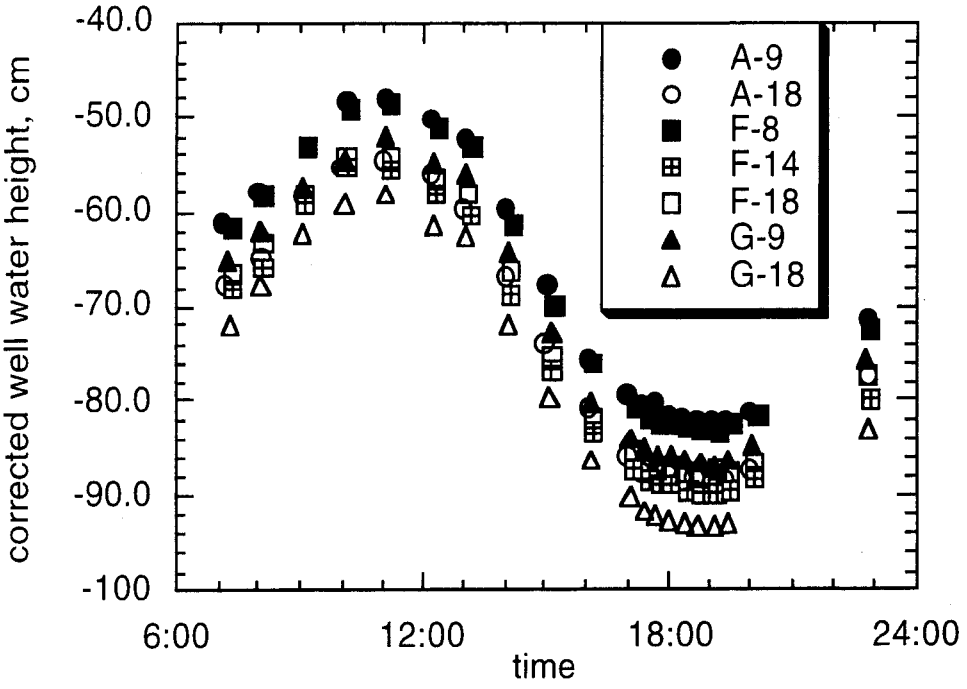

Figure 11. Water well height expressed as freshwater head. The elevation head for all wells are taken at the elevation of the bottom of the shallowest well, F-8.

Hydraulic gradients cannot be deduced from this corrected data because the salinity is known to vary laterally, and the head correction does not account for pressure differences due to variations in density laterally. The data here are insufficient to warrant the modeling needed to determine groundwater flow direction. Instead, the direction of wastewater flow was tracked using an artificial tracer test conducted by Chanton and Dillon (1998, unpub). The tidal data do show that the groundwater within the limestone is subjected to tidal effects. Additionally, the large difference between water levels in deep and intermediate wells can be primarily attributed to salinity differences. Much of the remaining variation between heads in the corrected data (Figure 11) is probably largely due to the simplifying assumptions of the correction or measurement error.

WATER CHEMISTRY

The data for the March and June 1998 samplings are tabulated in Appendix D and E, respectively. The March samples' pH readings for many of the wells were anomalously high, greater than 9, as a result of unset cement in the well installation (Appendix D). The high-pH wells were treated with acid in April of 1998. This treatment worked for the intermediate and deep wells, whose pH values rose to about 7 to 8 after treatment (June data Appendix E). Shallow wells within the mud remained acidic after treatment, as seen in the June sampling data for A-5 and B-5 during sampling rounds 2 to 6 (Appendix E). Overall, it appears that the acid treatment cleared the unset cement in well sampling the high porosity KLL.
Alkalinity results are given for the March 1998 sampling; however, the values measured for most of the wells are unreasonably large (Appendix D). This may be due to unset cement in some of the wells, which also caused high pH in some of the wells. However, there is not a one-to-one

correlation between high pH and alkalinity in the wells. The accidental use of impure distilled water during the analysis is another probable cause for the high alkalinities.

The groundwater within the mud layer has much higher ammonia and sulfide concentrations than groundwater from within the KLL, which suggests more reducing conditions. During the March sampling, sulfide concentrations greater than 5 mg/l were found only in wells within the mud layer, where the highest concentration was 58 mg/l (Appendix D). Ammonia also had high concentrations in the mud layer, from 8 to 18 ppm-N. Ammonia concentrations were low in the wastewater, which undergoes extended aeration during treatment.

Salinity, nitrate, and phosphate data for both sampling campaigns were contoured along the two well transects (Figures 12-17). Some assumptions were made in the contouring of the north-south transect. This transect crosses the line of injection wells, where it was assumed that a vertical plume of wastewater extended upwards from injection at 18 m to the base of the mud layer. The contours were then drawn approximately symmetrically around the injection well line. Better control on the plume geometry is needed in the north-south direction. Recently installed monitoring wells (Griggs and Kump, unpub. data) should provide added resolution. Figures 12-14, on which the March 1998 data were contoured along cross-sectional views of the two transects, show that the wastewater plume moved upward and eastward after injection at 18 to 27 m depth. This is best seen in the salinity distribution (Figure 12). Low-salinity wastewater was apparently confined beneath the mud-KLL contact, represented by the thick gray line, at all locations except C. Nitrate and phosphate distributions reflect the upward, and to a lesser extent eastward, movement of wastewater after injection (Figures 13-14). Phosphate appears to be less mobile than nitrate. Little north-south directed movement from the injection near well A was seen in nitrate. Low, but detectable phosphate concentrations in well G indicate that wastewater may have flowed to the south. Unfortunately, the nutrient results, especially phosphate, may be influenced by the highly alkaline conditions that occurred in some wells due to unset cement grout. Thus, patterns of nutrient flow were verified by comparison with the June sampling results.

Data from the comprehensive sampling round of June 1998 were contoured only for the limestone layer because wells from within the mud layer were not sampled (Figures 15-17). Low salinity water was again found in all of the intermediate wells, but salinities are higher in the deep wells close to injection (Figure 15) than they were in March 1998, indicating that the wastewater plume had contracted, perhaps in response to lower summer wastewater flow. During the March sampling campaign, there was a high rate of wastewater injection of 1300 to 2300 m^3/day. The extremely high rate of 2300 m^3/day occurred on the day of a rain event, March 9, 1998. In June 1998, the population of the resort-city of KCB was much lower and South Florida was experiencing a drought. These factors combined to account for a much lower rate of wastewater injection of 469 to 662 m^3/day. The lower flow of wastewater exerted less pressure at depth, and the ambient saline groundwater pushed closer to the injection wells. The difference in injection rate thus explains the higher salinities in the deep wells during the June sampling. Salinity distributions show that the wastewater flowed in a primarily upward and eastward in June (Figure 15), as in March, and this flow was reflected in the nitrate data (Figure 16). The phosphate distribution reflects this movement to a lesser extent (Figure 17). The nitrate and phosphate distributions along the north-south transect appear to show some minor movement to the northern well F.

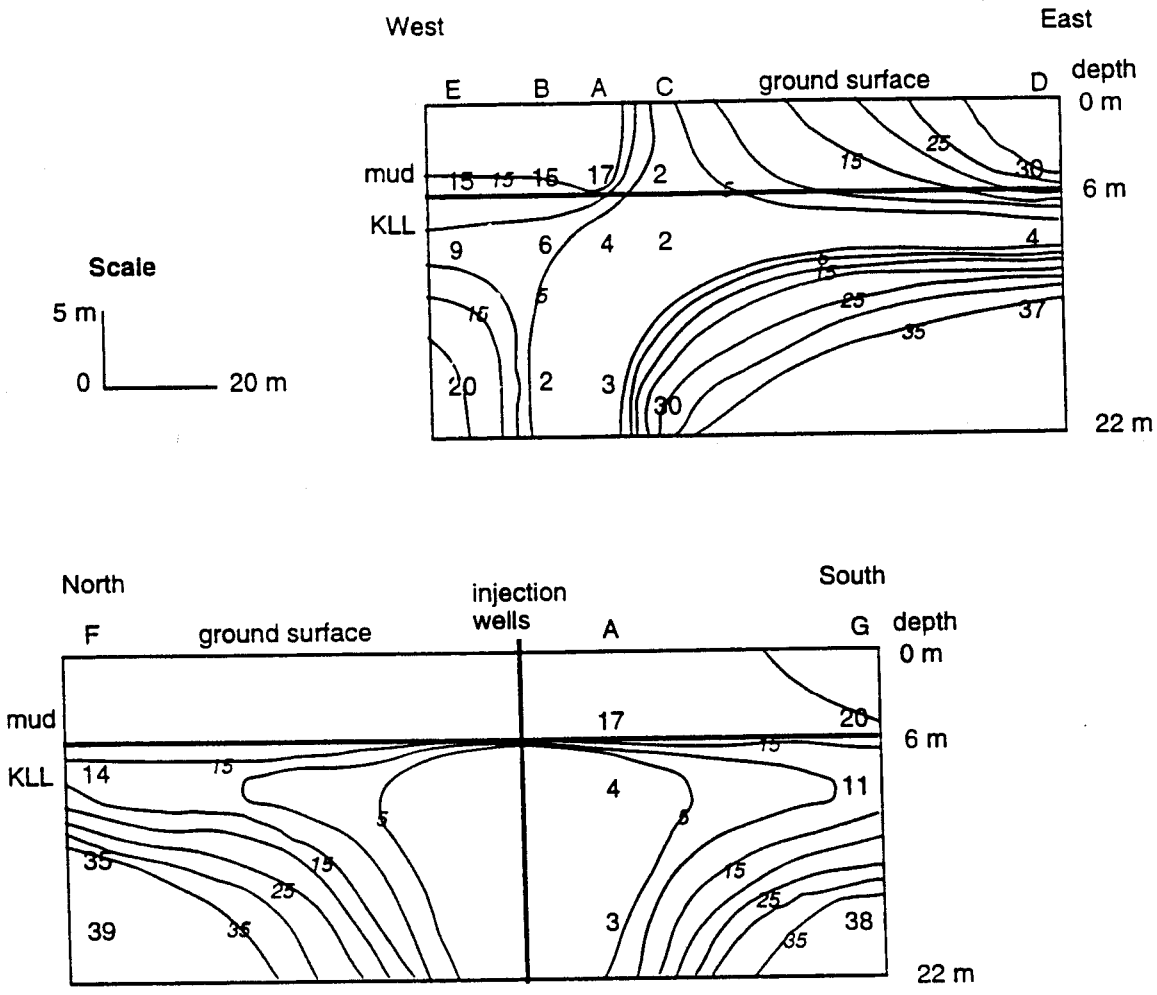

Figure 12. March salinity measurements are contoured along each transect with a contour interval of 5 psu.

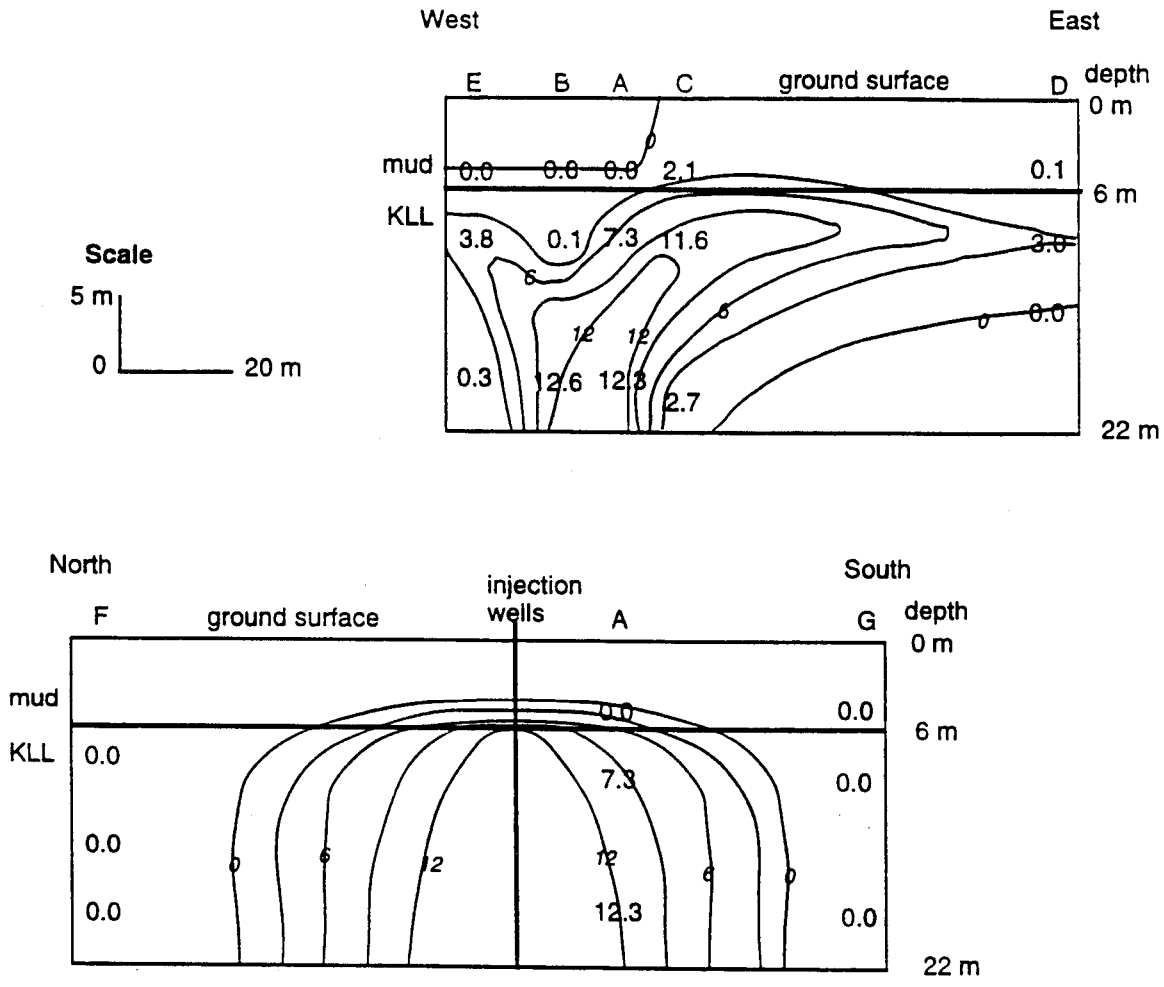

Figure 13. March nitrate measurements are contoured along each transect with a contour interval of 3 ppm-N.

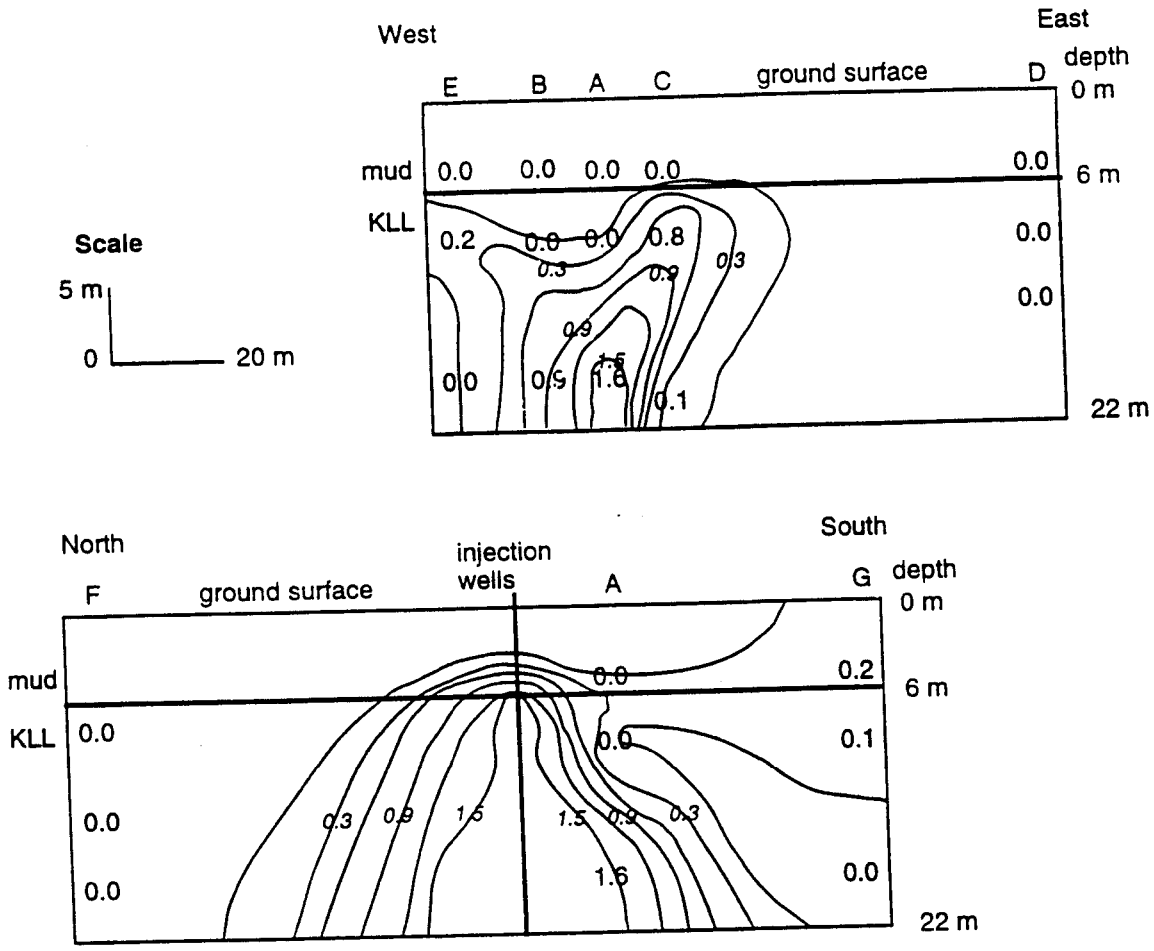

Figure 14. March phosphate measurements are contoured along each transect with a contour interval of 0.3 ppm-P.

Elemental analyses of the June 1998 groundwater samples (Appendix E) show that those elements known to be conservative in seawater were positively correlated with salinity. These include Mg ($R^2 = 0.91$), Na ($R^2 = 0.87$), K ($R^2 = 0.67$), Sr ($R^2 = 0.48$), and Ca ($R^2 = 0.31$). However, according to the linear correlation of concentration against salinity, at salinities around that of seawater all of these appeared in concentrations lower than seawater (Table 2). There was quite a bit of scatter in the data and some high-salinity samples did have Ca and Sr concentrations close to that of seawater. The concentrations of these elements were approximately sixty percent of what seawater ratios would predict, except for potassium, which was found in very low concentrations. Sparingly soluble elements such as Al, Ba, Mn, and Si did not necessarily correlate with salinity. While Mn correlated with salinity, Al and Ba concentrations varied little between low and high-salinity samples. One element, Si, showed a weak negative correlation with salinity ($R^2 = 0.272$). Fe and Ti are below their detection limits of 0.02 ppm in all of the waters analyzed. Overall, the concentrations of the major elements seem to be underestimated in these analyses.

Table 2. The predicted concentration at 35 psu was determined by a linear correlation of groundwater sample concentration with salinity. As the last column shows, the predicted concentration at 35 psu is only a fraction of seawater concentration at 35 psu for all of the major cations.

Element	Concentration in SW of 35 psu, ppm*	Concentration Predicted 35 psu, ppm by	% of Seawater Concentration Predicted
Ca	412	225	55
K	399	16	4
Mg	1283	780	61
Na	10782	6750	63
Sr	7.9	4.8	61

* Millero and Sohn, 1992

OXYGEN ISOTOPE RESULTS

A large difference in the $\delta^{18}O$ of wastewater and deep groundwaters far from injection was found in the June 1998 samples (Table 3). The wastewater was depleted in ^{18}O compared to SMOW, with an average $\delta^{18}O$ of -2.05‰ vs. SMOW for samples taken June 1-6 (Appendix E). The deep groundwaters far from the wastewater injection were comparatively enriched in ^{18}O, with $\delta^{18}O$ values from 1.23 to 1.39‰ vs. SMOW. Samples from the shallow wells within the mud layer were not taken in the June sampling campaign. To determine the oxygen isotopic composition of waters from within the mud layer, selected samples from the March sampling campaign were analyzed (Table 4).

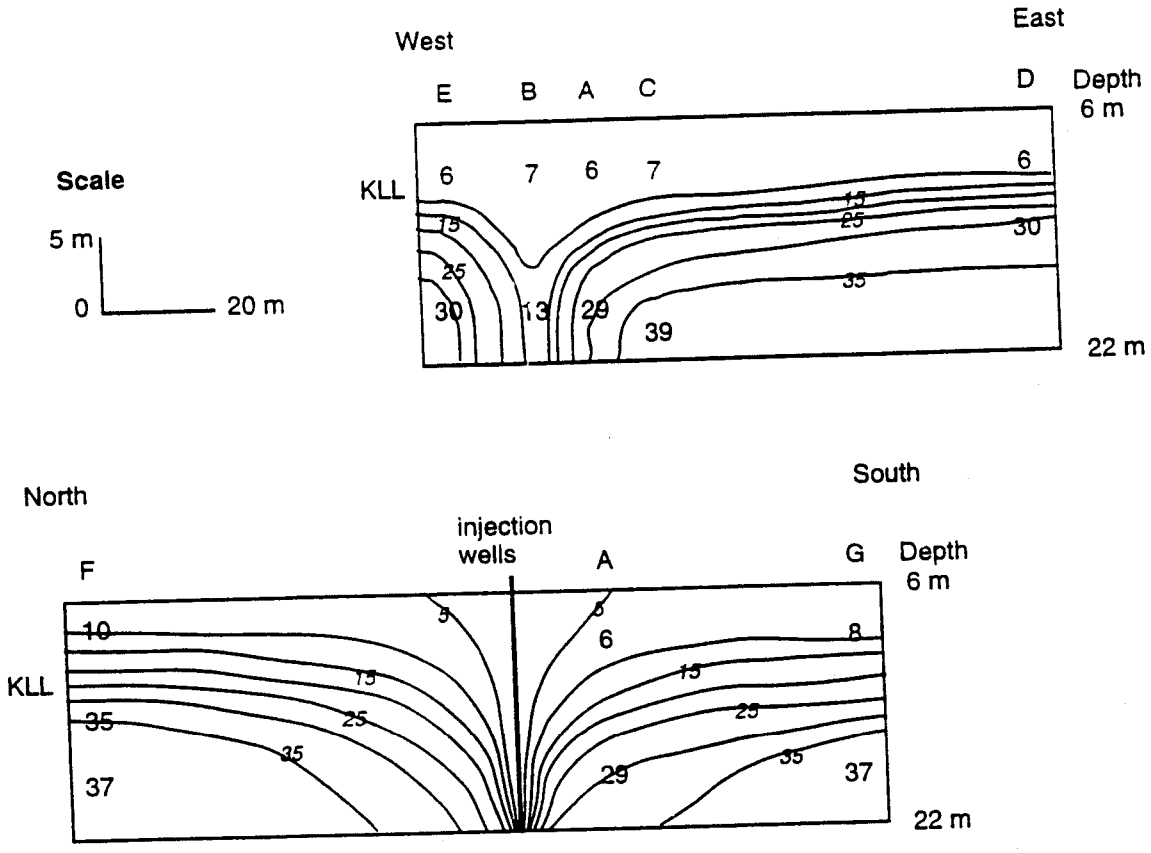

Figure 15. June salinity measurements are contoured along each transect with a contour interval of 5 psu

Table 3. Oxygen isotope measurements of the June 1998 well and wastewater samples, and two rain samples.

Well-Depth (m)	$\delta^{18}O$ vs. SMOW (‰)*
A-9	-1.91
A-18	0.4
B-9	-1.9
B-18	-1.25
C-9	-2.29
C-19	1.2
D-9	-2.15
D-13	1.33
E-9.	-1.93
E-18	0.59
F-8	-1.98
F-14	1.25
F-18	1.23
G-9	-1.55
G-18	1.39
MW	-0.16

MW = monitoring well *uncertainty of ±0.15 ‰

Sample	$\delta^{18}O$ vs. SMOW (‰)*
Rain	
rain 1/26/98	-5.53
rain 3/9/98	-2.80
Wastewater	
WW	-2.14
W1	-1.86
W2	-2.05
W3	-1.94
W4	-2.2
W5	-2.14
Wastewater Average	-2.06 ± 0.13

The two deeper groundwater samples at well B from March were also analyzed to look for $\delta^{18}O$ variations between the two sampling campaigns (Table 4). These wells are close to the wastewater injection and show a lower $\delta^{18}O$ during this campaign, reflecting the lower $\delta^{18}O$ of the wastewater in March.

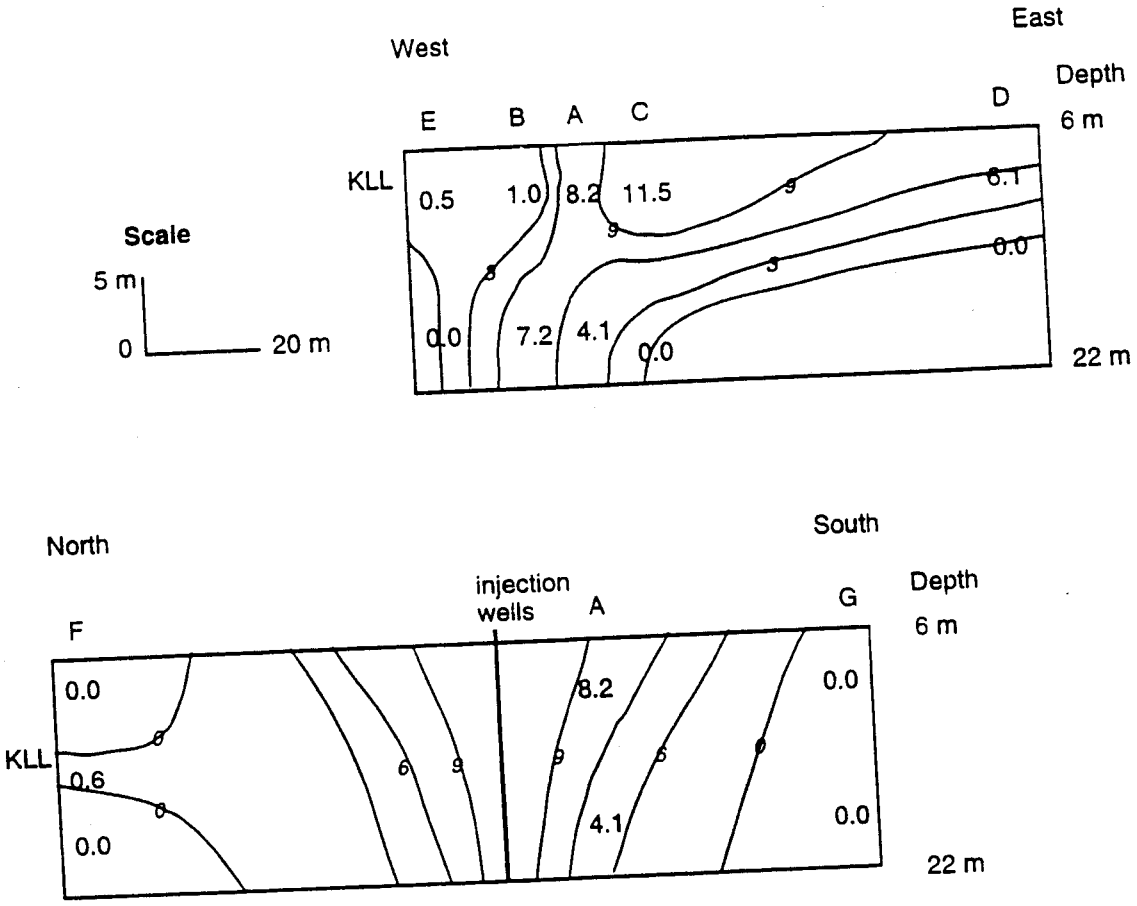

Figure 16. June nitrate measurements are contoured along each transect with a contour interval of 3 ppm-N.

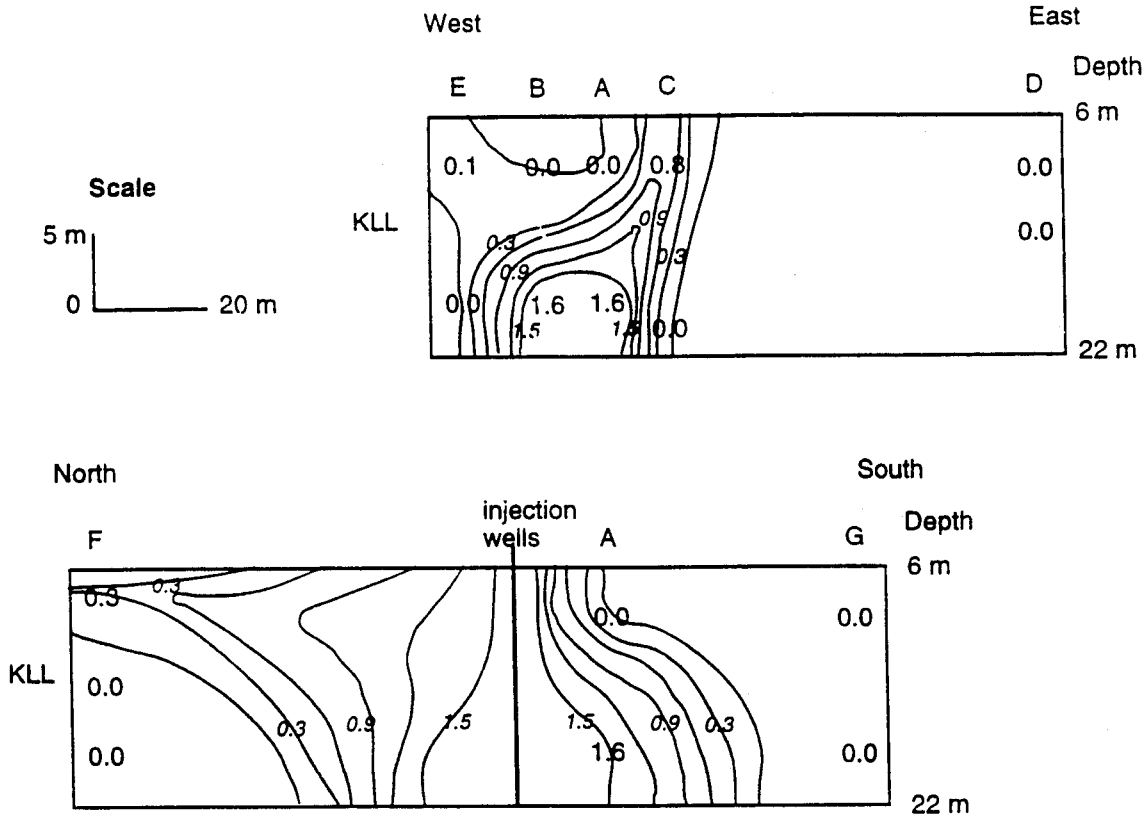

Figure 17. June phosphate measurements are contoured along each transect with a contour interval of 0.3 ppm-P.

Table 4. Oxygen isotope and salinity results of selected March 1998 samples.

Sample	$\delta^{18}O$ vs. SMOW (‰)
A-5	-1.81
B-5	-1.48
B-9.	-1.98
B-18	-2.38
C-5	-2.62
WW	-2.42

uncertainty of ±0.15 ‰

DISCUSSION

NATURAL WASTEWATER TRACERS

Oxygen isotopic and salinity measurements were used as natural tracers of the wastewater. A strong direct relationship exists between the samples' $\delta^{18}O$ and salinities (Figure 18), especially for those wells from within the KLL. In using $\delta^{18}O$ and salinity as natural tracers within the KLL, its was assumed that wastewater was the only source of ^{18}O-depleted, low-salinity water to this aquifer. The March results show that the salinities of wells within the mud layer are generally higher than deeper wells at the same location. The inverse salinity gradient makes it highly unlikely that rainwater is recharging the KLL from above and the source for the low-salinity water underneath the mud-limestone contact. Additionally, the low topography of the region would not support discharge of freshwater below this mud layer. These arguments support the simplifying assumption that the groundwater within the limestone at the site is composed of mixtures of ambient groundwater and wastewater only.

Oxygen isotopic compositions and salinities of June samples were used to generate two linear mixing models of wastewater and ambient groundwater (Table 5). The average of the six wastewaters was used as the wastewater end-member for these models, with a $\delta^{18}O$ of -2.06‰ and a salinity of 5.0 psu. The average of the deep wells at G and F was used as the groundwater end-member for these models because of their large distance from the wastewater injection wells. Averaging yielded a groundwater end-member with a $\delta^{18}O$ of 1.31‰ and a salinity of 36.9 psu. The uncertainty in the $\delta^{18}O$ measurements added an uncertainty of ±4% wastewater to the model based on oxygen isotopic measurements.

The oxygen isotope mixing model agreed well with the mixing model that is based on salinity (Table 5). The average absolute raw difference between the models is 4% wastewater, which is within the uncertainty of the oxygen-isotope model. Some calculated percentages were negative or greater than 100%. These unrealistic results stem from the fact that the models are calculated using a wastewater of constant salinity and $\delta^{18}O$ across the study area. In reality, the wastewater's salinity and $\delta^{18}O$ change with time and different regions of the wastewater plume represent different wastewaters.

Nitrate and phosphate-based mixing models generally yield dramatically lower wastewater percentages (Table 5). These models were calculated in a manner similar to the salinity and oxygen-isotope-based models also using June sampling campaign results. Again, the

average of nutrient concentrations from deep wells F and G was used as the groundwater end-member, and the wastewater nutrient concentrations used as the wastewater end-member. The fact that these nutrient based models yield such lower wastewater percentages provides evidence for nonconservative transport of these species.

The oxygen isotope results for six samples collected during the March 1998 sampling campaign were tested to see if linear mixing models could approximate samples from within the mud layer. In these calculations, the March 1998 wastewater was used as the wastewater end-member. Assuming that ambient groundwaters are seasonally invariant, the groundwater end-member in the June models was used. Sample salinities were used to determine the percentage of wastewater in a wastewater-groundwater mix of that salinity. The $\delta^{18}O$ of this theoretical groundwater-wastewater mixture was then calculated and compared to the actual $\delta^{18}O$ of the sample (Table 6). The measured $\delta^{18}O$ of the two March samples from within the KLL were within 0.02‰ of the calculated $\delta^{18}O$. The measured $\delta^{18}O$ of the three wells within the mud layer differed from the calculated results by 0.25 to 1.01‰. This suggests that a simple wastewater-groundwater mixture did not accurately model waters within the mud layer; meteoric water within the mud may be causing the diversion from the model. A more detailed analysis of the uncertainties of this model and the measurements is needed to confirm the finding based on these three samples that the water within the mud cannot be represented by a mixture of only ambient groundwater from 18 m and wastewater.

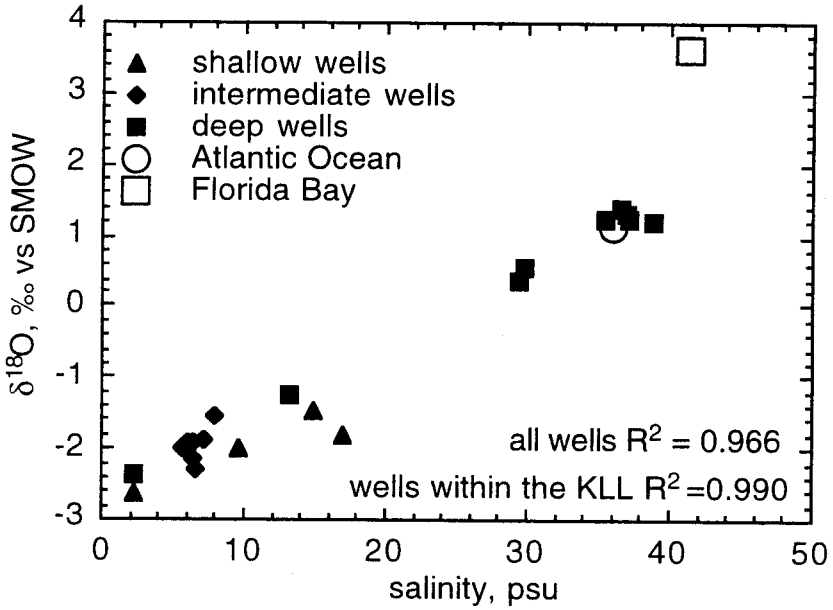

Figure 18. The oxygen isotope results for the well samples (solid samples) are plotted as against salinity along with Bohlke et al.'s (1997) data for Atlantic Ocean water offshore of the Florida Keys and Swart et al.'s data for Florida Bay water (1989).

Table 5. Results of linear mixing models of June 1998 groundwater and wastewater based on $\delta^{18}O$, salinity, nitrate, and phosphate measurements.

Sample	% WW based on $\delta^{18}O$	% WW based on salinity	% WW based on nitrate	% WW based on phosphate
A-9	96	97	48	0
A-18	27	23	24	48
B-9	95	93	6	0
B-18	76	74	42	46
C-9	107	95	68	23
C-20	3	-6	0	0
D-9	103	95	36	0
D-14	-1	0	0	0
E-9	96	96	3	2
E-18	21	22	0	0
F-8	98	85	0	8
F-14	2	5	3	0
F-18	2	-1	0	0
G-9	85	91	0	1
G-18	-2	1	0	0

% WW is percent wastewater uncertainty of ±4% wastewater based on 0.15‰ uncertainty in $\delta^{18}O$

Table 6. Oxygen isotope and salinity results of selected March 1998 samples along with model values of % wastewater and $\delta^{18}O$. Samples from within the mud layer are in bold.

Sample	$\delta^{18}O$ vs. SMOW (‰)	Salinity (psu)	% WW predicted by salinity	$\delta^{18}O$ predicted by % WW	% error of model
A-5	-1.81	17	56	-0.80	56
B-5	-1.48	15	62	-1.01	32
B-9	-1.98	5.7	89	-2.00	0.64
B-18	-2.38	2.3	98	-2.36	0.99
C-5	-2.62	2.2	99	-2.37	9.65
WW	-2.42	1.7			

uncertainty of ±0.15‰ measured value used as true value

The salinity and oxygen isotope models can be used to interpret the flowpath of wastewater after injection. Figure 19 shows the results of the $\delta^{18}O$-based mixing model on cross-sections cut along the two transects, with values greater than 100% set to 100% and negative values set to 0%. The pattern seen is quite similar to the salinity distribution during the

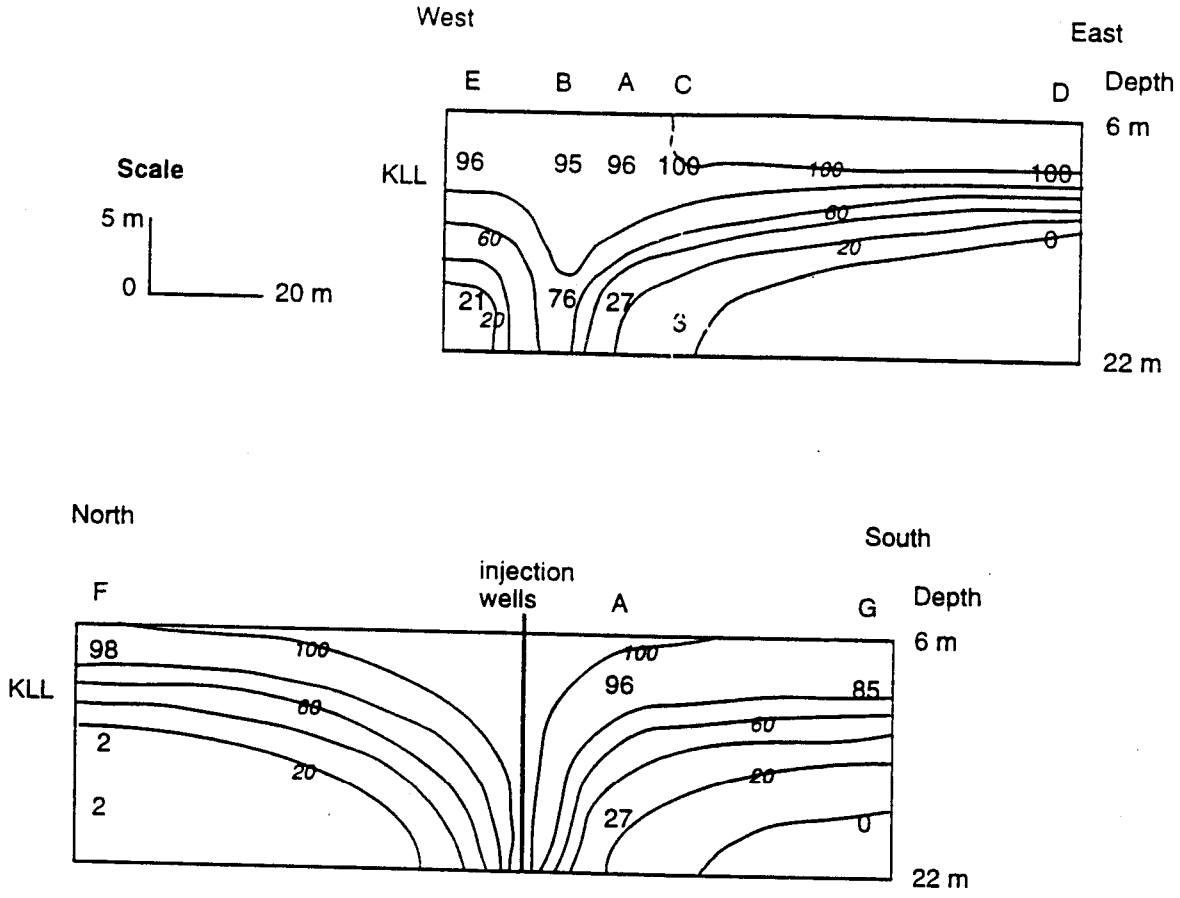

Figure 19. In this figure, the percentage of each sample calculated as wastewater-derived is contoured along the two well transects. This presents the results of the oxygen-isotope based mixing model. The data are contoured in intervals of 20% wastewater.

June sampling campaign (Figure 15). The results show that after injection at 18 to 27 meters into the saline groundwater, the wastewater immediately buoyantly advects upwards. The base of the mud layer confines this upward flow, and wastewater then flows outwards forming a large broad plume under this contact. After five years of continuous injection, a broad wastewater plume has developed across the entire study area under the mud-KLL contact.

In this isotope tracer study, the groundwater-wastewater mixing model was only applicable in the KLL, which is not recharged by rainwater. In rainwater-recharged aquifers of the Florida Keys, using $\delta^{18}O$ to trace wastewater would be more complicated. Finding a diagnostic isotopic signature for the Florida Keys wastewater that would distinguish it from rainwater would be difficult. Swart et al. (1989) measured the oxygen isotopic composition of 110 samples of South Florida rainwater over a three-year period. They found a large range in $\delta^{18}O$, from -8‰ to 0.0‰ (the two rain samples of this study fell within this range), with a weighted average of -2.67‰ (Swart et al., 1989). The $\delta^{18}O$ of KCB wastewater was found to be approximately -2.0‰, which is close to this rainwater average. A more comprehensive and longer duration of sampling than the one presented here would be needed to trace wastewater in a formation subjected to meteoric recharge. Three waters would be mixing in those situations: wastewater, rain, and saline groundwater. The two-component model used to trace KCB wastewater would not apply.

Typical groundwater contaminant plumes are cigar-shaped, but the oxygen isotope results delineate a plume that extends outwards is all directions. A broad plume like this results from two aquifer characteristics: a high transverse dispersivity (Freeze and Cheery, 1979) or a non-uniform flow field. Both of these characteristics are present in the KLL groundwater system. The complicated groundwater flow system includes flow due to density contrasts and the periodic reversal of groundwater flow direction due to tides. These factors caused a very dispersive groundwater system, which lead to the formation of a this extensive plume.

WASTEWATER TRACER TEST (REFER TO FSU FINAL REPORT)

Salinity and oxygen isotopic composition were used in the previous section to differentiate wastewater from ambient groundwater, but they cannot be used to determine the transport direction and velocity of a patch of wastewater after injection. Chanton et al (unpub. data) performed a tracer test during the June sampling campaign to determine this. On June 8, 1999, they poured a slug of water saturated with SF_6, a non-reactive gas, into the injection well trough. The monitoring wells and two canals closest to the plant, one to the east and one to the west (locations Figure 2), were then sampled for a period of up to 130 days.

During the monitoring period the tracer peaked in both canals and five of the twenty-one wells in the study area. The SF_6 peaked in two deep wells close to injection, A-18 and B-18; two intermediate wells close to injection, A-9 and C-9; and one intermediate well far from injection, D-9 (Table 7). Other wells, including those within the mud layer, had only background SF_6 concentrations. Vertical and horizontal transport velocities were calculated using an injection point at 18 meters deep at the location of the main injection well. The fastest horizontal transport velocity was to the eastern canal, which had a higher SF_6 concentration than the western canal even though it is at a much greater distance (Figure 2). Rapid SF_6 transport to the east to intermediate wells D and C also occured. These data show that after injection at 18 m, the main transport of the patch was upwards and eastwards, towards well C-9, where the highest concentration of SF_6 was detected. The vertical velocities show that rapid buoyant transport to this well. Dispersion of the patch resulted in SF_6 peaking in wells A-18 and B-18

Table 7. Here, SF6 tracer concentration and transport velocities from the wastewater injection wells (Chanton et al., unpub. data) are compared with nutrient samples taken the day before the tracer test began. Results are shown for those wells in which the tracer peaked.

Sample	peak [SF_6], nM	SF_6 arrival time, days	horizontal SF_6 velocity, m/day	vertical SF_6 velocity, m/day	[NO_3], ppm-N	[phosphate], ppm-P
A-9	0.51	60	0.27	0.16	8.18	BDL
A-18	0.33	20	0.80	NA	4.10	1.63
B-18	1.95	10	1.5	NA	7.17	1.57
C-9	4.0	7	2.53	1.53	11.5	0.79
D-9	0.8	55	1.30	0.15	6.09	BDL
east canal	0.004	65	3.05	0.24	NM	NM
west canal	0.0012	53	1.52	0.20	NM	NM

BDL = below detection limit, NA= not applicable, NM = not measured

within twenty days. The patch continued to flow east under the mud layer, and reached well D-9 and the east canal at 55 and 65 days, respectively. At the same time, slow dispersion resulted in SF_6 peaks in the west canal at 53 days and well A-9 at 60 days. The test results agree well with the salinity and oxygen isotope data, which reflect the upward and eastern transport of wastewater after injection. A transport direction to the east is consistent with the observation that the groundwater flow in the Keys is generally from Florida Bay towards the Atlantic Ocean.

NUTRIENT UPTAKE

Nitrate and phosphate-based mixing models show that these species were not conserved in the groundwater (Table 5). This is also demonstrated in Figures 20-21, in which nitrate and phosphate concentrations are plotted against salinity for all samples (including shallow wells). A tie line in each plot connects the wastewater samples with samples from deep well G and F, which are presumed to be ambient groundwaters. Conservative mixtures of groundwater and wastewater would plot along this line. Only the sample from B-18, which is close to the injection well and is influenced by wastewater soon after injection, fits in this category. However, the majority of samples plot below the mixing line for phosphate and nitrate, indicating that uptake or removal has occurred. The June 1999 samples of well A-18 (deep well A) were enriched with respect to nitrate and phosphate. In March, this well had low-salinity, high-nutrient water. The nutrient enrichment in A-18 in June may have come from phosphate and nitrate desorption or dissolution of soluble phases after the wastewater plume contracted. This explains why the phosphate based mixing model results over-predict the percentage of wastewater in A-18 based on June results (Table 5).

Denitrification, nitrate ammonification, and adsorption are probable mechanisms for the observed nitrate removal (Figure 20). Nitrate is known to absorb onto the surface of calcium carbonate (Singh and Sekhon, 1978). Alternatively, bacterial metabolism may be responsible for nitrate depletion. Bohlke et al. (1997) measured excess $N_2(g)$ in groundwater around the wastewater injection well at KML; they conclude that this is probably the result of denitrification of wastewater nitrate to $N_2(g)$. Sulfide is known to inhibit the activity of denitrifiers (Chalamet, 1985) and sulfide in the groundwaters may be limiting the rate or extent of denitrification at KCB, perhaps favoring nitrate ammonification.

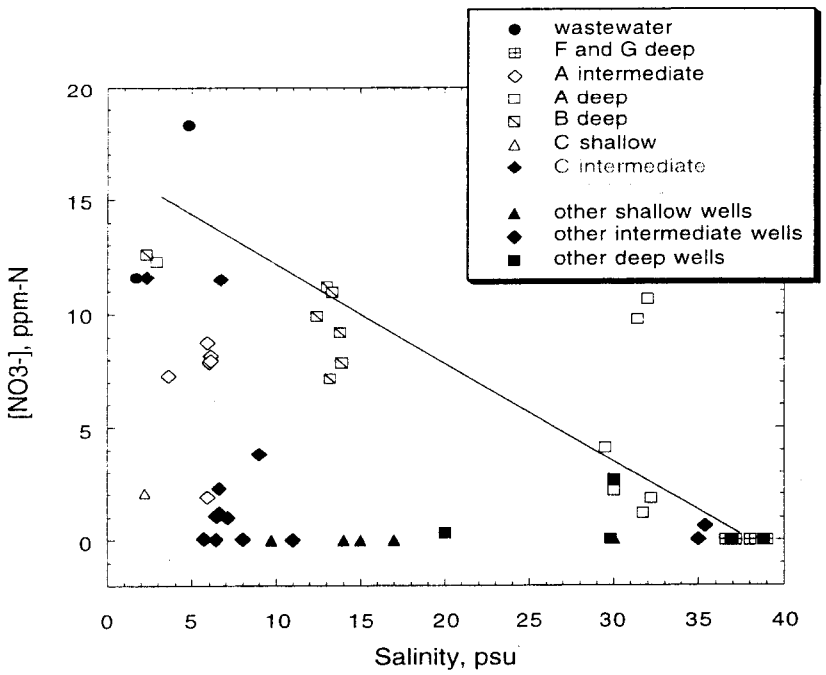

Figure 20. All samples are plotted on this graph of nitrate against salinity. The tie-line connects ambient groundwaters with wastewater.

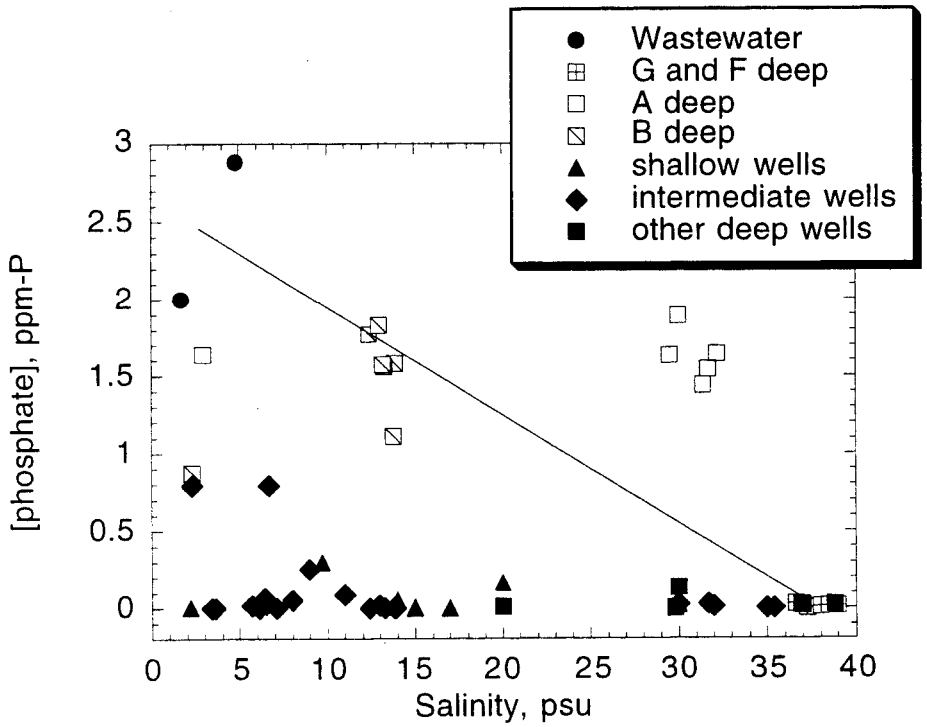

Figure 21. All samples are plotted on this graph of phosphate against salinity. The tie-line connects ambient groundwaters with wastewater.

N_2 is the typical end product of denitrification, but NH_3 also forms through nitrate dissimilation or ammonification (review in Golterman, 1985). In this study, it does not appear that the conversion of nitrate to ammonia is a major nitrate removal mechanism. No relationship between salinity and ammonia was observed (Figure 22). The shallow wells within the mud layer generally show elevated ammonia compared to deeper wells within the KLL. The two wells in the KLL that did show elevated ammonia, B-9 and G-9, one of which is close to the wastewater injection, while the other is quite far away (G-9).

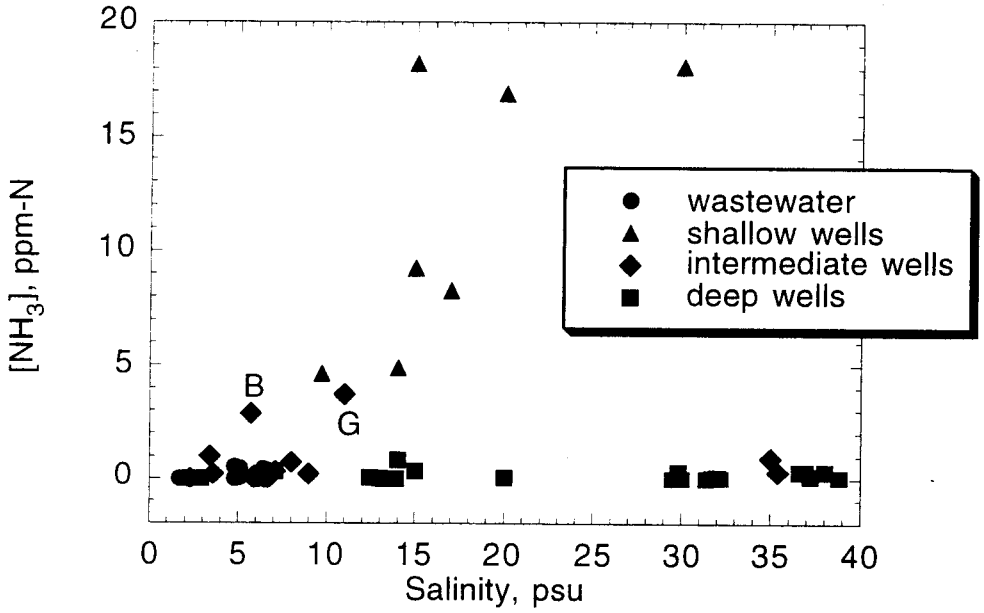

Figure 22. All samples are plotted on this graph of ammonia against salinity.

Phosphate depletion is more extensive than nitrate depletion. This is demonstrated in Figure 23, in which the data for the June 1998 samples are plotted. The x-axis of Figure 23 is the ratio of the sample nitrate concentration to the concentration expected in a conservative mixture of wastewater and groundwater of the same salinity. The y-axis is the same ratio calculated for phosphate concentrations. In this plot, samples equally depleted in both nutrients would fall along a 1:1 line, marked with the double line. However, most of samples are depleted in both species and plot near the origin. Again, well A-18 appears to be enriched in phosphate. This probably results from the removal of phosphate fixed onto the limestone surface during periods of high wastewater injection rates when A-18 was in the wastewater plume (as seen in March 1998). Of the remaining samples, more were preferentially depleted in phosphate. All of these especially phosphate depleted waters were from the intermediate sampling depths. Apparently, phosphate removal occurs before the wastewater buoyantly advects upwards after injection. This leaves the pool of wastewater below the mud layer depleted in phosphate. Potential phosphate removal mechanisms are discussed in the next section.

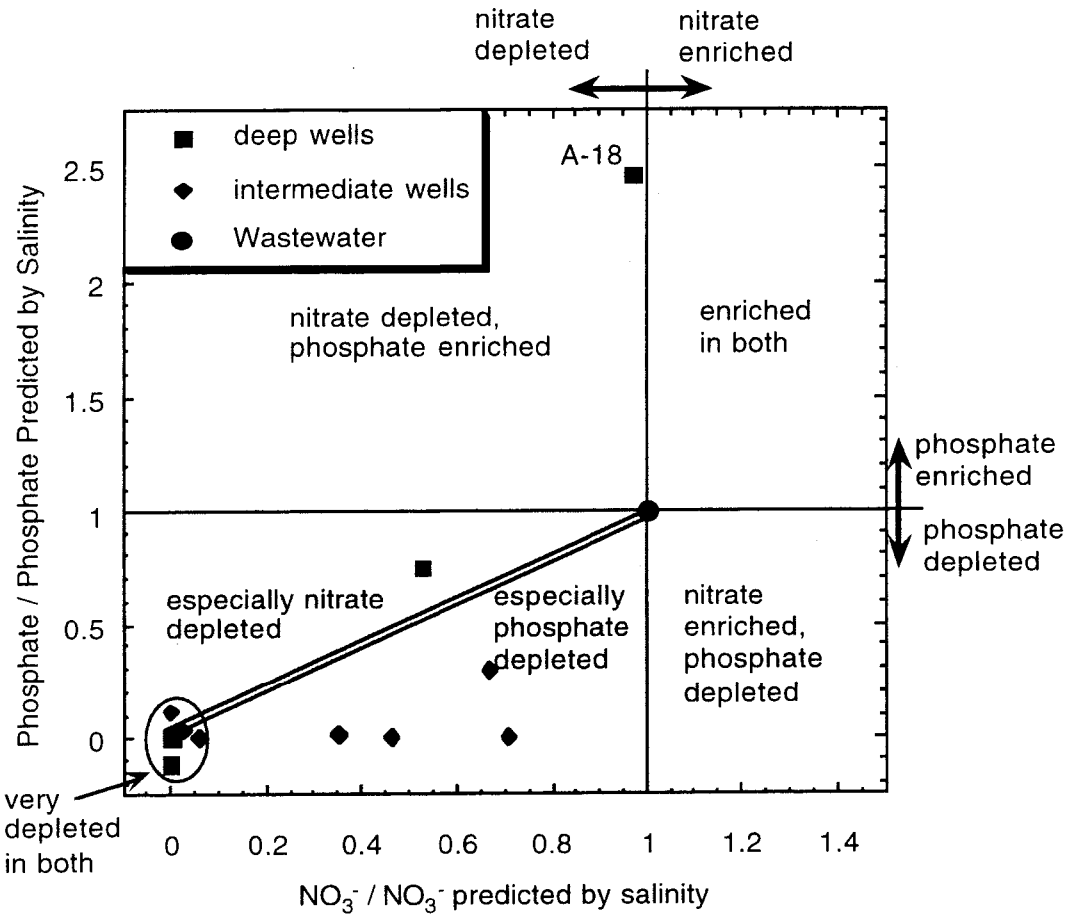

Figure 23. June 1998 samples from the comprehensive sampling round are plotted to show relative depletion of nitrate and phosphate.

A comparison of the SF_6 tracer test results (Chanton et al., unpub. data) with nutrient samples taken the day before the tracer test began (June 1998 comprehensive sampling) provides further evidence for preferential phosphate uptake in the groundwater. All wells in which SF_6 peaked had high nitrate concentrations (Table 7), while other wells had nitrate concentrations of ≤1.10 ppm-N. However, the only wells with high phosphate were the three with SF_6 arrival times within twenty days (Table 7). All other wells had phosphate concentrations of 0.3 ppm-P or lower. Thus, the SF_6 test results agree with other evidence that neither nutrient is conserved after injection, but phosphate removal proceeds at a much faster rate than nitrate removal.

PHOSPHATE UPTAKE BY CARBONATE FLUORAPATITE PRECIPITATION

This work demonstrates that a sink for phosphate exists in the aquifer at KCB. Others have also observed uptake of phosphate in Florida Keys groundwater. Monaghan (1996) found that wastewater-phosphate injected at the KML site was preferentially removed in comparison to

nitrate. La Pointe et al. (1990) observed phosphate removal from septic system effluent in the Keys. Perhaps the best documented evidence for phosphate uptake comes from the work of Corbett et al. (in review), who performed two phosphate injection experiments at the KML site. In their first experiment, a slug of water with an initial concentration of 0.83 M dissolved KH_2PO_4 and 46.2 M SF_6, a soluble gas that acts as a conservative tracer, was injected through the wastewater injection well at the site. Within five days and five meters of travel through the KLL, 85% of the injected phosphate had been removed. This percentage is normalized to the conservative tracer to remove dispersion and diffusion effects. However, because of the large amount of phosphate salt required, the density of the injectate solution was much larger than that of wastewater. Thus, the buoyant nature of the wastewater was not mimicked. To allow for a more dilute solution without compromising the phosphate detection limit, a similar experiment was conducted using radioactive (^{33}P) labeled phosphate. During this experiment 95% of the phosphate, again normalized to the conservative tracer, was removed in 2 days at five meters away from the injection well. This section will discuss possible phosphate removal mechanisms that explain these findings.

Phosphate is generally not mobile in most soils or lithologies; it precipitates with most metals and adsorbs onto clays and metal oxides (Isenbeck-Shröter et al., 1993). However, this is not a factor at the study site where metals exist in low concentrations in the groundwater and the rock is almost exclusively carbonate with low iron. Carbonate fluorapatite (CFA) precipitation is a more reasonable sink for wastewater-phosphate in the carbonate bedrock of the Florida Keys and was suggested by Monaghan (1996) and Lapointe et al. (1990). Calcium carbonate is known to convert, or be replaced by, carbonate apatite. Ames (1959) was the first to present laboratory work which shows that calcite converts to a carbonate apatite in phosphate-rich solutions. Textural evidence of natural CFA replacement of calcite in phosphorites has been reported by Manheim et al. (1980) and Cullen (1980), among others. Lamboy (1993) reports that while calcite can be replaced by CFA, it is more commonly formed by precipitation of CFA after carbonate dissolution.

The composition of CFA is quite variable and crystals are usually not homogeneous. A general formula for CFA is (Nathan, 1984):

$$Ca_{10-a-b-c}Na_aMg_b(PO_4)_{6-x}(CO_3)_{x-y-z}(CO_3{\cdot}F)_y(SO_4)_zF_2$$

Where: $x = y + a + 2c$
c = number of Ca vacancies

The solubility of CFA is low, but because of its variable composition a range of solubilities has been measured (Chien and Black, 1976; Jahnke, 1984).

The geochemical speciation code PHREEQC (Parkhurst, 1985) was used to determine if CFA precipitation is thermodynamically feasible in the groundwater and wastewater collected during June of 1998. The phases used are the most and least soluble CFA samples from Chien and Black (1976) whose solubilities and compositions are given in Table 8. Because phases must be charge balanced, the literature compositions were adjusted by equally distributing excess charge among the ions of the opposite sign. PHREEQC used the input data to calculate the activities of species in solution (Parkhurst, 1985). The appropriateness of using PHREEQC for seawater solutions will be demonstrated below. PHREEQC was used to calculate the saturation indices of the two natural CFAs from Chien and Black (1976), given in Table 8, in selected June 1998 samples (A-18, C-9, F-18, G-9, 8-18, and wastewater) which were chosen based on their different salinities and nutrient concentrations.

Table 8. Compositions of CFAs used in PHREEQC simulations along with the log of its equilibrium solubility constant (K_{eq}).

Sample	Description	log K_{eq}	Reported Composition	Excess Charge (eq)	Balanced Composition
CB IN	natural CFA from India	-121 least soluble of CB	$Ca_{9.93}Na_{0.05}Mg_{0.02}(PO_4)_{5.77}$-$(CO_3)_{0.23}F_{2.09}$	0.09	$Ca_{9.93}Na_{0.05}Mg_{0.02}(PO_4)_{5.78}$-$(CO_3)_{0.245}F_{2.12}$
CB NC	natural CFA from North Carolina	-114.4 most soluble of CB	$Ca_{9.54}Na_{0.33}Mg_{0.13}(PO_4)_{4.80}$-$(CO_3)_{1.20}F_{2.48}$	0.39	$Ca_{9.54}Na_{0.33}Mg_{0.13}(PO_4)_{4.84}$-$(CO_3)_{1.27}F_{2.48}$

CB- samples from Chein and Black (1976).

The chemical composition of each sample solution was written into PHREEQC input files. Measured nutrient, pH, fluoride, alkalinity and elemental concentrations of these samples were used. The concentrations of SO_4^{2-}, Cl^-, and Br^- were approximated by multiplying their seawater concentrations (Millero and Sohn, 1992) by the ratio of sample salinity to seawater salinity. Because sulfide was not measured in June of 1998, March 1998 sulfide results were used to approximate sulfide concentrations. One sample, F-18, had phosphate concentrations below detection, so the phosphate concentration was approximated as the detection limit of 0.01 ppm-P. PHREEQC used to input files to speciate each solution. It then used the solubility of the CFAs in Table 8 to calculate the saturation index of each mineral as:

$$\text{Saturation Index} = \log [\text{Ion Activity Product} / K_{eq}] \quad (7)$$

A positve saturation index means that a sample is supersaturated while a negative saturation index indicates the solution in undersaturated with respect to the phase.

The PHREEQC calculations show that all of the samples were extremely supersaturated with respect to the two phases (Table 9). The high-nutrient groundwaters were more supersaturated with respect to these two CFAs than the wastewater, presumably because of the higher calcium concentrations in the groundwater. These calculations show that samples with detectable phosphate are supersaturated with CFA. Therefore, CFA precipitation is a sustainable mechanism of phosphate removal at KCB given its low solubility and the high void space in the KLL.

Table 9. PHREEQC results for saturation indices two natural CFAs (Table 8) in selected June 1998 samples.

sample	solution character	Saturation Index of CB IN	Saturation Index of CB NC
A-18	high salinity, high nutrients '	23.22	20.04
C-9	low salinity, high nutrients '	22.58	19.46
F-18	high salinity, low nutrients ' #	10.31	9.63
G-9	low salinity, low nutrients	17.90	16.14
G-18	high salinity, low nutrients '	10.06	9.21
WW'	low salinity, high nutrients	21.63	17.77

' charge balance originally >0.01 eq, Na^+ used to balance charge

no detectable PO_4^{3-}, June detection limit of 0.01 ppm P used in input file

While CFA precipitation in the groundwaters is thermodynamically favored, this does not prove that it occurs in the field. Because of this, phosphate and fluoride concentrations in the groundwater samples were compared to look for evidence of CFA precipitation. Plotting fluoride and phosphate against salinity shows that in both species the intermediate wells samples lie below the conservative mixing line of wastewater and ambient groundwater, represented by F-18 and G-18) (Figures 24-25). These low-salinity samples appear to be depleted wastewater. The fluoride removal may be unrelated to phosphate; for example, Machusak and Kump (1997) observed fluoride depletion in the groundwater within KLL offshore of the Fiesta Key, but did not observe phosphate depletion. However in support of CFA precipitation, McGowen (1999, unpub. data) found a molar ratio of fluoride to phosphate depletion in the KCB groundwaters of 0.326. This F:P ratio is similar to the molar ratio found in CFA synthesized on a calcite seed of 0.214 (Gulbrandsen et al., 1984), and it is close to the molar ratio of F to P depletion of 0.394 observed in porewaters of the Peru margin, where phosphorites are currently forming (Froelich et al., 1988). Thus, the water chemistry provides evidence that the thermodynamically favored process of CFA precipitation is occurring at KCB.

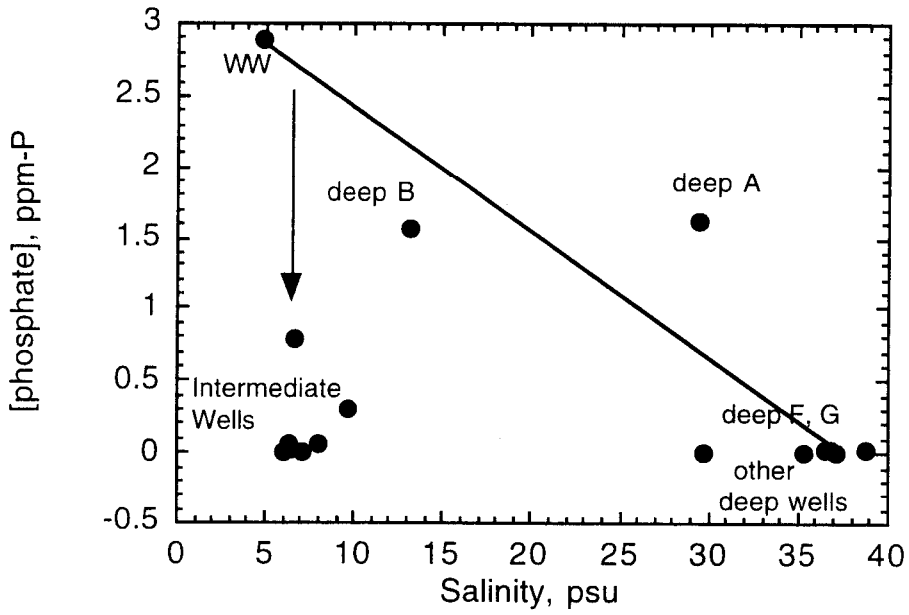

Figure 24. June 1998 phosphate results for the comprehensive sampling are plotted against salinity. The arrow marks the direction which wastewater would plot as phosphate was removed.

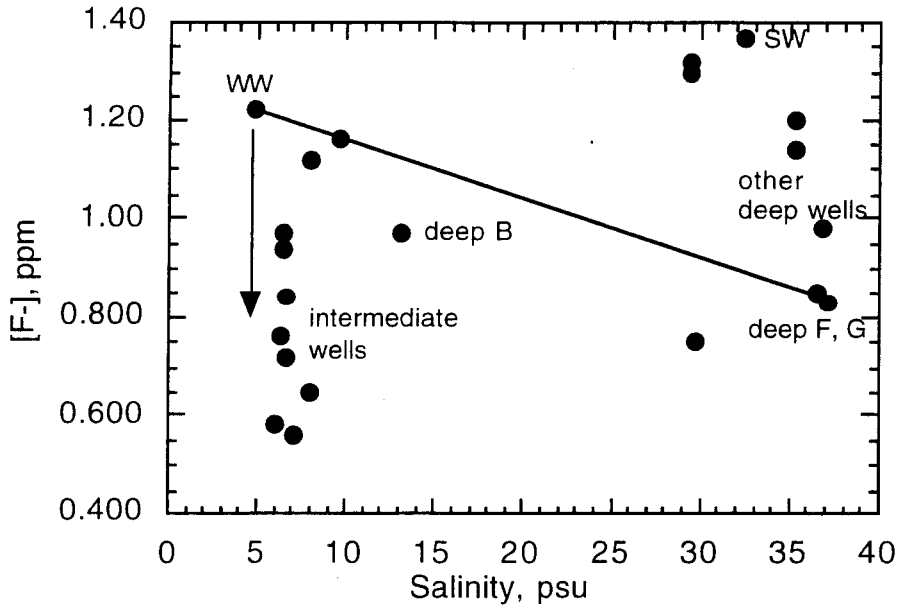

Figure 25. June 1998 fluoride results for the comprehensive sampling are plotted against salinity. The arrow marks the direction which wastewater would plot as fluoride was removed.

Contrary to what would be expected if wastewater phosphate is precipitating as CFA, no preferential phosphorous enrichment of rock samples of cores from near the wastewater injection wells was observed. Calculations were made to determine the concentration of phosphorous expected in the KLL if all phosphate injected had been adsorbed or precipitated. This was done to see if the phosphorous enrichment expected would be detectable using the methods employed. The calculation was performed assuming that all phosphate had been uniformly distributed within a 15 m diameter half-cylinder of KLL south of the injection wells that extended from top of the wastewater injection interval at 18.3 m to the base of the mud at 6 meters:

Given: (8)

wastewater phosphate concentration = 2 ppm P = 2.0 mg P/l ww
wastewater injection rate = 757000 l ww/day
time of injection = 5 yr

height of KLL half-cylinder = 12.3 m
density of calcite = 2.71 g/cm^3 (Morse and Mackenzie, 1990)
porosity of KLL = 0.5
radius of KLL half-cylinder = 15 m

Total P (kg P_2O_5) =
[PO_4^{3-}] (mg P/l ww)*inj rate (l ww/day)*365 (day/year)(1kg/10^6mg)*(141.95 kg P_2O_5/61.94 kg P)*(5 years)

Total P = 6330 kg P_2O_5

Mass of rock (kg) = height (m)*radius(m)$^2\pi$/2*porosity*density (g/cm^3)(1 kg/1000 g)* (100 cm)^3/ 1 m^3
Mass of rock (kg) = 5,890,000 kg

wt % P_2O_5 = (mass P_2O_5 (kg) * 100% / (mass of rock (kg) + mass of P_2O_5 (kg))
wt % P_2O_5 = 0.11 wt %

The stated detection limit for the phosphorous bulk analysis is 0.01 wt % P_2O_5; thus, the calculated enrichment of 0.11 wt % P_2O_5 is detectable. However, the range of phosphorus concentration in the cores far from injection, F and G, was from 0.02 to 0.18 wt % P_2O_5 (Appendix B). So if all wastewater phosphate injected was taken up within this short distance, phosphate concentrations in the rock might still be within the range of natural phosphate variability. Surface analytical techniques or a more detailed sampling in these cores may detect areas of wastewater phosphorous enrichment that were missed by this analysis. It is not surprising that X-ray diffraction of the bulk rock samples, which requires 1 wt % P in a well-crystallized phase for detection (Ruttenburg, 1992), did not detect any phosphate minerals.

The field data did not lead to a definite determination of the process that is removing wastewater-derived phosphate. Circumstantial evidence for CFA precipitation was discovered; the well waters are supersaturated with CFA, and the depletion of groundwater phosphate and fluoride were related in a ratio consistent with CFA stoichiometry. However, CFA was not found using bulk analysis or X-ray powder diffraction of core material. The mechanism by which KLL immobilizes phosphate was investigated through a laboratory study that examines the interaction between KLL and phosphate solutions (see below).

CONCLUSIONS OF FIELD STUDY

- Wastewater injected between 18 to 27 m depth at Key Colony Beach flows buoyantly upwards until blocked by the mud-Key Largo Limestone contact at 6 m below the surface. Afterwards, the general flow direction of the wastewater is to the east, although significant dispersion is evidenced by the large extent of the wastewater plume in all directions. After five years of wastewater injection, a large pool of relatively low-salinity wastewater exists under the mud layer. The full extent of this anthropogenic freshwater lens is unknown because it extends beyond the locations of monitoring wells in all directions.

- Wastewater-derived nitrate uptake is occurring in the groundwater. The nitrate sink is unknown; it potentially is adsorption onto the limestone, although nitrate ammonification or denitrification are the most likely possibilities.

- Wastewater-derived phosphate is immobilized in the Key Largo Limestone. The apparently coupled phosphate and fluoride depletion, along with the supersaturation of carbonate fluorapatite, supports the hypothesis that carbonate fluorapatite precipitation removes phosphate from the groundwater. Although no analytical evidence was discovered for carbonate fluorapatite, this secondary mineral may be present below analytical detection limits.

COLUMN EXPERIMENTS

INTRODUCTION

The results of the fieldwork at KCB suggest that uptake of wastewater-phosphate occurs within the KLL, but the process responsible was not identified. The apparent coupling of phosphate and fluoride uptake and the fact that groundwater samples are supersaturated with respect to carbonate fluorapatite (CFA) support the hypothesis that precipitation of this mineral is responsible for phosphate removal.

This section will discuss experiments conducted to observe the interaction of KLL and phosphate. In these experiments, pieces of KLL from cores drilled at the Keys Marine Laboratory on Long Key, Florida (Figure 1) were reacted with phosphate-enriched solutions over a period of several weeks. Wastewater, distilled water, and seawater were used as proxies for the different groundwater solutions at KCB. The goal of these experiments was to determine if the wastewater-phosphate uptake at KCB could be attributed to interaction with the KLL surface.

CALCIUM CARBONATE AND PHOSPHATE

Any reaction immobilizing phosphate through interaction with calcite would occur near or on the mineral surface. Many researchers have observed phosphate uptake by powdered calcite (Stumm and Leckie, 1970; Griffin and Jurniak, 1973 and 1974; Kitano et al., 1977; DeKanel and Morse, 1978; Avnimelech, 1980; Brown, 1980; Freeman and Rowell, 1981; House and Donaldson, 1986). The interpretation of these experiments was complicated by the fact that phosphate uptake involves more than one mechanism: phosphate adsorption, precipitation of a calcium phosphate phase, and even precipitation of multiple calcium phosphate phases have been proposed. Phosphate uptake typically occurs in two stages, an initial rapid uptake, which is attributed to adsorption, followed by a period of slower uptake (Stumm and Leckie, 1970; Jurniak and Griffin, 1973 and 1974; Kitano et al., 1977; DeKanel and Morse, 1978; Brown, 1980; Freeman and Rowell, 1981). All these authors attributed the later uptake to calcium-phosphate precipitation except DeKanel and Morse (1978), who proposed a second, slower mechanism of phosphate adsorption while not ruling out precipitation.

The phosphate concentration of the solution reacted with calcite is one factor that determines which process occurs. Griffin and Jurinak (1973) found that heterogeneous nucleation is the dominant mechanism of phosphate uptake at concentrations greater than 0.6 ppm P. At concentrations lower than this, adsorption alone can explain observed phosphate uptake (Griffin and Jurinak, 1973; House and Donaldson, 1986).

Some authors have found that multiple calcium phosphate phases are formed when dissolved phosphate reacts with calcium carbonate. Initial precursor phases subsequently

convert to more stable, insoluble precipitates (Stumm and Leckie, 1970; Freeman and Rowell, 1981). In eight to ten-day experiments conducted by Stumm and Leckie (1970) with initial solution phosphate concentrations of 3.2 ppm P, an amorphous calcium phosphate phase precipitated first and then converted to hydroxylapaptite. Griffin and Jurinak (1974) formed the same sequence of phases when they reacted a solution with of 0.2 ppm P phosphate with powdered calcite at 41 °C for one day. Freeman and Rowell (1981), in experiments with initial solution phosphate concentrations of up to 500 ppm P, found that dicalcium phosphate (DCP, $CaH[PO_4]*2H_2O$) formed rapidly and then partially converted to octa-calcium phosphate (OCP, $Ca_8H_2[PO_4]_6*5H_2O$), which is less soluble, in twenty days. In these studies, not only was the degree of saturation important to the number and type of precipitates formed, but also the length of the experiment. If these experiments had been shorter, only one phosphate precipitate might have been detected.

These literature results show that different precipitates can be formed through interaction of calcite with phosphate, depending on the amount of phosphate in solution (essentially the saturation state of the solution) and the duration of the experiment. Of the calcium phosphate precipitates, the apatite group is the most stable. It may be that the heterogeneously formed phases and surface complexes are apatite precursors. Apatite formation is known to be slow, and may not be observed within the duration of most experiments.

CARBONATE FLUORAPATITE

As discussed above, carbonate fluorapatite (CFA) is one of the thermodynamically stable, insoluble apatite minerals that can form through interaction of calcite with phosphate solutions. CFA precipitation has been implicated as a possible sink for wastewater-phosphate in the Florida Keys (Lapointe et al., 1990; Monaghan, 1996). This is feasible given its low solubility (Chien and Black, 1976; Jahnke, 1984), thermodynamic stability, occurrence in phosphate enriched marine waters as phosphorite deposits (reviews in Föllmi, 1996; Jarvis et al., 1994), and tendency to replace calcite (Ames, 1959).

The studies discussed above did not find evidence that CFA was one of the heterogeneously nucleated phosphate phases. However, most of these experiments were performed in fluoride-free solutions. Stumm and Leckie's (1970) experimental work did show that fluoride increases the rate of hydroxylapatite precipitation. They suggested that fluorapatite was also precipitating. It is possible that some of the other phases observed in experiments with phosphate and calcite are CFA precursors, and CFA could not form within the duration of the experiments. This hypothesis is supported by the work of Gulbrandsen et al. (1983), who found that an amorphous phosphate and then a crystalline magnesium phosphate phase preceded CFA precipitation onto calcite and apatite seeds in seawater. CFA was formed in theses experiments only after ten years (Gulbrandsen, 1983). Van Cappellen (1991) found that DCP and OCP were precursors to fluorapatite precipitation. Thus, some of the same phases that are precipitated through calcite-phosphate interaction are known fluorapatite precursors.

The inhibition of carbonate fluorapatite formation by magnesium has been demonstrated (VanCappelen, 1991; Gulbrandsen et al., 1983). This is an important consideration in the KLL, where magnesium concentrations in the groundwaters range from 94 to 1061 ppm Mg (Appendix E). Gulbrandsen et al. (1983) found that it took ten years to form apatite from precursors in seawater solutions with initial phosphate concentrations of 28-32 ppm-P and seeded with apatite and calcite. Seawater levels of magnesium thus cause a lag in the onset of apatite formation, a time much longer than the duration of most experiments.

While literature results show that solutions with wastewater concentrations of phosphate will induce heterogeneous precipitation of a calcium phosphate phase, there is a range of phases that can form in what is likely a time-dependent process. CFA precipitation is a

reasonable end product to expect, but its slow precipitation kinetics and inhibition by magnesium may make it unlikely to form during experiments lasting several months.

METHODS

EXPERIMENTAL DESIGN

The experiments were designed to monitor the chemistry of a phosphate solution constantly circulated through KLL. Two experimental apparatuses were used, each for a separate experiment. The critical component of each apparatus was a column of KLL 26-28 cm long and 5 cm wide that was slid into a 5.1 cm diameter PVC pipe (Figure 26). The limestone was not rinsed or washed before being placed into the PVC. This pipe was enclosed on each end with connectors attached to tubing that led to a solution reservoir. A peristaltic pump attached to this tubing pumped solution from the reservoir upwards through the column and then back to the sampling reservoir (Figure 26). A Fisher Scientific Mini Peristaltic Pump was used, which circulated the solutions at a rate of approximately 8 ml/minute. This pump uses a small length of silicone tubing that was changed every three to four weeks. The rest of the tubing in the Column 1 experiment was larger silicone tubing that fits a faster Masterflex peristaltic pump, which rapidly mixed the solutions at a rate of 3-7 liters per minute after mini-pump silicone tubing or solution changes. The rapid mixing ensured that the new solution would begin uniformly reacting with the limestone immediately. In the Column 2 experiment only a 60-cm section of this silicone tubing was used, and all other tubing used on the system was made of PVC.

The sampling reservoir was a two-liter glass bottle with a glass outlet near the bottom through which the solution was sampled. This outlet was fitted with a plastic clamp, which was opened for sampling (Figure 26). The solution in the reservoir was constantly stirred with a magnetic stirrer to maintain solution homogeneity. The solution reservoir was capped by a rubber stopper through which two short glass tubes passed, one to let solution into the reservoir and one to let solution out (Figure 26). Each glass tube had plastic tubing attached at either end to maintain the solution loop. The rubber stopper also had a small hole cut through it, which vented the system to the atmosphere, to keep the pressure within the system constant as sampling reduced the solution volume.

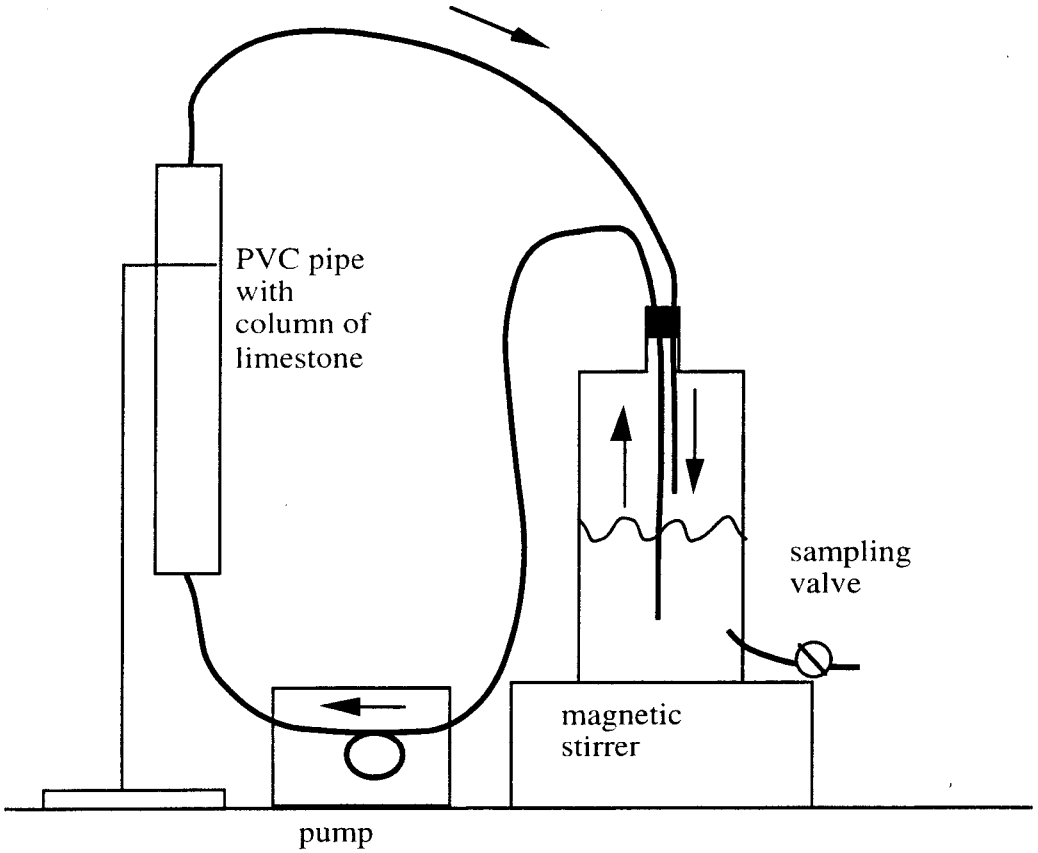

Figure 26. Schematic of the experimental design is not drawn to scale.

The experimental system held only approximately two liters of solution; sampling depleted this volume. Sampling occurred periodically, with more intense sampling after changes in the solution, when the reactions were most rapid. The volume of sample depended on the analyses to be performed. Approximately 10 ml was needed when only pH and phosphate were measured. However, when fluoride analyses were also desired, the minimum sample volume was 30 ml.

Information on the core material for Column 1 and Column 2 is given in Table 10. The core material was tightly packed in the column, but some large voids were open on the outside of the limestone column. Presumably, some solution flowed outside the rock, and it cannot be assumed that the solution moved uniformly through the core. However, even in the field, such preferred flowpaths exist (e.g., Monaghan, 1996).

Table 10. Characteristics of Column 1 and Column 2.

	Depth in core KML 7B, m	Length, cm	Diameter, cm	Weight, g
Column 1	11.3	28	5	935.3
Column 2	7.2	26.1 cm	5	833.0

COLUMN 1 EXPERIMENT

Column 1 was primarily used to investigate the interaction of phosphate-enriched seawater with KLL. After an initial test period with tap water to test for leaks in the system, seawater was added and the solution was allowed to react with the limestone overnight. The seawater added was low-nutrient seawater collected in the Gulf Stream off of the Florida Keys. It was not treated in any way before it was poured into the column. This was followed by three phosphate enrichments of that seawater solution over the next six months (Table 11), to investigate the phosphate uptake potential of the limestone. Next, the column was drained and low-nutrient Gulf Stream seawater was added to investigate phosphate desorption (Table 11). Column 1 was then drained and the last solution, phosphate and fluoride in distilled water, was added.

When a solution was removed from the experimental apparatus, the pump was stopped and the solution was drained from the column into the sampling reservoir. The column was allowed to drain for about two hours. The drained solutions were then removed from the reservoir and analyzed for salinity, alkalinity, and elemental concentrations.

Table 11. Changes made during the Column 1 experiment.

Date	Change	Purpose	Fast pump used?
7/14/1999	tapwater added	test for leaks	no
7/14/1999	column drained, seawater added	equilibrate with seawater	no
7/15/1999	phosphate standard added	phosphate enrichment	no
8/4/1998	phosphate standard added	phosphate enrichment	no
10/13/1998	phosphate standard in seawater added	phosphate enrichment, increase volume of solution	yes
1/6/1999	column drained, seawater added	desorb-dissolve phosphate	no
2/24/1999	column drained, distilled water added	equilibrate with distilled water	no
2/25/1999	fluoride and phosphate in distilled water added	phosphate and fluoride enrichment in distilled water	no
4/27/1999	column drained	end experiment	

When a change in a solution was made, the solution was added into the sampling reservoir by removing the stopper at the top and pouring the solution in. The solution was then mixed throughout the system with the Fischer mini-pump. In the middle of the experiment, the faster Masterflex pump was used for one mixing, but mechanical failure took this pump out of service for later solution changes (Table 11).

The Column 1 experiment was completed on April 27, 1999 when it was determined that the final solutions phosphate concentration had relatively constant for over a week (Table 11). The system was drained, and the PVC surrounding the column was cut with a hacksaw and removed from the KLL column. The reacted KLL was photographed, then placed back in the PVC pipe. The direction of the flow during the experiment was labeled on the pipe. Lastly, the whole apparatus was then wrapped in plastic and put in a freezer for storage for later analysis.

COLUMN 2 EXPERIMENT

Column 2 was used to investigate the reaction of phosphate in distilled water and wastewater-phosphate with the KLL (Table 12). During this experiment, solution changes and the draining of the column was carried out in the same manner as in the Column 1 experiment. Initially, the system was reacted with distilled water overnight before an addition of phosphate. After equilibrating with this phosphate solution for a period of two months, the column was drained and distilled water was added to observe phosphate removal from the reacted limestone surface.

Table 12. Change made in the Column 2 experiment.

Date	Change	Purpose	Fast pump used?
12/9/1998	added distilled water	equilibrate with distilled water	no
12/10/1998	add phosphate	phosphate enrichment	no
2/28/1999	column drained, distilled water added	desorb-dissolve phosphate	no
3/17/1999	column drained, KCB wastewater added	wastewater-phosphate enrichment	yes
4/5/1999	column drained, KCB wastewater poisoned with $HgCl_2$ added	wastewater-phosphate enrichment without biological activity	yes
5/18/1999	found that leak drained column, experiment ended		

In the second phase of the Column 2 experiment, wastewater was reacted with the KLL column (Table 12). KCB wastewater frozen since collection in November of 1998 was used. In the first attempt, begun on March 17, 1999, the wastewater added was not poisoned, in order to minimize interferences between phosphate and the poison. The experiment was kept covered with a cardboard box to prevent biological activity by minimizing light. However, this action did not prove effective in preventing algal growth. For the second wastewater enrichment on April 5, 1999, the column was drained and wastewater poisoned with 40 mg $HgCl_2$ per liter was added. Again, the apparatus was kept covered. Unfortunately, a leak drained the column, which ended the experiment on May 18, 1999. However, the poisoned wastewater reacted sufficiently to show the mode of wastewater-phosphate reaction. As in the Column 1 experiment, the KLL column of the Column 2 experiment was removed from it PVC housing and visually inspected. The whole apparatus was then wrapped in plastic and put in a freezer for storage.

SAMPLING PROCEDURE

During sampling, it was important to keep track of the volume of solution taken out of the system to allow for a mass balance to be made. Samples were taken in graduated cylinders. The volume of the sample was read and recorded immediately with an estimated accuracy of $\pm$ 0.2 ml. Samples were stored in plastic screwcap bottles stored at 4 °C until analysis. When pH measurements of the samples began, after the third addition of phosphate-enriched seawater to Column 1, the sampling procedure changed. After the sample volume was read, samples were poured into clean and dry beakers for pH measurement. After a pH measurement was made, the sample was placed in plastic screwcap bottles and stored as before.

NUTRIENT, pH, SALINITY AND ALKALINITY ANALYSIS

All column experiments were analyzed for phosphate by the same method used for the field samples with minor modifications. In order to conserve sample volume, samples were not analyzed in replicate. Since the data were a time series, samples were only re-analyzed when irregularities in the concentration versus time graph were found. Many samples required small dilutions, 1:5 to 1:2, to reach the range of the analytical method, which is 0 to 1 ppm-P. These samples were diluted with the matrix of the sample, low-nutrient seawater or distilled water (also used for wastewater samples), by pipetting in the appropriate volume of sample and dilution matrix into a small Erlenmeyer flask; this solution was then mixed thoroughly. Ten percent of the samples were re-analyzed on a different day as a quality control (results in Appendix I)

Beginning on 10/13/1998 samples were analyzed for pH with a Hanna HI model 9023 portable pH and temperature meter. This meter was standardized each day with pH 7 and 10 buffers. After each sample measurement, the pH 7 buffer was read as a quality control check.

The column experiment samples were analyzed for fluoride following the procedure used for the field samples. Tonya McGowen, Penn State undergraduate student, analyzed the samples from Column 1 during the third seawater phosphate enrichment, from October to December 1998. The author performed all later fluoride analyses using the same technique and equipment. Because of the small sample size, replicate analyses could not be performed. Instead, a large sample of seawater was analyzed during each analytical period to ensure consistent results (results in Appendix I).

During the wastewater enrichments of Column 2, nitrate analyses were made of selected samples. The nitrate analytical procedure of the field study was used. The only modification was that the samples were not run in replicate. The samples had to be diluted so that nitrate concentrations were within the range of the method, 0 to 1 ppm-N. Since all of the samples are in a low-salinity wastewater matrix, they were diluted in distilled water and run with distilled water standards.

The large volume samples collected after each time a column was drained were analyzed for salinity and alkalinity. Salinity measurements were made with an Orion model 115 conductivity meter standardized with a 15 mS (8 psu) standard. Alkalinity titrations were performed with standard hydrochloric acid in the same method as the field samples. However, not all alkalinity analyses were performed within 24 hours, but up to one month later on samples that had been stored in a refrigerator a 4 °C.

ELEMENTAL ANALYSIS

Selected samples were filtered and analyzed by atomic absorption flame emission spectrophotometry (AA-FES). Samples were analyzed for Ca, K, Mg, and Na. The samples were filtered with inline membrane filters to remove particles, most importantly fragments of the limestone column. Samples were drawn into a 3 cc syringe and then pushed through the filter. The first cc of sample was filtered was discarded to rinse the filter, the remainder of the filtrate was collected. Approximately 4 cc of sample was filtered and collected in this manner. The samples were then diluted 1:25 with distilled water in volumetric flasks. These dilutions were then sent to the Material Research Laboratory, Penn State for analysis by AA-FES. Ten percent of the samples were diluted in replicate for analysis as a quality control check.

RESULTS

COLUMN 1

The evolution of the Column 1 experiment can be followed in Figure 27 (data in Appendix F), which shows the changes in the chemistry of the solution through time. After each phosphate addition, an initial period of rapid phosphate uptake was followed by a longer period of slower uptake (Figure 27 A). The period of rapid uptake also corresponds to a rapid pH change (Figure 27 B). The pH change was greater when the distilled water solution was added at the end of the experiment. The later, slower phosphate uptake proceeded to an apparent equilibrium concentration of approximately 0.8 ppm P (marked by a double horizontal line in Figure 27 A) after each addition of phosphate. The same equilibrium concentration was reached by removing phosphate from the column surface after seawater with a phosphate concentration of less than 0.01 ppm P was added to the pre-reacted column. The third addition of phosphate-enriched seawater approached did not reach equilibrium because sampling depleted the solution volume before equilibrium was attained.

Fluoride concentrations varied little during the Column 1 experiment (Figure 27 C, data Appendix F). Fluoride measurements were made on samples after the third seawater phosphate enrichment and on samples after the addition of phosphate and fluoride in distilled water. In the seawater solution, there appears to be no fluoride uptake over a forty-eight day period during which the phosphate concentration dropped 2.86 ppm P (Figure 29). Additionally, McGowen (unpub.) showed that the fluoride concentration measured just before the third phosphate enrichment, 1.07 $\pm$ 0.3, is very close to the concentration calculated by assuming that seawater fluoride had been conserved since the beginning of the experiment, 1.15ppm F. The last solution to react in this experiment was phosphate and fluoride in distilled water. The first three days this solution reacted the fluoride concentration dropped from approximately 1.45 ppm F to 1.20 ppm F, which is close to the range of error for the fluoride measurements of approximately $\pm$ 0.1. The fluoride concentration then remained constant for the remainder of the experiment, while phosphate removal continued. The ratio of the fluoride taken up by the column to the phosphate taken up in the distilled water addition is 0.27; this F/P ratio is within the range of laboratory synthesized apatite. For example, Gulbrandsen et al. (1984) synthesized a CFA with a F/P ratio of 0.214 on a calcite seed, and Janke (1984) homogeneously precipitated CFAs had F/P ratios of 0.38 to 0.42. However, the brief period of fluoride removal was not coupled with the more sustained phosphate uptake (Figure 29). While no fluoride uptake was observed in the seawater solution; a small but potentially significant amount of fluoride uptake occurred in the distilled water solution.

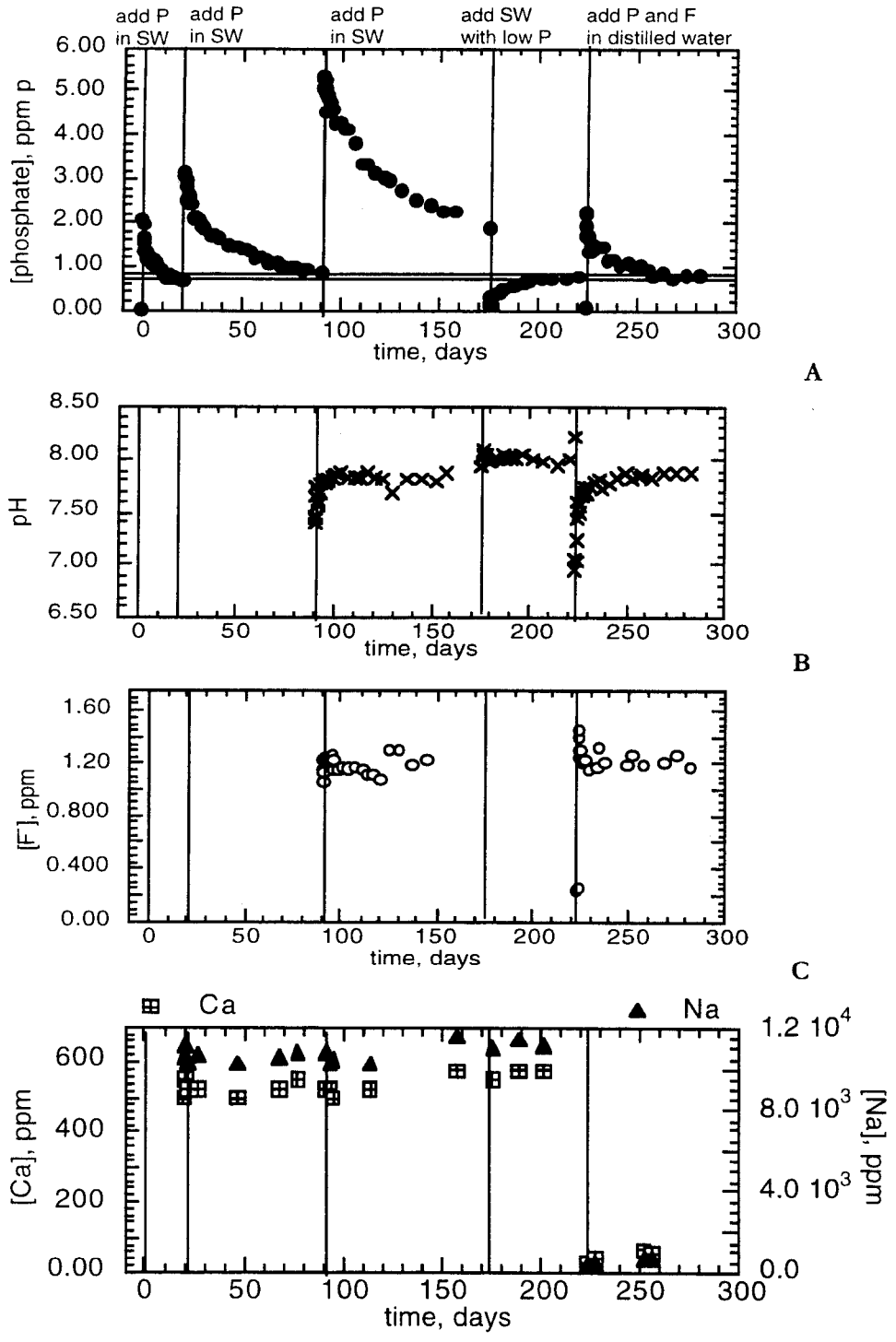

Figure 27. The solution phosphate (A), pH (B), fluoride (C), along with total calcium and sodium (D) through the Column 1 experiment are shown. The vertical lines, labeled at the top, give the time when changes to the solution were made.

The concentrations of sodium, calcium, magnesium, and potassium during the experiment largely reflect the salinity of the experimental solution (Figure 27 D, Appendix F). As seen in Figure 27 D, the calcium and sodium concentrations were nearly constant as seawater solutions reacted with the column. Calcium and sodium concentrations were quite low immediately after the last phosphate addition, which was in distilled water. By the end of the experiment, however, their concentrations had risen to 65 ppm Ca and 650 ppm Na. Magnesium and potassium concentrations showed similar trends (data Appendix F). The concentrations of the major cations did not change during the seawater phase of the experiment; any interaction with the KLL is insufficient to measurably alter their concentrations. The last solution of phosphate and fluoride in distilled water apparently dissolved the column material as it reacted, releasing the cations from both calcite dissolution and possibly salt dissolution.

The changes in the amount of phosphate on the column surface during the Column 1 experiment is shown in Figure 28. After the initial addition of phosphate in seawater (marked as 1 on Figure 28), the system begins with no phosphate fixed on the limestone but a relatively high concentration of phosphate in solution. Phosphate was taken up by the rock as the system proceeded to equilibrium, marked by the double line, in the direction noted by the arrow labeled absorption-precipitation. The second seawater phosphate addition, marked by a 2, brought the system back to a relatively high concentration of phosphate in solution. After this enrichment, the solution again proceeded to the same equilibrium as the first. After the third phosphate addition, at 3, the solution approached but never reached equilibrium before the solution volume was depleted. After the third addition, the system was drained and low-phosphate seawater was added at 4. This solution initially had a low phosphate concentration while the limestone had a relatively large amount of phosphate on its surface. The system reacted to this solution change by releasing phosphate from the limestone surface. Next, the column was drained and distilled water was added at 5. The solution was allowed to react overnight, then phosphate and fluoride was added at 6. The system then reached the same equilibrium as before, even in a low-ionic strength solution. The equilibrium points at the end of each reaction period (with the exception of the third seawater addition which did not reach equilibrium) should fit an adsorption isotherm if that is the overall mechanism for phosphate uptake. However, each solution ultimately reaches the same equilibrium phosphate concentration, regardless of the amount already fixed on the limestone surface which does is not consistent with absorption isotherms. Thus, these data are not consistent with phosphate uptake by adsorption for the long-term reaction. Initial rapid adsorption remains a possibility.

When the KLL column was removed from its PVC housing at the end of the experiment, evidence for localized alteration of the limestone was apparent.
An area of dark orange-yellow discoloration was observed at the end of the column where solution entered (Figure 29). This suggests that not all surfaces of the KLL were equally reacted. An analysis of the reacted surfaces of this limestone remains a direction of future work.

COLUMN 2

The Column 2 experiment was conducted to examine the phosphate-KLL interaction in low-ionic strength solutions, distilled water and wastewater. After the first addition of phosphate in distilled water (Figure 30 A), phosphate concentration decreased rapidly at first, and then the phosphate uptake slowed (data Appendix G). A rapid rise in the pH of solution also occurred after the phosphate addition (Figure 30 B). This solution was very slow to reach a point where the phosphate concentration was at equilibrium, judged by having the same phosphate concentration for over a week. In an attempt to pinpoint the equilibrium concentration, the column was drained and distilled water added to approach equilibrium from undersaturated conditions. The system reacted to this addition by initially raising the phosphate

concentration to the level at the end of the first addition, but then phosphate concentration dropped to very low levels. Again, a rapid pH rise occurred as the solution reacted.

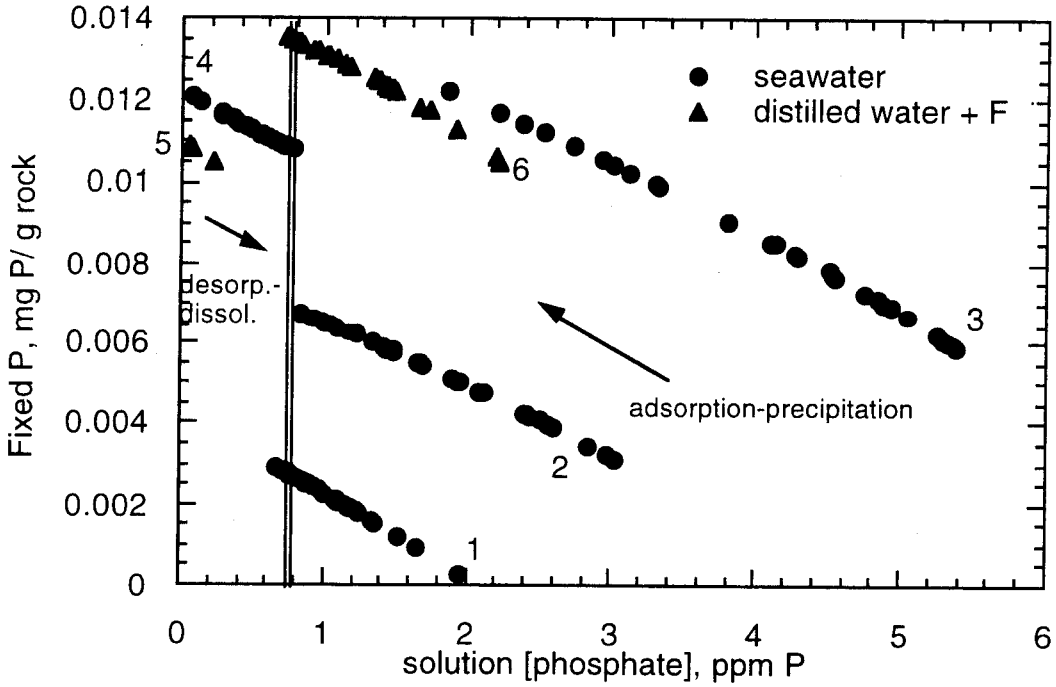

Figure 28. Phosphorous removed by the rock is plotted against solution phosphate concentration for the Column 1 experiment. The numbers are referred to in the text.

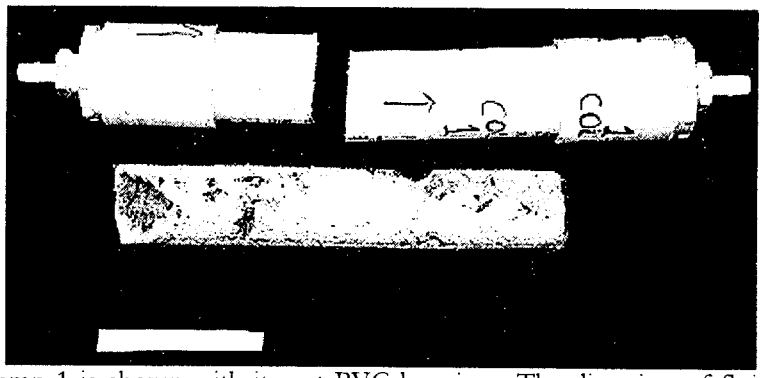

Figure 29. Column 1 is shown with its cut PVC housing. The direction of fluid flow was from left to right, note the large yellow spot where fluid entered the column. Scale bar is 10 cm long.

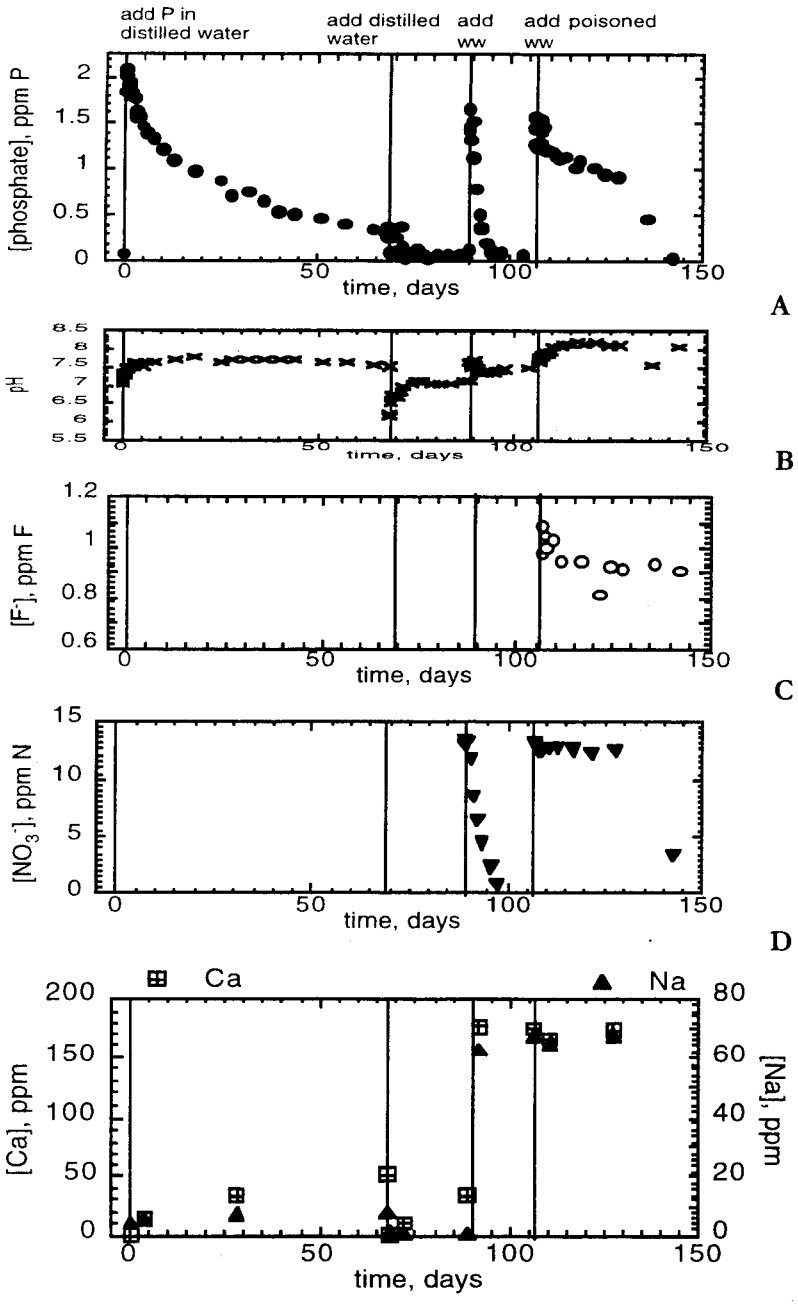

Figure 30. The solution phosphate (A), pH (B), fluoride (C), nitrate (D) along with total calcium and sodium (E) through the Column 2 experiment are shown. The vertical lines, labeled at the top, give the time when changes to the solution were made

Next, the column was drained and wastewater was added to investigate the reaction of phosphate in a wastewater matrix. The subsequent uptake of phosphate was quite rapid (Figure 30 A) and coincided with a rapid drop in the nitrate concentration (Figure 30 D). This, along with green growth observed in the experimental tubing, showed that the phosphate uptake was due to biological activity. The ratio of nitrate to phosphate uptake was 19.9, which is close to the average ratio of nitrogen to phosphorous in phytoplankton of 16 (Anderson and Sarmiento, 1994). Thus, the uptake of nitrate and phosphate in the wastewater solution was probably due to algal growth.

For the last addition to Column 2, wastewater poisoned with $HgCl_2$ was reacted in an attempt to observe the uptake of wastewater-phosphate by the KLL without biological activity. During the first twenty days this solution reacted phosphate uptake occurred, while the nitrate concentration in the solution remained fairly constant (Figure 30 D) which suggest algal growth did not occur. However, after twenty days the phosphate and nitrate concentrations dropped abruptly; the ratio of N removed to P removed was approximately 24. Additionally, an unusually low pH was measured and the solution appeared cloudy. Apparently, after an approximately twenty-day lag time, algae were able to resume growth in the mercury solution. Preventing biological activity from interfering with the phosphate-rock interaction proved difficult in the wastewater solutions. Because of the biological activity that occurred in the Column 2 experiment, the amount of phosphate adsorbed onto the KLL of Column 2 cannot be determined.

Although biological activity disrupted the poisoned wastewater addition twenty days after it began the relationship between phosphate and fluoride in the earlier part of the reaction can be interpreted. Phosphate concentrations dropped throughout the first twenty days, quickly during the first three days and then slowly between three and twenty days as observed when other solutions were reacted in the experiments. Fluoride uptake only occurred during the first five days after the poisoned wastewater addition (Figure 30 C). This brief period of fluoride uptake is similar to fluoride uptake observed in the distilled water solution reacted at the end of the Column 1 experiment. The ratio of fluoride immobilized to phosphorous immobilized in this during the first twenty days of after wastewater addition is 0.408. This F/P ratio is within the range of CFAs synthesized by Gulbrandsen et al. (1984) (F/P ratio of 0.214) and Janke (1984) (F/P ratios of 0.38-0.42).

During the first half of the Column 2 experiment, distilled water solutions were reacted. Figure 30 E shows the concentrations of calcium and sodium against time during the Column 2 experiment (data Appendix G). After the first addition of phosphate to distilled water, calcium and sodium concentrations rise as the solution reacts with the limestone, presumably as the result of calcite and salt dissolution or through the release of adsorbed sodium. The same behavior was observed during the distilled water desorption-dissolution phase of the experiment. In contrast to the distilled water solutions, the wastewater contains sufficient calcium and sodium to mask any release of these ions from the KLL (Figure 30 E). The magnesium and potassium results show similar trends.

Contrary to the Column 1 experiment, the KLL of the Column 2 experiment showed no obvious alteration when examined after the conclusion of the experiment. The differences could result from the fact that the KLL of Column 1 was reacted with more phosphate for a longer time period, or that the Column 1 experiment was conducted in (for the most part) high-calcium seawater solutions with concentrations of 400 to 500 ppm Ca.

DISCUSSION

KINETICS OF THE PHOSPHATE-KLL INTERACTION

The phosphate data from the Column 1 experiment were fit to different rate laws, but it was found that no rate law could accurately describe both the initial period of rapid reaction and the slower later period of reaction. However, both periods of uptake agreed well with separate second order rate laws. This is given by the equation:

$$d[PO_4^{3-}]/dt = -k[PO_4^{3-}]^2 \qquad (9)$$

where: $[PO_4^{3-}]$ = phosphate concentration (ppm P)

t = time, days

k = rate constant (1/ppm P/day)

The linear form of the solution to this equation is:

$$1/[PO_4^{3-}]_t = kt + 1/[PO_4^{3-}]_0 \qquad (10)$$

where: $[PO_4^{3-}]_t$ = phosphate concentration at time t (ppm P)

$[PO_4^{3-}]_0$ = phosphate concentration at time 0 (ppm P)

The data was fit to second order rate laws by plotting the inverse of the phosphate concentration on the abscissa against time. The linear regression of this plot is in the form of equation 10, with a slope equal to the rate constant, k.

For the column 1 experiment, the initial rapid first reaction described the first two to five days of reaction, while the second slower reaction described later phosphate uptake (Figure 31 A). The correlation coefficients for the linear plot shows that data fit the second order rate expressions reasonably well (Table 13). The data for the seawater desorption phase of the experiment yield negative rate constants since phosphate was released rather than removed (Figure 31 B). The averages of the rate constants show a large scatter, but generally the rate constants of the first reaction are an order of magnitude larger than the rate constants of the second reaction (Table 13).

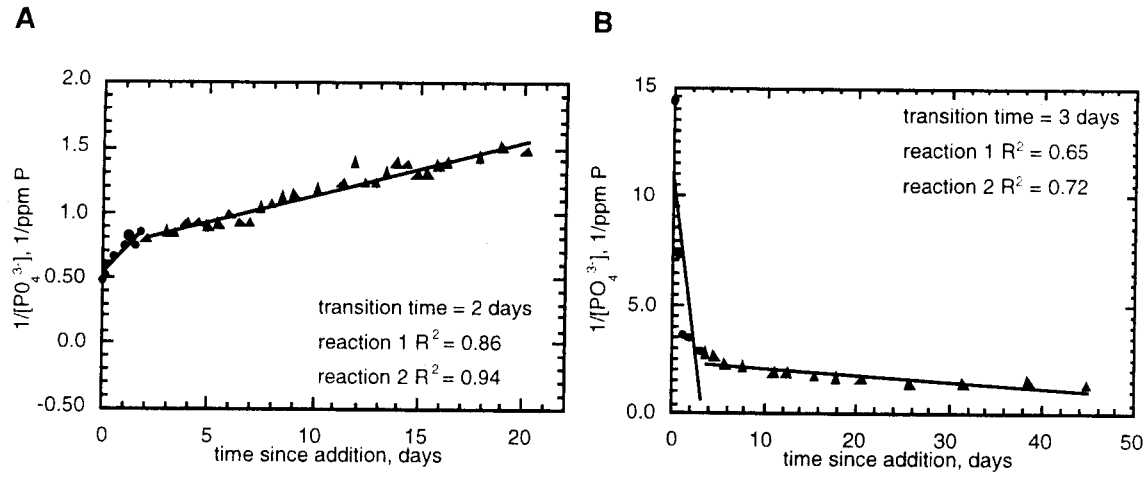

Figure 31. The data for the first seawater phosphate addition (A) and the seawater desorption phase (B) of the Column 1 experiment are plotted here as second-order reactions.

Table 13. Kinetic constants for the Column 1 experiment is shown along with the length of time during which reaction 1 occurred and the correlation coefficient for second order plot (as in Figure 31).

	Reaction 1 k, (ppm P*day)$^{-1}$	Reaction 1 R^2	Length of Reaction 1, days	Reaction 2 k, (ppm P*day)$^{-1}$	Reaction 2 R^2
first SW addition	0.18	0.86	2	0.041	0.94
second SW addition	0.33	0.82	2	0.011	0.99
third SW addition	0.0077	0.64	5	0.0039	0.99
desorption	-3.4	0.65	3	-0.030	0.72
DI with F addition	0.13	0.82	2	0.013	0.84
Average ± Std. Dev.	0.2 ± 0.1*			0.02 ± 0.01#	

* desorption not included #opposite of desorption included

For the Column 2 experiment, the data for the distilled water phosphate addition and the poisoned wastewater addition were also fit to second-order rate laws (Figure 37, Table 14). Only a single second-order rate constant was needed to describe the distilled water addition

kinetics (Figure 32 A); this yielded a rate constant similar to that of Phase 2 in the Column 1 experiment. The results for the poisoned wastewater addition were more similar to the Column 1 experiment; although the data for the beginning of this addition are quite scattered and did not fit any rate law well (Figure 32 B). However, the later data fit well to a second order rate law similar to the Phase 2 of the Column 1 experiment. Unfortunately this reaction did not reach equilibrium before being disrupted by the onset of biological activity after twenty days. However, given the kinetic similarity between the rate constant for the second reaction of this addition and those of the Column 1 experiment, it is reasonable to assume that the poisoned wastewater solution would have reached a similar equilibrium if given enough time.

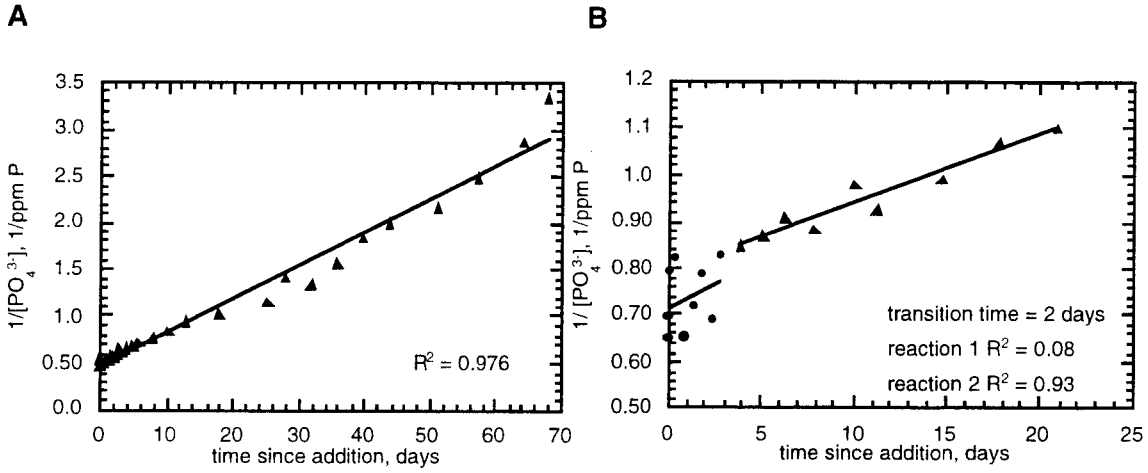

Figure 32. The data for the first phosphate addition (A) and the poisoned wastewater addition (B) to the Column 2 experiment are plotted as second-order reactions.

Table 14. Kinetic constants for the Column 2 experiment along with the length of time during which reaction 1 occurred and the correlation coefficient for each plot (as in Figure 32).

	Reaction 1 k, (ppm P*day)$^{-1}$	Reaction 1 R^2	Length of Reaction 1, days	Reaction 2 k, (ppm P*day)$^{-1}$	Reaction 2 R^2
first DI addition	N.A	na	na	0.036	0.98
poisoned WW addition	0.018	0.080	3	0.015	0.93

It is unknown why these reactions empirically fit second-order rate laws. The need for two separate kinetic equations to accurately describe the phosphate uptake demonstrates that there are two sequential reactions removing phosphate. The processes most likely responsible for this two-stage uptake are discussed in the next section.

PHOSPHATE PRECIPITATION

The phosphate kinetics suggests that two reactions occurred with respect to phosphate during the experiments. The Column 1 experiment repeatedly approached the same equilibrium phosphate concentration after each phosphate addition (Figure 28). This implies that a precipitation reaction occurred that determined the equilibrium concentration. The alkalinity and major ion data collected was not comprehensive enough to characterize the precipitate or precipitates formed. Instead, potential precipitates were identified by calculating the saturation states of calcium phosphate phases (Table 15) that other researchers reported had formed through calcite-limestone interaction in the experimental solution. A phase that found to be saturated after the phosphate solutions reacted could be identified as a likely precipitate. Because of the high magnesium concentration of the seawater solutions, four magnesium phosphates were also included. Table 15 lists the dissolution equation for each phase and the log of the equilibrium constant (K_{eq}) for that reaction. The references used for the solubility constants for crystalline phosphate phases (CFA, DCP, DCPD, DMPT, FA, HA, OCP, TMP, and TMT) were chosen based on those in the compilation of thermodynamic data for phosphate minerals by Viellard and Tardy (1984). These are well established and others have found similar results. However, the solubilities of the amorphous phases (ACP1, ACP2) of Christoffersen et al. (1990) are based on only one study.

The geochemical speciation code PHREEQC was used to calculate the saturation indices of the phosphate phases (Table 15) for each sample analyzed for calcium, magnesium, potassium, and sodium. These concentrations along with the phosphate results were written into PHREEQC input files for each sample. Fluoride and pH results were also included; if they were not measured then results for the nearest sample in time were used. The alkalinity measured for each solution drained from the column was used for samples taken while that solution reacted (data Appendices F and G). Since very few alkalinity measurements were made, the approximation of using these measurements for many samples is a potential source of error. Another source of potential error is that the chloride and sulfate concentrations written into each input file were estimated by multiplying the sodium concentration by the ratio of that element's concentration to sodium in seawater (Millero and Sohn, 1992). The input files for PHREEQC were also written so that the chloride concentration was adjusted to maintain a charge balance. The PHREEQC output files for each sample gives the saturation indices (according to equation 7) for each phase, along with the concentration of each aqueous species and complex.

PHREEQC calculates the activity of species using the Truesdell and Jones equation (Parkhurst, 1985) which is appropriate for a range of ionic strength from zero to approximately two moles/kg, but is most accurate at low ionic strength (Langmuir, 1997). To check the results of PHREEQC at seawater ionic strength of 0.7, the saturation index of calcite in three column samples in a seawater matrix were calculated according to the method of seawater apparent equilibrium constants of Morse and Mackenzie (1990). In this method, the equilibrium constants for the carbonate system and calcite dissolution have been adjusted for seawater activities. The

Table 15. Solubility equations of phosphate phases which were used in calculations.

Phase	Solubility Equation	log K_{eq}	Source
Amorphous Calcium Phosphate 1 (ACP1)	$Ca(PO_4)_{0.74}H_{0.22}(s) = Ca^{2+}(aq) + 0.74PO_4^{3-}(aq) + 0.22H^+(aq)$	-10.64	Christoffersen et al., 1990
Amorphous Calcium Phosphate 2 (ACP2)	$Ca(PO_4)_{0.74}H_{0.22}(s) = Ca^{2+}(aq) + 0.74PO_4^{3-}(aq) + 0.22H^+(aq)$	-11.47	Christoffersen et al., 1990
Anhydrous Trimagnesium Phosphate (ATMP)	$Mg_3(PO_4)_2(s) = 3Mg^{2+}(aq) + 2PO_4^{3-}(aq)$	-23.28	Racz and Soper, 1968
Carbonate Fluorapatite (CFA)	$Ca_{9.54}Na_{0.33}Mg_{0.13}(PO_4)_{4.84}(CO_3)_{1.27}F_{2.48}(s) = 9.54Ca^{2+}(aq) + 0.33Na^+(aq) + 0.13Mg^+(aq) + 4.84PO_4^{3-}(aq) + 1.27CO_3^-(aq) + 2.48F^-(aq)$	-121	Chien and Black, 1976
Dimagnesium Phosphate Trihydrate (DMPT)	$MgHPO_4 \cdot 3H_2O(s) = Mg^{2+}(aq) + HPO_4^{2-}(aq) + 3H_2O(l)$	-5.83	Racz and Soper, 1968
Dicalcium Phosphate (DCP)	$CaHPO_4(s) = Ca^{2+}(aq) + HPO_4^{2-}(aq)$	-6.66	Lindsay and Moreno, 1960
Dicalcium Phosphate Dihydrate (DCPD)	$CaHPO_4 \cdot 2H_2O(s) = Ca^{2+}(aq) + HPO_4^{2-}(aq) + 2H_2O(l)$	-6.56	Moreno et al., 1960 a
Fluorapatite (FA)	$Ca_5(PO_4)_3F(s) = 5Ca^{2+}(aq) + 3PO_4^{3-}(aq) + F^-(aq)$	-59.6	McCann, 1968
HYDOXYLAPATITE (HA)	$Ca_{10}(PO_4)_6(OH)_2(s) = 10Ca^{2+}(aq) + 6PO_4^{3-}(aq) + 2OH^-(aq)$	-114	Brown, 1960*
Octocalcium Phosphate (OCP)	$Ca_4H(PO_4)_3(s) = 4Ca^{2+}(aq) + H^+(aq) + 3PO_4^{3-}(aq)$	-46.9	Moreno et al., 1960 b
TRIMAGNESIUM PHOSPHATE 22-HYDRATE (TMT)	$Mg_3(PO_4)_2 \cdot 22H_2O(s) = 3Mg^{2+}(aq) + 2PO_4^3(l) + 22H_2O(l)$	-23.7	Racz and Soper, 1968
Trimagnesium Phosphate Octahydrate (TMO)	$Mg_3(PO_4)_2 \cdot 8H_2O(s) = 3Mg^{2+}(aq) + 2PO_4^3(l) + 8H_2O(l)$	-25.2	Taylor et al., 1963

* in PHREEQC internal database (Parkhurst, 1995)

three calculated saturation indices were 0.10, 0.34, and 0.68, while corresponding saturation indices calculated by PHREEQC were 0.06, 0.26, and 0.63. The hand-calculated saturation indices are all only slightly larger than those calculated using PHREEQC. The error using PHREEQC was considered negligible and it was used to calculate the speciation of the seawater samples.

The results of the PHREEQC calculations show that none of the crystalline phases in Table 15 controlled the equilibrium phosphate concentrations observed in the experiments. The crystalline magnesium phosphates were undersaturated in all of the solutions. This was also the case for the crystalline calcium phosphates DCP, DCPD, and OCP. At the opposite end of the spectrum the apatite minerals CFA (saturation indices from 17.55 to 28.92) and fluorapatite (saturation indices 7.63 to 13.32) were extremely supersaturated in all samples with fluoride and thus also out of equilibrium. The fluoride results indicate that these minerals did not precipitate.

ACP2 was the phase that PHREEQC calculated as closest to equilibrium. ACP2 is an amorphous phosphate that homogeneously precipitated by Christoffersen et al. (1990), who determined its solubility. After each phosphate solution was reacted in the experiment, whether it was in seawater, distilled water, or wastewater, ACP was slightly undersatured (Table 16). According to the PHREEQC calculations, calcite was also near saturation after each solution reacted (Table 16). These results show a phase similar to ACP2 may be responsible for the equilibrium concentration observed after each solution reacted.

Table 16. Saturation indices calculated by PHREEQC of ACP2, CBP, and calcite after each solution was reacted in Experiment 1 and 2.

Experiment	Solution Reacted	ACP2 Saturation Index	Calcite Saturation Index
1	first SW phosphate addition	-0.56	0.29
	second SW phosphate addition	-0.67	0.06
	third SW phosphate addition	-0.12	0.40
	seawater desorption	-0.24	0.61
	DI with F and phosphate addition	-0.71	-0.13
2	first DI phosphate addition	-0.92	-0.08
	DI desorption	-1.59	-0.68
	poisoned WW addition	-0.21	0.48

The PHREEQC calculations also show that the pH rise observed after solutions were added to Column 1 and 2 are likely the result of the equilibration of the carbonate system with the solutions (Figures 27 B, 30 B). The speciation results for carbon dioxide are most accurate

for those samples whose alkalinities measured, the large-volume samples collected when the columns were drained. These solutions were speciated by PHREEQC, which also calculated the saturation for carbon dioxide (according to equation 7 except a gas dissolves into the solution instead of a mineral). The results show that the solutions were undersaturated with carbon dioxide even after weeks of reacting with the limestone (Table 17). Thus, the pH rise observed after each solution was added could be the adjustment of the carbonate system in to approach equilibrium with respect to carbon dioxide.

Table 17. PHREEQC calculations of the carbon dioxide saturation of solutions after they were reacted in one of the two experiments and drained from the system.

Experiment	Reacted Solution Drained	Date Drained	CO_2 Saturation Index	$[CO_2]$, mmoles/l
Column 1	third seawater phosphate addition	1/6/1999	-3.24	0.0016
Column 1	low phosphate seawater	2/24/1999	-3.30	0.0014
Column 1	phosphate and fluoride in distilled water	4/27/1999	-2.99	1.54
Column 2	phosphate in distilled water	2/28/1999	-2.35	0.15
Column 2	phosphate-free distilled water	3/17/1999	-2.01	0.33

A two-phase phosphate uptake was observed in the experiments. The saturation state calculations show that the second period of uptake is most likely due to precipitation of an amorphous phase similar to ACP2. The initial rapid uptake observed could be through the rapid formation of a metastable phase, but also through phosphate adsorption. Many researchers have observed an initial rapid uptake of phosphate onto calcite, which they attribute to adsorption (Freeman and Rowell, 1981; Brown, 1980; Kitano et al., 1978; Griffin and Jurinak, 1974 and 1973; Stumm and Leckie, 1970). These same authors also observed, as in this study, a second slower precipitation reaction. Avnimelech (1980) formed a calcium-bicarbonate-phosphate surface complex through phosphate interaction with calcite. The formation and adsorption of this complex could be how the initial phosphate uptake occurs. Although the mechanism of the initial phosphate uptake observed in the column experiments is unknown, a comparison of the experimental results to the literature suggests adsorption is the most likely mechansism.

The poorly-characterized phosphate precipitate that formed during the second phase of the experiment is not a stable phase; thus, the equilibrium observed is a metastable equilibrium. At the end of each reaction period, all solutions were supersaturated with the more stable apatite minerals. The order of these phases in increasing degree of supersaturation and thermodynamic stability is hydroxylapatite, fluorapatite, and carbonate fluorapatite. This is also the order that they would form from the experimental solution, since more soluble phases precipitate first (Steffel and Van Cappellen, 1990). Given a longer period to react, the amorphous calcium phosphate that presumably formed on the limestone would have converted to a more stable phase with a lower equilibrium phosphate concentration, as in the work of

Gulbrandsen et al. (1983), Stumm and Leckie (1970), and Griffin and Jurinak (1974). However, the formation of apatite is kinetically slow; it took ten years for carbonate fluorapatite to form in phosphate and fluoride-enriched seawater through precursors on a calcite seed in the experiments of Gulbrandsen et al (1983).

EXTRAPOLATION OF COLUMN RESULTS TO THE FIELD DATA

Phosphate removal in the experiments occurred through an initial rapid removal of phosphate, followed by the slower formation of a precipitate that reached a metastable equilibrium. It is likely that sequential uptake reactions of wastewater-phosphate occur in the groundwater of KCB. The phosphate distribution observed during the March and June 1998 sampling campaigns was after five years of wastewater injection at KCB and phosphate mobility is low. Thus, the precipitation mechanism is effective at removing phosphate. As wastewater flows out from the injection wells, its phosphate concentration drops due adsorption and the precipitation of metastable phases, such as an amorphous calcium phosphate. Metastable phases generally form rapidly at higher degrees of saturation first (Steffel and Van Cappellen, 1990). Further away from the injection wells these phases become undersaturated (Figure 36) and more stable phases, hydroxylapatite and carbonate fluorapatite, are more likely to crystallize directly and further remove phosphate from the wastewater. Given that more insoluble phases will form when groundwater phosphate concentrations around the wastewater wells decrease, it is unlikely much precipitated phosphate can become remobilized.

CONCLUSIONS OF EXPERIMENTAL WORK

- When solutions enriched with phosphate were reacted with columns of Key Largo Limestone, two periods of phosphate uptake were observed. The first was a rapid uptake lasting two to five days, while the second slower uptake proceeded to equilibrium. In seawater solutions, the equilibrium concentration was approximately 0.8 ppm-P; this equilibrium was also reached from undersaturated conditions. When distilled water solutions were reacted with the limestone, phosphate uptake proceeded in the same manner, although the same equilibrium concentration was not always reached. The reaction of phosphate in a wastewater solution poisoned with $HgCl_2$ also occurred in the same mode, but the reaction was interrupted by biological activity before reaching equilibrium. The two stages of phosphate uptake fit separate second-order reactions and are due to two different reactions.

- The initial uptake resulted from either phosphate precipitation or adsorption. The second, slower reaction reached equilibrium with a metastable phosphate phase. Saturation state calculations show that an amorphous calcium phosphate phase is the most likely precipitate formed during the second reaction. The equilibrium concentration observed is metastable. If the solutions had been

allowed to react with the limestone longer, less soluble phases might have formed in the order of decreasing supersaturation: hydroxylapatite, fluorapatite, and carbonate fluorapatite.

CONCLUSIONS AND DIRECTIONS OF FUTURE WORK

OVERALL CONCLUSIONS

At Key Colony Beach, one of the largest wastewater injection sites in the Florida Keys, phosphate concentrations in the dominant flow direction were found to be reduced to between 40 to 28 percent of the wastewater concentration within 15 meters of injection. Wastewater-derived water has formed a large plume in the Key Largo Limestone underneath the carbonate mud layer. The horizontal extent of this plume is unknown because it extends beyond the monitoring wells in all directions, but it reaches outwards from the main injection wells at least 30 m to the east, 80 m to the west, 70 m to the north, and 80 m to the south.

Batch-type column experiments have shown that phosphate concentration is reduced from an initial concentration of 3.14 to 1.41 ppm P to a metastable equilibrium of 0.8 to 0.3 ppm P over a period of twenty to seventy days through interaction with the Key Largo Limestone in saline, low-salinity, and wastewater solutions. Thus, wastewater-limestone interaction can account for the phosphate uptake observed in the groundwater of Key Colony Beach.

The column experiments show phosphate removal can be attributed to uptake onto the Key Largo Limestone surface. The stable mineral carbonate fluorapatite was not synthesized in the experiments, metastable precipitates formed instead. Two sequential reactions occurred that fit separate second-order rate laws with respect to phosphate. The initial reaction lasted two to five days and rapidly removed phosphate, through adsorption or a precipitation reaction. The second slower reaction was caused by the precipitation of a phosphate phase that reached metastable equilibrium. Saturation state calculations indicate that an amorphous calcium phosphate phase probably controlled the equilibrium phosphate concentration. If the solutions had been allowed to react with the limestone longer, less soluble phases might have formed in the order of decreasing supersaturation: hydroxylapatite, fluorapatite, and carbonate fluorapatite.

This study has shown that phosphate is largely removed from wastewater injected into the Key Largo Limestone through interaction with the limestone. Thus, less phosphate is bioavailable when wastewater that has been disposed of into the groundwater discharges into canals or other surface waters. Experiments show that this phosphate removal occurs through precipitation of a metastable phase, and it is unlikely that the removed phosphate will become remobilized. The wastewater-phosphate loading of surface waterbodies surrounding wastewater injection wells is greatly decreased due to phosphate uptake by the Key Largo Limestone.

FUTURE WORK

FUTURE WORK AT KEY COLONY BEACH

At the field site the geometry of the wastewater plume and the wastewater flowpaths along with the fate of wastewater nitrogen should be further constrained to understand the impact of wastewater disposal. Salinity and nutrient results from wells recently installed by Griggs et al. (unpub. data) should further constrain the geometry of this anthropogenic freshwater lens. Nitrate was found to be the more mobile of the two dominant nutrient species in KCB wastewater, nitrate and phosphate. The fate of this nitrate was not a focus of this study. However, determining the mechanism and effectiveness of nitrate removal, along with its potential discharge to nearby canals is needed for a complete understanding of the ecological impact of wastewater disposal into the KLL.

FUTURE EXPERIMENTAL WORK

Further work is needed to characterize the phosphate precipitates formed during the experiments. Experiments of a longer duration would also be useful in understanding if and when more stable precipitates would form such as hydroxylapatite, fluorapatite, and carbonate fluorapatite. Also, examinations of the reacted surface should be conducted.

An investigation of the phosphate bound to the reacted limestone presents some challenges. First, those elements that are potential components of possible secondary phases are also components of the limestone substrate: calcium, carbonate, phosphate, and fluoride. The solubility calculations presented in this work suggest that those phases that most likely formed are poorly to non-crystalline, so they can not be identified by X-ray diffraction. Furthermore, the amount of phosphate taken up by each column was small; Column 1 immobilized only about 12.6 mg during the course of the experiment, and Column 2 removed between 2.7 and 5.35 mg phosphorous. Because of these factors, bulk analyses are not sufficient to determine the form of phosphate on the KLL; an analysis of the reacted surface is required.

To examine the reacted limestone surface, a scanning electron microscope (SEM) equipped with an energy dispersive spectrometer could be used to map the relative concentration of phosphorous, while x-ray photoelectron spectroscopy (XPS) could be used to determine quantitative Ca/P ratios on the surface. This is similar to the approach Salingar and Kochva (1994) used to study powdered calcite with CBP overgrowths. SEM is a valuable tool for imaging surfaces and it has the large depth of field necessary to image the rough surface of the KLL (McIntyre et al., 1995). EDS often complements SEM on the same machine; EDS can be used to get relative concentrations of elements across the surface of a sample, even in rough areas (McIntyre et al., 1998). However, for quantitative analysis by EDS or XPS, a smooth surface is desirable (Reed, 1996). A polished section of the reacted core material could be analyzed with XPS. The section could be cut and polished as a cross-section through the reacted surface. In this procedure, a sample of the column material containing some of the outer surface would be impregnated with a low-viscosity cold-setting epoxy under moderate vacuum (Reed, 1996). After hardening, this section could be polished smooth as a cross-section through the surface. The XPS could give quantitative ratios of Ca/P ratios across this polished section and show if Ca/P ratios decrease towards the surface. Also EDS could be used to generate a map of relative phosphate concentration across the polished section. This would also determine if surface phosphate enrichment was uniform across the surface or confined to patches of overgrowth. Such an examination of the reacted surfaces of the columns would aid in interpreting the mode of phosphate uptake, and test the conclusion that a secondary amorphous calcium phosphate has formed.

REFERENCES

American Public Health Association. (1985) Standard Methods for the Examination of Water and Wastewater, 16th Edition. AHPA.

Ames L.L. (1959) The genesis of carbonate apatites. Economic Geology **54**, 829-841.

Anderson L.A. and Sarmiento J.L. (1994) Redfield ratios of remineralization determined by nutrient data analysis. Global Biogeochemical Cycles. **8**, 65-80.

Avnimelech Y. (1980) Calcium-carbonate-phosphate surface complex in calcareous systems. Nature **288**, 255-257.

Berner R. A. and Morse J.W. (1974) Dissolution kinetics of calcium carbonate in sea water IV. Theory of calcite dissolution. American Journal of Science **274**, 108-134.

Bodkin, J.B. (1977) Determination of fluorine in silicates by use of an ion-selective electode following fusion with lithium metaborate. The Analyst **102**, 409-413.

Bohlke J.K., Plummer L.N., Busenberg E., Coplen T.B., Shinn E.A., and Schlosser, P.L. (1997) Origins, Residence times, and nitrogen chemistry of marine ground waters beneath the Florida Keys and nearby offshore areas. In U.S. Geological Survey Program on the South Florida Ecosystem- Proceedings of the Technical Symposium in Ft. Lauderdale, Florida, August 25-27, 1997, pp. 6-7. USGS Open-File Report 97-385.

Broecker W.S., Peng T.H. (1992) Tracers in the Sea. pp. 26-27. Lamont-Doherty Geological Observatory.

Brown J.L. (1980) Calcium phosphate precipitation in aqueous calcitic limestone suspensions. Journal of Environmental Quality **9**, 641-644.

Brown W.E. (1960) Behavior of slightly soluble calcium phosphate as revealed by phase-equilibrium calculations. Soil Science **90**, 51-57.

Chalemet A. (1985) Effects of environmental factors on denitification. In Denitrification in the Nitrogen Cycle. (ed. H.L. Golterman), pp. 7-29. Plenum Press.

Chiappone M. (1996) Site Characterization for the Florida Keys and Environs, Volume 1: Geology and Paleontology of the Florida Keys and Florida Bay, pp. 6. The Preserver.

Chien, S.H. and Black C.A. (1976) Free energy of formation of carbonate apatites in some phosphate rocks. Soil Science Society of America Journal **40**, 234-239.

Christoffersen M.R., Christoffersen J., and Kibalczyc W. (1990) Apparent solubilities of two amorphous calcium phosphates and of octacalcium phosphate in the temperature range 30-42°C. Journal of Crystal Growth **106**, 349-354.

Coniglio M. and Harrison R.S. (1983) Holocene and Pleistocene caliche from Big Pine Key, Florida. Bulletin of Canadian Petroleum Geology **31**, 3-13.

Craig H. (1957) Isotopic standards for carbon and oxygen and correction factors for mass-spectrometric analysis of carbon dioxide. Geochemica et Cosmochemica Acta **12**. 133-149.

Craig, H. and Gordan L.I. (1965) Deuterium and oxygen 18 variations in the ocean and the marine atmosphere. In Stable Isotopes in Oceanographic Studies and Paleotemperatures. (ed. E. Tongiorgi), pp. 9-130. Consiglia Nazionale Delle Ricerche Laboratorio Di Geologia Nucleare.

Cullen D.J. (1980) Distribution, composition and age of submarine phosphorites on Chatham Rise, East of New Zealand. In Marine Phosphorites. (ed. Y. K. Bentor), pp. 139-152. SEPM Special Publication 29.

Cunningham K.J., McNeill D.F, Guertin J.A., Ciesielski P.F., Scott T.M., and de Verteuil L. (1998) New Tertiary stratigraphy for the Florida Keys and southern peninsula of Florida. Geological Society of America Bulletin **110**, 231-258.

Custodio E. (1987) Salt-fresh water interrelationships under natural conditions. In Groundwater problems in coastal areas (ed. E. Custodio and G.A. Bruggeman), pp. 14-96. Unesco Studies and Reports in Hydrology 45.

Deines P. (1970) Mass spectrometer correction factors for the determination of small isotopic composition variations of hydrogen and oxygen. Inter. J. of Mass Spectrometry and Ion Physics **4**, 238-295.

DeKanel J. and Morse J.W. (1978) The chemistry of orthophosphate uptake from seawater onto calcite and aragonite. Geochimica et Cosmochimica Acta **42**, 1335-1340.

Dunham R.J. (1962) Classification of carbonate rocks according to depositional texture. In Classification of carbonate rocks. (ed. W.E. Ham), pp. 108-121. Memoir American Association of Petroleum Geologist 1.

Enos P. and Sawatsky L.H. (1981). Pore networks in carbonate sediments. Journal of Sedimentary Petrology **51**, 961-985.

Enos P. (1977) Holocene sediment accumulations of the South Florida Shelf Margin. In Quaternary Sedimentation in South Florida (ed. P. Enos and R.D. Perkins), pp. 1-130. Geology of Society of America Memoir 147.

Epstein S. and Mayeda T. (1953) Variation of O^{18} content of waters from natural sources. Geochemica et Cosmochemica Acta **4**. 213-224.

Feiner S.J. (1991) City of Key Colony Beach. In The Monroe County Environmental Story (ed. J. Gato), pp. 204-205. The Monroe County Environmental Education Task Force.

Fölmi K.B. (1996) The phosphorus cycle, phosphogenesis and marine phosphate-rich deposits. Earth-Science Reviews **40**, 55-124.

Fouqurean J.W., Zieman J.C., and Powell G.V.N. (1992) Relationships between porewater nutrients and seagrasses in a subtropical carbonate environment. Marine Biology **114**, 57-65.

Freeman J.S. and Rowell D.L. The adsorption and precipitation of phosphate onto calcite. Journal of Soil Science **32**, 75-84.

Freeze R.A. and Cherry J.A. (1979) Groundwater. pp. 400-401. Prentice Hall.

Froelich P.N., Arthur M.A., Burnett W.C., Deakin M., Hensley V., Jahnke R., Kaul L., Kim K.-H., Roe K., Soutar A., and Vathakanon C. (1988) Early diagenesis of organic matter in Peru continental margin sediments: phosphorite precipitation. Marine Geology **80**, 309-343.

Gallagher D. (1991) Impact of the built environment of the natural environment of the Florida Keys. In The Monroe County Environmental Story (ed. J. Gato), pp. 226-228. The Monroe County Environmental Education Task Force.

Golterman H.L. (1985) Denitrification: appraisal and concluding remarks. In Denitrification in the Nitrogen Cycle (ed H.L. Golterman), pp. 1-6. Plenum Press.

Griffin R.A. and Jurinak J.J. (1974) Kinetics of the phosphate interaction with calcite. Soil Science Soc. of America Proc. **38**, 75-79.

Griffin R.A. and Jurinak J.J. (1973) The interaction of phosphate with calcite. Soil Science Soc. of America Proc. **37**, 847-850.

Gulbrandsen R.A., Roberson, C.E. and Neil S.T. (1984) Time and crystallization of apaptite in sewater. Geochemica et Cosmochimica Acta. Geochimica et Cosmochimica Acta **48**, 213-218.

Halley R.B., Vacher H.F., and Shinn E.A. (1997) Geology and hydrogeology of the Florida Keys. In Geology and Hydrology of Carbonate Islands. (ed. H.L. Vacher, and T. Quinn T), pp. 217-248. Developments in Sedimentology 54.

Hanson C.F. (1980) Water resources of Big Pine Key, Monroe County, Florida. U.S.G.S. Open-File Report 80-447.

Harrison R.S. and Coniglio M. (1985) Origin of the Pleistocene Key Largo Limestone, Florida Keys. Bulletin of Canadian Petroleum Geology **33**, 350-358.

Henry J.A., Portier K.M, and Coyne J. (1994) The Climate and Weather of Florida. pp. 23. Pineapple Press.

Hoffmeister J.E. and Multer H.G. (1968) Geology and origin of the Florida Keys. Geological Society of America Bulletin **79**, 1487-1502.

Horita J., Cole D.R., and Wesolowski D.J. (1993) The activity-composition relationship of oxygen and hydrogen isotopes of mixed salt solutions from 50 to 100°C and geochemical implications. Geochimica et Cosmochimica Acta. **57**, 4703-4711.

House W.A. and Donaldson L. (19860 Adsorption and coprecipitation of phosphate on calcite. Journal of Colloid and Interface Science **112**, 309-324.

Isenbeck-Schröter M., Döring U., Möller A., Schröter J., and Mattheß G. (1993) Experimental approach and simulation of the retention process limiting orthophosphate transport in groundwater. Journal of Contaminant Hydrology **14**, 143-161.

Kitano Y., Okumura M., and Idogaki M. Uptake of phosphate ions by calcium carbonate. Geochemical Journal **12**, 29-37.

Kohout F.A. (1987) Aquifer-estuary fresh-salt water balance, Miami, Florida. In Groundwater Problems is Coastal Areas. (ed. E. Custodiao, E and G.A. Bruggman), pp. 249-272. Unesco Studies and Reports in Hydrology 45.

J.C.P.D.S. (1992) Powder Diffraction File. J.C.P.D.S.

Jahnke R. A. (1984) The synthesis and solubility of carbonate flourapatite. American Journal of Science **284**, 558-78.

Jarvis I., Burnett W.C., Nathan Y., Almbaydin S.M., Attia A.K.M., Castro L.N., Flicoteaux R., Hilmy M.E., Husain V., Qutawnah A.A., Serjani A., and Zanin Y.N. (1994) Phosphorite geochemistry: State-of-the-art and environmental concerns. Eclogae. geol Helv. **87**, 643-700.

Juster T.C. and Vacher H.L. (1994) Permeability structure of Holocene carbonate mud sediments from Florida Bay and implications to diagenesis. Abstracts with Programs, Geological Society of America **26**, 411.

Lamboy M. (1993) Phosphatization of calcium carbonate in phosphorites: microstructure and importance. Sedimentology **40**, 43-62.

Langmiur D. (1997) Aqueous Environmental Geochemistry. pp.142. Prentice-Hall.

Lapointe B.E. (1989) Macroalgal production and nutrient relations in oligotrophic areas of Florida Bay. Bulletin of Marine Science **44**, 312-323.

Lapointe B.E. (1987) Phosphorous- and nitrogen-limited photosynthesis and growth ofGracilaria tikvalhiae (Rhodophyceae) in the Florida Keys: an experimental field study. Marine Biology **93**, 561-568.

Lapointe B.E. and Clark M.W. (1992) Nutrient inputs from the watershed and coastal eutrophication in the Florida Keys. Estuaries **15**, 465-476.

Lapointe B.E., O'Connell J.D. and Garrett G.S. (1990) "Nutrient couplings between on-site sewage disposal systems, groundwaters, and nearshore surface waters of the Florida Keys." Biogeochemistry **10**, 289-307.

Lide D.R. (ed). (1996) CRC Handbook of Chemistry and Physics, 77th Ed. CRC Press.

Lindsay W.L. and Moreno E.C. (1960) Phosphate phase equilibria in soils. Soil Science Soc. of America Proc. **24**, 99-102.

Machusak D.D. and Kump L.R. Environmental controls on groundwater chemistry in an offshore island aquifer: Fiesta Keys, Florida. Aquatic Geochemistry **3**, 129-167.

Manheim F.T., Pratt R.M., and McFarlin P.F. (1980) Composition and origin of phosphorite deposits of the Blake Plateau. In. Marine Phosphorites. (ed. Y.K. Bentor), pp. 117-137. SEPM Special Publication 29.

McCann H.G. (1968) The solubility of fluorapatite and its relationship to that of calcium fluoride. Archives of Oral Biology **13**, 987-1001.

McIntyre N.S., Davidson R.D, Hyder I.Z., and Brennunstühl A.M. (1998) Corrosion and surface analysis: an integrated approach involving spectroscopic and electrochemical methods. In. Handbook of Surface and Interface Analysis (ed. J.C. Rivière and S. Myhra), pp. 643-696. Marcel Dekker.

McKenzie D.J. (1990) Water-Resources Potential of the Freshwater Lens at Key West, Florida. U.S.G.S. Water-Resources Investigations Report 90-4115.

Millero F.J. and Sohn M.S. (1992) Chemical Oceanography. pp.70. CRC Press.

Monaghan L.B. (1996) The Hydrogeochemical Behavior of Wastewater-Derived Nutrient Elements in the Groundwaters of Long Key, Florida. MS Thesis, The Pennsylvania State University.

Moreno E.C., Brown W.E., and Osborn G. (1960a) Solubility of dicalcium phosphate dihydrate in aqueous systems. Soil Science Soc. of America Proc. **24**, 94-98.

Moreno E.C., Brown W.E., and Osborn G. (1960b) Stability of dicalcium phosphate dihydrate in aqueous solution and solubility of octocalcium phosphate. Soil Science Soc. of America Proc. **24**, 99-102.

Morse J.W. and Mackenzie F.T. (1990) The Geochemistry of Sedimentary Carbonates. pp. 26-31. Developments in Sedimentology 48.

Nathan Y. (1984) The mineralogy and geochemistry of phosphorites. In Phosphate Minerals (ed. J.O. Nriagu J.O. and P.B. Moore), pp. 275-291. Springer-Verlag.

N. O. A. A. (1995) Florida Keys National Marine Sanctuary Draft Management Plan/Environmental Impact Statement: Volume II. U. S. Government Printing Office: 1995-386-543/25601.

O'Neil J.R., Adami L.H., and Epstein S. (1975) Revised value for the ^{18}O fractionation between CO_2 and H_2O at 25°C. Journal of Research, USGS **3**, 632.

O'Neil J.R. and Truesdell A.H. (1991) Oxygen isotope fractionation studies of solute- water interactions. In Stable Isotope Geochemistry: A Tribute to Samuel Epstein. (ed. H.P. Taylor, J.R. O'Neil., and I.R. Kaplan), pp. 17-25. The Geochemical Society, Special Publication 3.

Ogden L.C., Porter J.W., Smith N.P., Szmant, A.M., Jaap W.C. and Forcucci D. (1994) A long-term interdisciplinary study of the Florida Keys seascape. Bulletin of Marine Science **54**, 1059-1071.

Ovide K. (1991) The task of delivering potable water to the Florida Keys. In The Monroe County Environmental Story (ed. J. Gato), pp. 275-276. The Monroe County Environmental Education Task Force.

Parkhurst D.L. (1995) User's Guide to PHREEQC - A Computer Program for Speciation, Reaction-Path, Advective-Transport, and Inverse Geochemical Calculations. USGS Water Resources Investigations Report 95-4227.

Perkins R.D. (1977) Depositional Framework of Pleistocene Rocks in South Florida. In Quaternary Sedimentation in South Florida (ed. P. Enos and R.D. Perkins), pp. 131-196. Geology of Society of America Memoir 147.

Racz G.J. and Soper R.J. (1968) Solubility of dimagnesium phosphate trihydrate and trimagnesium phosphate. Canadian Journal of Soil Science **48**, 265-269.

Reed, S.J.B. (1996) Electron Microprobe Analysis and Scanning Electron Microscopy in Geology. pp. 177-180. Cambridge University Press.

Rude P.D. and Aller R.C. (1991) Flourine mobility during early diagenesis of carbonate sediment: An indicator of mineral transformations. Geochimica et Cosmochimica Acta **55**, 2491-2509.

Ruttenberg K.C. (1992) Development of a sequential extraction method for different forms of phosphorous in marine sediments. Liminology and Oceanography **37**, 1460-1482.

Schomer, N.S. amd Drew, R.D. (1982) An ecological characterization of the lower Everglades, Florida Bay, and the Florida Keys. U.S. Fish and Wildlife Service FWS/OBS 82/58.1.

Schuyler, S.S. (1987) The Effects of Acid Precipitation on Two Soils of Pennsylvania. MS Thesis: The Pennsylvania State University.

Shinn E.A., Reese R.S. and Reich, CD. (1994). Fate and Pathways of Injection-Well Effluent in the Florida Keys. U.S.G.S. Open-File Report 94-276.

Shinn E.A., Reich C.D., Hickey D., and Tihansky A. (1997) Geology and hydrology of the Florida Keys: ground water flow and seepage. In U.S. Geological Survey Program on the South Florida Ecosystem- Proceedings of the Technical Symposium in Ft. Lauderdale, Florida, August 25-27, 1997, pp. 81-82. USGS Open-File Report 97-385.

Singh B. and Selhon G.S. (1978) Leaching nitrate in calcareous soils as influenced by its adsorption on calcium carbonate. Geoderma **20**, 271-279.

Steefel C.I, and Van Cappellen P. (1990) A new kinetic approach to modeling water-rock interaction: The role of nucleation, precursors, and Ostwald ripening. Geochimica et Cosmochimica Acta **54**, 2657-2677.

Stumm W. and Leckie J.O. (1970) Phosphate exchange with sediment; its role in the productivity of surface waters. Advances in Water Pollution Research **2**, III-26/1 - III-26/16.

Sullivan K.M., Chiappone M., and Lott C. (1996) Site Characterization for the Florida Keys and Environs, Volume 9: Controversites and Conservation Issues, pp. 35. The Preserver.

Swart P.L. and Kramer P.A. (1997). Geology of mud islands in Florida Bay. In Geology and Hydrology of Carbonate Islands. (ed. H.L. Vacher, and T. Quinn T), pp. 249-274. Developments in Sedimentology 54.

Swart P.K., Sternberg L.D.S.L., Steinen R. and Harrison S.A. (1989) Controls on the oxygen and hydrogen isotopic composition of the waters of Florida Bay, U.S.A. Chemical Geology (Isotope Geoscience Section) **79**, 113-123.

Taylor A.W., Frazier A.W., Gurney E.L., and Smith J.P. (1963) Solubility products of di- and trimagnesium phosphates and the dissociation of magnesium phosphate solutions. Transactions of the Faraday Society **59**, 1585-1589.

Thompson M. and Walsh J.N. (1989) Handbook of Inductively Coupled Plasma Spectometry. Champman and Hall.

UNESCO (1981) Background Papers and Supporting Data on the International Equation of State of Seawater. Unesco Technical Papers in Marine Science No. 38.

USEPA. (1996) Water Quality Protection Program for the Florida Keys National Marine Sanctuary, First Biennial Report to Congress. Office of Water, USEPA.

USEPA. (1983) Methods for Chemical Analysis of Water and Wastes. EPA-600/4-79- 020. Environmental Monitoring and Support Laboratory, USEPA.

Vacher, H.L., M.J. Wightman, and M.T. Stewart. (1992) Hydrology of meteoric diagenesis: Effect of Pleistocene stratigraphy on fresh-water lenses of Big Pine Key, Florida. In Quaternary Coasts of the US: Marine and Lacustrine Systems (ed. C.H. Fletcher III and J.F. Wehmiller), pp. 213-220. SEPM Special Publication 48.

Van Cappellen P.S. (1991) The formation of marine apatite: A kinetic study. Ph.D. Disertation, Yale University.

Viellard P. and Tardy W. (1984) Thermochemical properties of phosphates. In Phosphate Minerals (ed. J.O. Nriagu J.O. and P.B. Moore), pp. 275-291. Springer-Verlag.

APPENDIX A. SURVEY RESULTS

Table A.1. Survey conducted 6/6/1999 by L. Kump and D. Ombalski. Distances in the x and y directions are from a benchmark at a latitude 24°43'29" N and a longitude of W 81°01'18". The positive x direction is to the East; the positive y direction is to the North. Elevations are relative to N.G.V.D. and were measured at top of each piezometer pipe. The average of x and y of the three piezometers in each nest was used to generate site maps and transects.

Well	x, m	y, m	elevation, m
A-5	16.517	-72.861	1.205
A-9	16.537	-72.881	1.205
A-18	16.49	-72.905	1.205
Average A	16.515	-72.882	1.205
B-5	4.791	-70.299	1.213
B-9	4.835	-70.275	1.220
B-18	4.785	-70.285	1.222
Average B	4.804	-70.286	1.218
C-5	29.736	-66.454	1.230
C-9	29.77	-66.419	1.229
C-20	29.742	-66.422	1.229
Average C	29.749	-66.432	1.229
D-5	91.35	-49.331	1.245
D-9	91.405	-49.309	1.249
D-14	91.395	-49.332	1.248
Average D	91.383	-49.324	1.248
E-5	-13.01	-62.227	1.128
E-9	-12.974	-62.192	1.127
E-18	-13.613	-62.198	1.129
Average E	-13.199	-62.206	1.128
F-8	11.986	30.018	1.119
F-14	11.968	30.007	1.120
F18	11.992	30.057	1.117
Average F	11.982	30.027	1.119
G-5	31.97	-116.42	1.212
G-9	31.983	-116.431	1.212
G-18	32.022	-116.397	1.212
Average G	31.992	-116.416	1.212

APPENDIX B. CORE ANALYSIS

Table B.1. Percent recovery of core sections based on core length.

Depth interval, m	Percent Recovery A	Percent Recovery B	Percent Recovery C	Percent Recovery D	Percent Recovery E	Percent Recovery F	Percent Recovery G
6.1-7.6	100	10	40	80	10	70	45
7.6-9.1	40	90	19	20	0	50	60
9.1-10.7	30	80	33	50	20	40	40
10.7-12.2	50	60	10	5	40	40	40
12.2-13.7	30	65	10	45	15	60	40
13.7-15.2	28	5	30		5	30	10
15.2-16.8	100	2	30		10	5	17
16.8-18.3	5	15	20		10	15	17
18.3-19.8			10				

Table B.2. Calculated porosity based on core weight. Values in bold are porosities calculated from cores with a percent recovery of 90% or greater.

Depth interval, m	porosity A	porosity B	porosity C	porosity D	porosity E	porosity F	porosity G
6.1-7.6	0.52	0.96	0.90	0.73	0.96	0.70	0.68
7.6-9.1	0.87	0.60	0.92	0.95	1.00	0.84	0.79
9.1-10.7	0.89	0.65	0.75	0.84	0.92	0.99	0.83
10.7-12.2	0.75	0.75	0.94	0.98	0.86	0.84	0.83
12.2-13.7	0.88	0.74	0.95	0.82	0.95	0.77	0.85
13.7-15.2	0.89	0.96	0.86		0.99	0.90	0.94
15.2-16.8	0.53	0.98	0.86		0.93	0.96	0.92
16.8-18.3	0.92	0.94	0.91		0.93	0.94	0.92
18.3-19.8			0.95				

Table B.3. Chemical analysis of core material.

Core	Depth, m	SiO_2, % wt.	Al_2O_3, % wt.	Fe_2O_3, % wt.	MnO, % wt.	MgO, % wt.	CaO, % wt.	Na_2O, % wt.	K_2O, % wt.	TiO_2, % wt.	P_2O_5, % wt.	Lost on ignition, % wt.
A	7.31	0.76	0.17	0.2	BDL	0.69	55.51	0.14	0.02	0.01	0.05	34.99
A	10.36	0.17	0.03	0.07	BDL	0.69	56.45	0.05	0.01	BDL	0.04	32.18
A	13.41	0.24	0.03	0.11	BDL	0.48	56.12	0.1	0.02	BDL	0.08	32.66
A	14.93	0.34	0.1	0.12	BDL	0.46	56.18	0.05	0.03	BDL	0.02	33
A	16.46	0.27	0.04	0.07	BDL	0.49	57.01	0.07	0.01	BDL	0.04	32.83
A	17.98	0.38	0.03	0.07	BDL	0.52	56.01	0.07	BDL	BDL	0.04	31.34
C	7.31	0.2	0.02	0.1	BDL	0.52	57.19	0.03	0.02	BDL	0.02	32.95
C	10.36	0.17	0.03	0.07	BDL	0.59	55.67	0.02	0.02	BDL	0.09	32.78
C	13.41	0.21	0.03	0.13	BDL	0.41	55.97	0.07	BDL	BDL	0.06	31.51
C	16.46	0.31	0.03	0.14	BDL	0.71	55.07	0.03	BDL	BDL	0.03	33.13
C	19.51	0.42	0.02	0.25	BDL	0.59	55.45	0.09	BDL	BDL	0.02	32.74
F	7.31	0.29	0.04	0.14	BDL	0.79	55.63	0.1	BDL	BDL	0.04	33.155
F	10.36	0.23	0.03	0.19	BDL	0.42	56.83	0.05	BDL	BDL	0.04	31.19
F	13.41	0.3	0.04	0.13	BDL	0.41	55.85	0.2	BDL	BDL	0.04	36.49
F	14.93	0.3	0.04	0.05	BDL	0.32	58.51	0.13	BDL	BDL	0.08	33.75
F	16.46	0.39	0.03	0.08	BDL	0.42	58.2	0.07	0.01	BDL	0.18	31.03
G	7.31	0.59	0.18	0.06	BDL	0.66	57.65	0.06	0.01	BDL	0.03	32.24
G	10.36	0.26	0.05	0.055	BDL	0.66	57.95	0.06	BDL	BDL	0.09	31.89
G	13.41	0.22	0.04	BDL	BDL	0.31	57.19	0.2	0.03	BDL	0.05	36.82
G	16.46	0.3	0.02	0.05	BDL	0.557	57.75	0.11	0.02	BDL	0.04	34.13

Core	Depth, m	Ba, ppm	Sr, ppm	Y, ppm	Sc, ppm	Zr, ppm	Be, ppm	V, ppm	F, ppm	X-ray Diffraction results
A	7.31	11	2529	BDL	BDL	19	BDL	BDL	400	calcite with minor aragonite
A	10.36	3	1999	BDL	BDL	15	BDL	BDL	280	calcite with minor aragonite
A	13.41	5	3143	BDL	BDL	16	BDL	BDL	350	calcite with minor aragonite
A	14.93	10	1684	BDL	BDL	21	BDL	6	250	calcite with minor aragonite
A	16.46	4	1581	BDL	BDL	16	BDL	BDL	200	calcite with minor aragonite
A	17.98	3	1538	BDL	BDL	14	BDL	BDL	180	calcite with minor aragonite
C	7.31	3	1876	BDL	BDL	15	BDL	BDL	170	calcite with minor aragonite
C	10.36	2	1526	BDL	BDL	15	BDL	BDL	180	calcite
C	13.41	3	3038	BDL	BDL	16	BDL	BDL	310	calcite with minor aragonite
C	16.46	3	970	BDL	BDL	4	BDL	BDL	150	calcite with minor aragonite
C	19.51	3	2061	BDL	BDL	15	BDL	BDL	170	calcite with minor aragonite
F	7.31	6	2292	BDL	BDL	2	BDL	BDL	280	calcite with minor aragonite
F	10.36	3	1302	BDL	BDL	18	BDL	BDL	180	calcite with minor aragonite
F	13.41	3	2717	BDL	BDL	16	BDL	BDL	390	calcite with minor aragonite
F	14.93	5	2102	3	BDL	9	BDL	5	350	calcite with minor aragonite
F	16.46	3	1141	3	BDL	9	BDL	BDL	180	calcite with minor aragonite
G	7.31	7	1765	BDL	BDL	11	BDL	BDL	250	calcite with minor aragonite
G	10.36	5	2309	BDL	BDL	11	BDL	5	300	calcite with minor aragonite
G	13.41	6	3715	2	BDL	11	BDL	BDL	480	calcite with minor aragonite
G	16.46	3	1774	BDL	BDL	10	BDL	BDL	210	calcite with minor aragonite

APPENDIX C. TIDAL STUDY RESULTS

Table C.1. Tidal survey results. Tidal survey was conducted on June 6, 1998. Monitoring well head values are normalized to an elevation of benchmark on plant monitoring well of zero centimeters. Actual elevation of benchmark is 1.213 m N.G.V.D. Freshwater head is calculated to a depth of well F-8.

Well	Time	Uncorrected head, cm	Freshwater head, cm
A-9	7:07	-64.4	-61.2
	8:00	-61.0	-57.7
	10:10	-51.7	-48.4
	11:04	-51.2	-47.9
	12:12	-53.6	-50.3
	13:02	-55.6	-52.3
	14:03	-63.1	-59.9
	15:01	-71.0	-67.8
	16:04	-78.8	-75.6
	17:02	-82.4	-79.2
	17:21	-83.7	-80.6
	17:40	-83.5	-80.4
	18:02	-84.7	-81.6
	18:21	-84.9	-81.8
	18:41	-85.3	-82.2
	19:02	-85.3	-82.2
	19:24	-85.3	-82.2
	20:00	-84.3	-81.2
	22:50	-74.4	-71.2
A-18	7:10	-83.0	-67.7
	8:01	-80.1	-64.7
	9:02	-73.8	-58.3
	10:01	-70.9	-55.3
	11:02	-70.1	-54.5
	12:11	-71.5	-55.9
	13:01	-75.2	-59.7
	14:02	-82.1	-66.8
	15:00	-89.1	-73.9
	16:02	-95.9	-80.9
	17:01	-100.8	-85.9
	17:20	-102.4	-87.5

	17:38	-103.0	-88.1
	18:00	-102.8	-87.9
	18:20	-103.0	-88.1
	18:40	-103.1	-88.2

Well	Time	Uncorrected head, cm	Freshwater head, cm
A-18	19:01	-103.4	-88.5
	19:23	-103.2	-88.3
	19:59	-102.0	-87.1
	22:49	-92.3	-77.2
F-8	7:23	-66.8	-61.7
	8:08	-63.2	-58.0
	9:10	-58.2	-53.0
	10:11	-54.3	-49.1
	11:13	-53.8	-48.6
	12:22	-56.3	-51.1
	13:12	-58.1	-52.9
	14:12	-66.4	-61.3
	15:13	-74.9	-69.9
	16:13	-81.2	-76.2
	17:11	-85.7	-80.7
	17:34	-86.6	-81.6
	17:49	-87.4	-82.4
	18:08	-87.4	-82.4
	18:29	-87.7	-82.7
	18:50	-87.9	-83.0
	19:13	-88.2	-83.3
	19:35	-87.4	-82.4
	20:11	-86.5	-81.5
	22:53	-77.54	-72.5
F-14	7:22	-86.4	-68.1
	8:08	-84.2	-65.8
	9:08	-77.6	-59.1
	10:10	-73.9	-55.3
	11:12	-74.3	-55.7
	12:20	-76.8	-58.2
	13:11	-78.8	-60.3
	14:11	-87.1	-68.8
	15:12	-94.9	-76.8
	16:12	-101.4	-83.5
	17:10	-105.1	-87.3
	17:34	-106.2	-88.4

17:48	-106.5	-88.7
18:07	-106.7	-88.9
18:28	-107.2	-89.4
18:49	-107.4	-89.6
19:12	-107.6	-89.9
19:33	-107.2	-89.4
20:09	-105.9	-88.1
22:53	-97.9	-79.9

Well	Time	Uncorrected head, cm	Freshwater head, cm
F-19	7:21	-85.6	-66.4
	8:07	-82.7	-63.4
	9:07	-77.7	-58.3
	10:09	-73.8	-54.3
	11:12	-73.9	-54.4
	12:19	-76.2	-56.7
	13:09	-77.7	-58.3
	14:10	-85.3	-66.1
	15:11	-94.5	-75.5
	16:11	-100.6	-81.8
	17:09	-103.9	-85.2
	17:33	-105.7	-87.1
	17:47	-105.7	-87.1
	18:06	-105.4	-86.7
	18:27	-106.2	-87.6
	18:48	-106.8	-88.2
	19:11	-106.0	-87.4
	19:32	-106.1	-87.5
	20:08	-105.3	-86.6
	22:52	-96.2	-77.3
G-9	7:14	-69.3	-65.1
	8:03	-66.2	-61.9
	9:05	-61.9	-57.6
	10:06	-59.0	-54.7
	11:06	-56.3	-52.0
	12:16	-59.4	-55.1
	13:05	-60.2	-55.9
	14:06	-68.6	-64.3
	15:09	-76.9	-72.7
	16:06	-84.3	-80.1
	17:05	-88.3	-84.2
	17:25	-89.2	-85.1
	17:44	-90.1	-85.6
	18:04	-90.1	-86.0
	18:25	-90.3	-86.2
	18:45	-90.7	-86.6
	19:07	-90.9	-86.8
	19:29	-90.5	-86.4
	20:03	-88.7	-84.6
	22:47	-80.0	-75.8

Well	Time	Uncorrected head, cm	Freshwater head, cm
G-18	7:17	-90.6	-71.8
	8:04	-86.5	-67.6
	9:04	-81.5	-62.5
	10:05	-78.2	-59.1
	11:05	-77.4	-58.2
	12:15	-80.5	-61.4
	13:04	-81.8	-62.8
	14:04	-90.7	-71.9
	15:06	-98.3	-79.7
	16:06	-104.7	-86.3
	17:06	-108.4	-90.1
	17:24	-110.1	-91.8
	17:42	-110.2	-91.9
	18:03	-110.9	-92.7
	18:24	-111.3	-93.1
	18:43	-111.4	-93.2
	19:06	-111.4	-93.2
	19:28	-111.3	-93.1
	22:52	-101.5	-83.0

Table C.2. Canal tidal study conducted the same day. Data is not relative to any benchmark.

time	tide (cm)
6:45	23.2
7:00	27.5
7:06	29.5
7:25	30.1
7:47	34.5
8:15	37.0
8:46	44.2
9:12	47.0
9:34	49.5
10:20	50.7
10:30	52.0
11:45	47.0
12:45	36.5
13:35	25.0
14:05	18.7
14:37	11.0
15:23	3.9
15:55	-1.1
16:05	-3.0
16:45	-5.0
18:19	-6.0
19:18	-1.7
19:33	0.5
20:00	3.9
20:40	10.7
20:55	13.5

APPENDIX D. MARCH 1998 WATER SAMPLING CAMPAIGN RESULTS

Table D.1. Field and nutrient analysis results for March water samples.

Sample	pH	Salinity, ppt	Alkalinity, mg/L	Sulfide, mg/L	[NH_3] ppm-N	[NO_3^-] ppm-N	[phosphate] ppm-P
A-5	11.9	17	24790	34	8.27	BDL	BDL
A-9	11.5	3.6	6260	<0.1	0.21	7.30	BDL
A-18	7.49	2.9	1465	<0.1	BDL	12.3	1.64
B-5	11.68	15	14540	36	18.2	0.005	0.005
B-9	8.68	5.7	640	4.1	2.85	0.063	0.020
B-18	7.55	2.3	1220	<0.1	BDL	12.6	0.874
C-5	7.10	2.2	4300	<0.1	BDL	2.09	BDL
C-9	7.71	2.3	1570	<0.1	BDL	11.6	0.792
C-20	7.53	30	1325	<0.1	BDL	2.68	0.134
D-5	9.54	30	1830	44	18.1	0.065	0.019
D-9	10.50	3.4	494.6	2.5	1.00	3.00	BDL
D-14	7.34	37	1430	1.2	0.335	0.009	0.018
E-5	8.12	15	1660	54	9.24	BDL	BDL
E-9	8.33	9	1265	0.6	0.211	3.81	0.251
E-18	7.39	20	1715	<0.1	0.826	0.313	0.011
F-8	7.66	14	2720	30	4.88	BDL	0.054
F-14	10.17	35	370	0.7	0.932	0.024	BDL
F-18	7.46	39	1100	0.9	0.05	BDL	0.007
G-5	10.11	20	2680	58	16.9	BDL	0.162
G-9	8.12	11	1310	14	3.72	BDL	0.087
G-18	7.36	38	1545	4.8	0.326	BDL	0.008
WW	7.21	1.7	325	<0.1	BDL	11.6	2.00

BDL = below detection limit (0.005 ppm N for NO_3^- and NH_3, 0.005 ppm P phosphate)
NA = measurement not available

APPENDIX E. JUNE 1998 WATER SAMPLING CAMPAIGN RESULTS

Table E.1. Field, nutrient, and fluoride analytical results for June water samples from the comprehensive sampling round.

Sample	pH	Salinity, psu	Alkalinity, m eq/L	[NH_3], ppm-N	[NO_3^-], ppm-N	[phosphate], ppm-P	[F-], ppm-F	Sulfide Present?
A-9	8.6	6.1	1.15	0.10	8.18	BDL	0.58	no
A-18	7.38	29.5	2.40	BDL	4.10	1.63	1.3	no
B-9	8.08	7.1	2.80	0.32	1.01	BDL	0.56	yes
B-18	7.65	13.2	2.40	BDL	7.17	1.57	0.97	no
C-9	7.64	6.7	2.52	BDL	11.5	0.79	0.84	no
C-20	7.42	38.8	2.45	0.06	BDL	0.02		yes
D-9	6.93	NA	4.80	BDL	6.09	0.02	1.08	no
D-14	7.45	36.9	2.80	0.31	0.011	0.02	1.12	yes
E-9	8.25	6.4	1.80	0.1	0.473	0.06	0.90	yes
E-18	7.49	29.8	3.50	0.31	0.034	BDL	0.89	no
F-8	7.69	9.7	4.80	4.61	BDL	0.30	1.16	yes
F-14	7.76	35.4	1.77	0.31	0.609	BDL	1.14	yes
F-18	7.56	37.2	2.32	0.12	BDL	BDL	0.83	yes
G-9	7.89	8	3.20	0.73	0.035	0.05	1.12	yes
G-18	7.49	36.6	2.70	0.33	0.014	0.02	0.85	yes
WW	6.94	4.8	1.70	0.51	18.3	2.88	1.22	no

BDL = below detection limit (0.002 ppm N for NO_3^-, 0.01 ppm P for phosphate, 0.025 ppm N for NH_3)
NA = measurement not available

Table E.2. Elemental analysis results of June water samples from the comprehensive sampling round.

Sample	[Al], ppm	[Ba], ppm	[Ca], ppm	[Fe], ppm	[K], ppm	[Mg], ppm	[Mn], ppm	[Na], ppm	[P], ppm	[Si], ppm	[Sr], ppm	[Ti], ppm
A-9	0.48	0.04	186	BDL	3.1	116	0.05	1335	BDL	2.6	1.7	BDL
A-18	0.66	0.02	392	BDL	27	939	0.19	8324	2.1	1.9	5.5	BDL
B-9	0.41	0.05	160	BDL	4.2	179	0.06	1748	BDL	2.1	1.9	BDL
B-18	0.52	0.03	204	BDL	9.1	428	0.11	3880	2.0	2.9	3.0	BDL
C-9	0.37	0.03	150	BDL	6.2	228	0.08	1833	1	3	2.4	BDL
C-20	0.61	0.02	394	BDL	21	1006	0.17	9069	BDL	1.1	6.1	BDL
D-9	0.54	0.03	256	BDL	3.4	145	0.09	1119	BDL	3	3.8	BDL
D-14	0.51	0.01	308	BDL	14	845	0.15	7736	0.6	1.3	3.7	BDL
E-9	0.49	0.04	163	BDL	4.2	94	0.05	1381	BDL	1.8	2.6	BDL
E-18	0.37	0.03	201	BDL	10	541	0.1	4964	BDL	1	3	BDL
F-8	0.51	0.02	167	BDL	7	328	0.09	3625	BDL	4.6	2.7	BDL
F-14	0.82	0.06	949	BDL	25	1061	0.27	9509	BDL	4.5	8.5	BDL
F-18	0.41	0.02	303	BDL	17	803	0.12	6711	BDL	0.73	4	BDL
G-9	0.40	0.03	193	BDL	8	277	0.09	2411	BDL	3.7	2.9	BDL
G-18	0.49	0.02	212	BDL	12	876	0.12	6142	0.6	0.78	3.6	BDL
WW	0.32	0.02	142	BDL	4.2	219	0.07	1578	2.8	1.6	1.9	BDL

Table E.3. Times and dates when June sampling rounds 2-6 occurred.

Round	Date	Time Began
2	6/8/1998	19:57
3	6/9/1998	8:03
4	6/9/1998	20:32
5	6/10/1998	8:56
6	6/10/1998	21:12

Table E.4. Salinity, pH, and nutrient analysis of June water samples of rounds 2-6.

Well	Round	pH	Salinity, psu	[NO_3], ppm N	[phosphate], ppm P	[NH_3], ppm N
A-5	2	NA	NA	0.175	13.5	37
	3	NT	NT	NT	NT	NT
	4	1.72	38.9	0.071	8.28	44.18
	5	2.44	36.3	0.118	9.36	46.22
	6	1.81	37.9	0.118	7.13	0.081
A-9	2	8.83	6.0	7.87	0.02	0.04
	3	8.74	5.9	8.76	0.02	BDL
	4	8.65	6.2	NT	NT	NT
	5	8.49	5.9	1.9	BDL	0.12
	6	8.61	6.1	7.96	0.026	0.03
A-19	2	7.4	30	2.2	1.89	BDL
	3	7.39	31.3	9.76	1.44	BDL
	4	7.45	32	10.65	BDL	0.08
	5	7.41	31.7	1.19	1.54	0.05
	6	7.33	32.2	1.82	1.64	0.02
B-5	2	3.2	27.3	0.071	3.81	75.6
	3	NT	NT	NT	NT	NT
	4	6.18	27.4	BDL	9.23	67.9
	5	6.85	26.8	BDL	5.27	61.6
	6	6.26	28.1	BDL	8.69	72.7
B-9	2	8.17	6.6	1.2	BDL	0.30
	3	7.83	6.5	NA	0.02	0.22
	4	8.20	6.4	1.08	BDL	0.43
	5	8.01	6.5	1.06	BDL	0.32
	6	8.06	6.6	2.28	BDL	0.39
B-18	2	7.41	12.4	9.92	1.77	0.06
	3	7.46	13.0	11.2	1.83	0.03
	4	7.54	13.8	9.2	1.11	NA
	5	7.55	13.9	7.85	1.58	BDL
	6	7.32	13.3	10.96	1.56	BDL

BDL = below detection limit (0.002 ppmN for NO_3, 0.01 ppm P for phosphate, 0.025 ppm N for NH_3)
NT = sample not taken

Table E.5. Nutrient concentrations and salinity of wastewater taken the workweek before the June sampling campaign. Samples taken approximately noon each day.

Collected	[NO_3], ppm N	[phosphate], ppm P	[NH_3], ppm N	salinity, psu
5/31/98	14.03	3.76	0.45	5.1
6/1/98	16	3.36	0.105	5.2
6/2/98	16.85	3.33	0.094	5
6/3/98	17.2	3.4	BDL	4.8
6/4/98	19.48	3.73	0.062	5.1

APPENDIX F. COLUMN 1 RESULTS

Table F.1. Phosphate, pH and fluoride results through time for Column 1 water samples.

sample	time (days)	[phosphate], ppm P	pH	[F-], ppm F	sum of P abs/g of rock (mg/g)
added seawater and equlibrated overnight					
0	0	0			
added phosphate					
1	0.007	2.06			
2	0.08	1.95			0.000242
3	0.17	1.65			0.000898
4	0.47	1.53			0.00116
5	0.96	1.34			0.00157
6	1.17	1.22			0.00183
7	1.50	1.35			0.00155
8	1.71	1.18			0.00192
9	2.05	1.24			0.00178
10	2.96	1.16			0.00195
11	3.41	1.19			0.00189
12	3.97	1.08			0.00211
13	4.48	1.09			0.00210
14	4.99	1.11			0.00206
15	5.46	1.10			0.00208
16	5.96	1.01			0.00226
17	6.45	1.09			0.00210
18	6.99	1.09			0.00210
19	7.47	0.96			0.00236
20	7.96	0.93			0.00242
21	8.45	0.89			0.00250
22	9.09	0.88			0.00252
23	10.15	0.85			0.00257
24	11.38	0.81			0.00265
25	11.96	0.72			0.00282
26	12.45	0.81			0.00265
27	12.95	0.81			0.00265
28	13.47	0.76			0.00274
29	13.95	0.72			0.00282
30	14.48	0.72			0.00281
31	14.95	0.77			0.00273
32	15.45	0.76			
33	15.97	0.73			0.00280
34	16.36	0.72			0.00286
35	17.96	0.70			0.00292
36	19.03	0.66			0.00292
37					
38	20.14	0.68			0.00290
added phosphate					
39	20.93	3.14			
40	21.10	3.03			0.00310
41	21.10	2.97			0.00322
42	21.27	2.84			0.00345
43	21.95	2.50			0.00406

sample	time (days)	[phosphate], ppm P	pH	[F-], ppm F	sum of P abs/g of rock (mg/g)
44	22.40	2.61			0.00387
45	22.96	2.56			0.00396
46	23.45	2.41			0.00422
47	23.95	2.43			0.00419
48	24.41	2.40			0.00423
45	22.96	2.56			0.00396
46	23.45	2.41			0.00422
47	23.95	2.43			0.00419
48	24.41	2.40			0.00423
49	25.33	2.11			0.00474
50	27.01	2.12			0.00473
51	27.94	2.08			0.00478
52	28.94	1.94			0.00503
53	29.95	1.96			0.00499
54	31.08	1.89			0.00511
55	34.14	1.69			0.00544
56	35.93	1.70			0.00543
57	37.94	1.68			0.00545
58	42.33	1.49			0.00576
59	43.97	1.48			0.00578
60	45.95	1.44			0.00584
61	48.11	1.42			0.00587
62	50.45	1.41			0.00551
63	51.97	1.41			0.00589
64	54.20	1.34			0.00599
65	56.08	1.17			0.00625
66	59.25	1.22			0.00618
67	62.140	1.17			0.00625
68	64.03	1.09			0.00637
69	64.99	1.08			0.00639
70	67.45	1.09			0.00637
71	70.09	1.04			0.00645
72	71.97	0.98			0.00654
73	75.40	1.00			0.00651
74	76.96	0.98			0.00653
75	80.10	0.92			0.00662
76	83.23	0.93			0.00660
77	90.98	0.84	7.74	1.07	0.00673
added phosphate and seawater					
78	91.00	5.04	7.45	1.14	
79	91.09	5.34	7.38	1.15	0.00600
80	91.17	5.30	7.44	1.13	0.00610
81	91.28	5.37	7.65	1.13	0.00594
82	91.43	5.39	7.56	1.23	0.00589
83	91.53	5.25	7.61	1.24	0.00621
84	91.92	5.05	7.68	1.23	0.00666
85	92.08	4.51	7.57	1.22	0.00785
86	92.28	5.06	7.58	1.24	0.00665
87	92.48	4.94	7.62	1.24	0.00691
88	92.96	4.89	7.69	1.26	0.00702

sample	time (days)	[phosphate], ppm P	pH	[F-], ppm F	sum of P abs/g of rock (mg/g)
89	93.46	4.84	7.77	1.23	0.00712
90	93.95	4.76	7.80	1.15	0.00728
91	94.40	4.53	7.79	1.15	0.00775
92	95.12	4.56	7.77	1.17	0.00769
93	96.11	4.27	7.79	1.16	0.00825
94	96.95	4.29	7.81	1.17	0.00821
95	98.95	4.30	7.82	1.14	0.00819
96	100.95	4.11	7.86	1.12	0.00854
97	104.01	4.14	7.87	1.10	0.00849
98	106.92	3.81	7.83	1.08	0.00908
99	111.02	3.33	7.83	1.30	0.00992
100	112.87	3.31	7.83	1.30	0.00995
101	116.86	3.13	7.87	1.19	0.01025
102	120.90	3.01	7.82	1.23	0.01045
103	124.86	2.94	7.81		0.01057
104	130.35	2.73	7.68		0.01090
105	137.88	2.53	7.81		0.01121
106	145.17	2.38	7.80		0.01144
107	152.09	2.22	7.78		0.01167
108	157.96	2.22	7.87		0.01167
109	174.93	1.86	7.92		0.01219
column drained , seawater added for desorption experiment					
110	175.23	0.07	8.09		0.01194
111	175.94	0.14	8.04		0.01166
112	176.30	0.28	8.03		0.01165
113	177.13	0.28	8.04		0.01153
114	178.22	0.35	7.98		0.01149
115	178.96	0.37	7.98		
116	179.99	0.39	7.99		0.01145
117	181.11	0.45	8.01		0.01134
118	182.92	0.48	8.02		0.01129
119	186.34	0.54	8.01		0.01118
120	187.94	0.55	7.99		0.01116
121	190.95	0.59	8.04		0.01110
122	193.14	0.64	8.00		0.01101
123	195.95	0.66	7.98		0.01098
124	201.04	0.73	7.95		0.01090
125	206.91	0.72	8.00		0.01092
126	213.93	0.71	8.06		0.01092
127	220.19	0.78	7.05	0.23	0.01082
column drained distilled water added					
128	223.48	0.07	8.20		0.10838
129	223.91	0.05	8.20	0.25	0.01088
130	223.99	0.22	6.95	1.39	0.01053
added phosphate and fluoride					
131	224.03	2.22	7.04	1.44	0.01053
132	224.09	2.20	7.23		0.01066
133	224.25	1.92	7.44		0.01128

sample	time (days)	[phosphate], ppm P	pH	[F-], ppm F	sum of P abs/g of rock (mg/g)
134	224.47	1.72	7.59	1.24	0.01172
135	224.85	1.72	7.57		0.01172
136	225.17	1.66	7.50	1.29	0.01185
137	225.47	1.36		1.20	0.01249
138	225.91	1.49	7.64		0.01222
139	226.46	1.44	7.69		0.01232
140	226.94	1.46	7.68	1.21	0.01228
141	227.39	1.33	7.74	1.22	0.01253
142	226.89	1.46	7.69		0.01228
143	227.89	1.37	7.74	1.14	0.01245
144	228.89	1.44	7.79		0.01232
145	230.83	1.42	7.81	1.17	0.01236
146	233.30	1.14	7.72	1.32	0.01287
147	235.11	1.18	7.84	1.21	0.01270
148	237.93	1.01	7.77		0.01309
149	240.93	1.07	7.83		0.01299
150	244.92	0.94	7.88	1.19	0.01321
151	249.13	1.03	7.81	1.27	0.01306
152	252.02	0.92	7.84		0.01323
153	256.21	0.74	7.85	1.19	0.01352
154	257.95	0.84	7.83		0.01336
155	262.90	0.72	7.88	1.20	0.01354
156	268.04	0.80	7.88	1.25	0.01343
157	274.94	0.82	7.88	1.17	0.01340
158	282.05	0.77		1.18	0.01347
drain	282.91				

Table F.2. Elemental analysis results for the Column 1 water samples.

Sample	Time, days	[Ca], ppm	[K], ppm	[Mg], ppm	[Na], ppm
36	19.02	500	525	1375	10575
38	20.14	550	550	1400	11100
42	21.27	525	500	1350	10300
50	27.01	525	525	1400	10700
60	45.95	500	500	1325	10175
70	67.45	525	525	1400	10575
74	76.96	550	550	1400	10750
80	91.17	525	550	1400	10775
90	93.95	525	525	1375	10350
91	94.49	500	525	1375	10425
100	112.87	525	500	1350	10275
108	157.96	575	575	1525	11600
110	175.23	550	525	1450	11025
120	187.94	575	550	1475	11425
124	201.04	575	550	1475	11150
132	224.09	25	19	45	375
142	226.89	37.5	25	62.5	500
152	252.02	62.5	30	85	675

Table F.3. Analytical results for solutions that were drained from Column 1.

Solution Drained	pH	Salinity, psu	Alkalinity, meq/L	[Ca], ppm	[K], ppm	[Mg], ppm	[Na], ppm
third SW addition 1/6/1999	7.92	36.3	1.62	600	575	1550	11925
SW desorption 2/24/1999	8.06	36.0	1.95	600	575	1525	11750
F and P in DI addition 4/27/1999	7.89	2.1	1.54	65	32.5	92.5	650

APPENDIX G. COLUMN 2 RESULTS

Table G.1. Phosphate, fluoride, and nitrate though time in the Column 2 water samples.

sample	time, days	[phosphate], ppm P	pH	[F⁻], ppm F	[NO_3^-], ppm N
distilled water added, equilibrated overnight, phosphate added					
0	0.00	0.085	7.02		
1	0.06	1.84	7.01		
2	0.15	2.04	7.12		
3	0.31	2.08	7.28		
4	0.50	2.00	7.34		
5	0.88	1.9	7.43		
6	1.24	1.95	7.47		
7	1.53	1.8	7.50		
8	2.07	1.81	7.47		
9	2.53	1.75	7.51		
10	3.00	1.55	7.55		
11	3.45	1.61	7.59		
12	3.96	1.54	7.55		
13	4.94	1.45	7.52		
14	5.94	1.37	7.60		
15	7.93	1.32	7.63		
16	10.23	1.20			
17	12.94	1.08	7.74		
18	18.10	0.98	7.75		
19	25.25	0.86	7.64		
20	27.96	0.71	7.71		
21	32.00	0.74	7.67		
22	35.99	0.64	7.67		
23	39.94	0.54	7.71		
24	43.98	0.50	7.67		
25	51.21	0.46	7.63		
26	57.24	0.40	7.60		
27	64.24	0.35	7.56		
28	68.02	0.30	7.52		
column drained, distilled water added					
29	68.33	0.26	6.13		
30	68.39	0.36	6.18		
31	68.61	0.34	6.51		
32	68.96	0.10	6.73		
33	69.28	0.31	6.72		
34	69.59	0.24	6.69		
35	70.04	0.089	6.75		
36	70.56	0.26	6.69		
37	71.06	0.87	6.92		
38	71.61	0.36	6.82		
39	72.00	0.16	6.99		
40	73.05	0.04			
41	74.09	0.05	7.02		
42	75.04	0.05	7.13		
43	76.04	0.11	7.11		
44	77.04	0.05	7.11		
45	78.98	0.04	7.07		

sample	time, days	[phosphate], ppm P	pH	[F⁻], ppm F	[NO_3^-], ppm N

46	81.45		7.04		
47	81.26	0.06	7.06		
48	84.076	0.05	7.08		
49	87.08	0.05	7.13		
50	89.21	0.12	7.09		
column drained, wastewater added					
51	89.24	1.45	7.63		12.9
52	89.30	1.65	7.52		
53	89.49	1.65	7.55		13.4
54	89.62	1.42	7.59		
55	89.97	1.30	7.68		13.2
56	90.30	1.50	7.57		
57	90.65	1.11	7.44		11.8
58	91.08	0.79	7.44		
59	91.58	0.78	7.30		8.41
60	92.11	0.49			
61	92.63	0.36	7.33		6.41
62	92.75	0.35	7.35		
63	93.71	0.19	7.41		4.36
64	94.78	0.14	7.37		
65	95.78	0.10	7.38		2.21
66	96.75	0.05	7.40		
67	97.69	0.10	7.43		0.82
68	not analyzed				
69	not analyzed				
70	103.61	0.05	7.48		
column drained, poisoned wastewater added					
71	106.73	1.43	7.71	1.08	
72	106.75	1.54	7.75	0.97	13.0
73	106.83	1.26	7.65	0.97	
74	107.13	1.22	7.73		12.9
75	107.60	1.53	7.82	1.05	
76	108.09	1.39	7.88	0.99	12.6
77	108.55	1.27	7.86		
78	109.07	1.45			12.4
79	109.55	1.21	7.94	1.03	
80	110.61	1.18	8.06		12.7
81	111.83	1.15	8.06	0.94	
82	112.94	1.19	8.13		12.7
83	114.54	1.13	8.14		
84	116.75	1.02	8.22	0.94	12.6
85	118.00	1.08	8.13		
86	121.48	1.01	8.18	0.82	12.3
87	124.50	0.93	8.09	0.92	
88	127.59	0.91	8.10	0.91	12.4
89	135.64	0.46	7.57	0.94	
90	142.36	0.05	8.06	0.91	3.33

Table G.2. Elemental analysis results of the Column 2 water samples.

Sample	Time, days	[Ca], ppm	[K], ppm	[Mg], ppm	[Na], ppm
2-1	0.06	BDL	4	4.5	42.5
2-11	3.45	15	5.75	9	87.5
2-20	27.96	35	7	16.75	130
2-28	68.04	52.5	8.25	19.75	145
2-30	68.39	BDL	1.25	0.75	2.25
2-39	72.00	10	0.75	1.75	7.50
2-50	89.21	35	0.5	3.25	6.00
2-60	92.11	177.5	62.5	155	1100
2-72	106.75	175	67.5	155	1125
2-80	110.60	165	65	157.5	1100
2-88	127.59	172.5	67.5	160	1125

BDL: below detection

Table G.3. Analytical results for waters drained from Column 2.

Solution Drained	pH	Salinity, psu	Alkalinity, meq/L	[Ca], ppm	[K], ppm	[Mg], ppm	[Na], ppm
DW phosphate addition 2/28/1999	7.52	0.6	2.58	47.5	8	20.75	142.5
distilled water desorption 3/17/1999	7.09	0.1	1.95	37.5	0.25	3.25	5.75
poisoned wastewater 5/17/1999	8.05	3.8	3.49	NM	NM	NM	NM

DW distilled water, NM not measured

APPENDIX H. FIELD STUDY QUALITY CONTROL RESULTS

Table H.1. March duplicate results for field and nutrient water analyses.

Analysis	Sample	Concentration	Duplicate Concentration	Percent Recovery
Alkalinity	E-30	1265	1255	99.2
	G-30	1310	1515	115
	D-45	1430	1422	99.4
Ammonia	A-30	0.23	0.19	80.7
	G-30	3.88	3.57	92.0
	D-45	0.33	0.37	109
Nitrate	A-30	7.3	7.11	97.4
	D-45	BDL	BDL	NA
	G-30	0.078	0.096	124
Phosphate				
	D-45	0.02	0.02	100
	G-30	0.05	0.08	144
Sulfide	F-60	0.9	0.9	100
	G-30	14	19	136
	C-65	BDL	BDL	NA

% recovery = (duplicate value / sample value)*100

Table H.2. June duplicate results for field and nutrient water analyses.

Analysis	Sample	Concentration	Duplicate Concentration	Percent Recovery
Nitrate	B-9 round 2	0.421	1.20	285
	F-18 round 1	BDL	0.009	NA
	B-9 round 1	1.01	0.234	23
	E-9 round 1	0.473	0.278	59
	F-14 round 1	0.609	0.715	117
Phosphate	F-18 round 1	BDL	0.02	NA
	G-18 round 1	0.02	0.03	135
	B-18 round 3	1.83	1.69	92
	A-18 round 6	1.64	1.66	101
Ammonia	B-9 round 1	0.32	0.37	117

	E-9 round 1	0.10	0.27	268
	F-14 round 1	0.31	0.20	62
	B-9 round 5	0.32	0.38	120
Alkalinity	E-9 round 1	90	73.75	82
	MW round 1	720	712	99

Table H.3. Triplicate interlaboratory comparison results for June water samples.

	NO_3^-, ppm N PSU	NO_3^-, ppm N FIU	NH_3, ppm N PSU	NH_3 ppm N FIU	Phosphate, ppm P PSU	Phosphate, ppm P FIT
B-18 round 1	10.7	7.17	BDL	0.00588	1.57	1.98
E-9 round 1	0.073	0.473	0.10	0.841	0.06	0.0963
G-18 round 1	0.009	0.0144	0.33	0.0227	0.02	0.0344
MW round 1	0.053	0.033	37.8	7.43	2.85	0.214
A-9 round 5	11.4	1.9	0.12	0.0311	BDL	0.0161

FIT = Florida International University
PSU = Penn State

Table H.4. Percent recoveries of duplicate analyses of elemental analysis of June water samples.

	Al	Ba	Ca	Fe	K	Mg	Mn	Na	P	Si	Sr	Ti
% recovery D-9	113	100	85	ND	118	94	100	102	ND	57	97	ND
% recovery E-18	157	100	137	ND	130	137	130	125	ND	130	150	ND

ND= none detected in one of the analyses.
% recovery = (duplicate value / sample value)*100

Table H.5. Percent Recoveries for duplicate analysis of bulk rock chemistry.

core	sample depth, m	SiO_2, % R	Al_2O_3, % R	Fe_2O_3, % R	MnO, % R	MgO. % R	CaO, % R	Na_2O, % R	K_2O, % R	TiO_2, % R	P_2O_5, % R	Lost on ignition, % R
A	10.36	253	167	57	ND	107	101	80	100	ND	125	82
F	16.46	79	100	138	ND	93	98	86	100	ND	17	100

ND= none detected in one of the analyses
% R= % recovery = (duplicate value / sample value)*100%

core	sample depth, m	Ba, % R	Sr, % R	Y, % R	Sc, % R	Zr, % R	Be, % R	V, % R	F, % R
A	10.36	167	102	ND	ND	67	ND	ND	100
F	16.46	100	97	67	ND	111	ND	ND	100

ND= none detected in one of the analyses
% R= % recovery = (duplicate value / sample value)*100

Table H.6. Duplicate results for oxygen isotopic composition measurements of June water samples.

Well-Depth, m	Data of sample analysis	Date of duplicate analysis	% Recovery
B-9	7/23/1998	07/29/1998	100
G-9	7/31/1998	8/3/1998	109
C-9	9/18/1998	9/24/1998	99

% Recovery = (duplicate value / sample value)*100

Table H.7. Oxygen isotopic composition measurements of reference water. Average of these values is 0.78 ± 0.06 ‰.

date	$\delta^{18}O$ beginning of day, ‰	$\delta^{18}O$ end of day, ‰
7/23/98	0.79	
7/29/98	0.85	0.83
7/31/98	0.68	0.81
8/3/98	0.81	0.83
9/18/98	0.69	0.72
10/2/98	0.7	0.66

APPENDIX I. COLUMN EXPERIMENTS QUALITY CONTROL RESULTS

Table I.1. Column 1 replicate phosphate analysis of water samples.

sample	[phosphate], ppm P	Replicate [phosphate], ppm P	Replicate % Recovery
24	0.81	0.86	106
39	3.14	3.44	109
41	2.97	2.98	100
46	2.41	2.77	115
50	2.12	2.11	100
56	1.70	1.59	94
57	1.68	1.79	106
62	1.41	1.65	117
65	1.17	0.96	82
80	5.30	5.45	103
90	4.76	4.70	99
104	2.73	2.95	108
123	0.66	0.68	103
131	2.22	2.25	101
132	2.20	2.20	100
140	1.46	1.42	97
145	1.42	1.18	103
148	1.01	0.98	97
151	1.03	0.92	89
154	0.84	0.86	103

% recovery = (replicate value / sample value)*100

Table I.2. Column 2 replicate phosphate analysis of water samples.

sample	[phosphate], ppm P	Replicate [phosphate], ppm P	Replicate % Recovery
4	2.00	1.90	95
8	1.81	1.74	96
13	1.45	1.38	95
21	0.74	0.77	105
35	0.09	0.06	67
73	1.26	1.44	114
77	1.27	1.33	105
80	1.18	1.10	93
81	1.15	1.19	103
84	1.02	0.91	89

% recovery = (replicate value / sample value)*100

Table I.3. Column 2 replicate nitrate analysis of water samples.

sample	$[NO_3^-]$, ppm N	Replicate $[NO_3^-]$, ppm N	Replicate % Recovery
78	12.4	12.7	102
82	12.7	12.6	99

% recovery = (replicate value / sample value)*100

Table I.4. Fluoride analysis of the seawater that which was used as a reference during each analytical period. Average seawater concentration equals 1.45 ± 0.08 ppm F.

date	$[F^-]$ beginning of day, ppm F	$[F^-]$ end of day, ppm F
4/22/1999	1.50	1.47
4/28/1999	1.54	1.47
5/26/1999	1.34	1.37

Table I.5. Replicate results for elemental analysis of Column 1 and 2 water samples.

Sample analyzed in replicate	% Recovery [Ca]	% Recovery [K]	% Recovery [Mg]	% Recovery [Na]
Column 1 drained 2/24/1999	96	100	102	100
Column 1 #153	132	133	100	128
Column 2 drained 2/22/1999	110	100	96	102
Column 2 drained 3/17/1999	93	ND	92	104